

เซ็นเซอร์ชนิดใหม่ฐานกรดโบโรนิก/ฟลูออเรสซินที่เรืองแสงและเปลี่ยนสีได้
สำหรับคอปเปอร์และโซดาในดีไอออน

นางสาวศิรินันท์ กุลชาติ

วิทยานิพนธ์นี้เป็นส่วนหนึ่งของการศึกษาตามหลักสูตรปริญญาวิทยาศาสตรมหาบัณฑิต
สาขาวิชาเคมี ภาควิชาเคมี
คณะวิทยาศาสตร์ จุฬาลงกรณ์มหาวิทยาลัย
ปีการศึกษา 2553
ลิขสิทธิ์ของจุฬาลงกรณ์มหาวิทยาลัย

NEW BORONIC ACID/FLUORESCEIN BASED FLUORESCENT AND COLORIMETRIC
SENSORS FOR COPPER AND CYANIDE IONS

Miss Sirinan Kulchat

A Thesis Submitted in Partial Fulfillment of the Requirements
for the Degree of Master of Science Program in Chemistry

Department of Chemistry

Faculty of Science

Chulalongkorn University

Academic Year 2010

Copyright of Chulalongkorn University

Thesis Title NEW BORONIC ACID/FLUORESCEIN BASED FLUORESCENT
AND COLORIMETRIC SENSORS FOR COPPER AND CYANIDE
IONS
By Miss Sirinan Kulchat
Field of Study Chemistry
Thesis Advisor Assistant Professor Boosayarat Tomapatanaget, Ph.D.

Accepted by the Faculty of Science, Chulalongkorn University in Partial
Fulfillment of the Requirements for the Master's Degree

..... Dean of the Faculty of Science
(Professor Supot Hannongbua, Dr.rer.nat.)

THESIS COMMITTEE

..... Chairman
(Assistant Professor Warinthorn Chavasiri, Ph.D.)

..... Thesis Advisor
(Assistant Professor Boosayarat Tomapatanaget, Ph.D.)

..... Examiner
(Assistant Professor Soamwadee Chaianansutcharit, Ph.D.)

..... External Examiner
(Gamolwan Tumchareon, Ph.D.)

ศรินทร์ กุลชาติ : เซ็นเซอร์ชนิดใหม่ฐานกรดโบโรนิกฟลูออเรสเซนต์ที่เรืองแสงและเปลี่ยนสีได้สำหรับคอปเปอร์และไซยาไนด์ไอออน. (NEW BORONIC ACID/FLUORESCENT BASED FLUORESCENT AND COLORIMETRIC SENSORS FOR COPPER AND CYANIDE IONS) อ. ที่ปรึกษาวิทยานิพนธ์หลัก : ผศ.ดร. บุษยรัตน์ ธรรมพัฒน์กิจ, 101 หน้า.

งานวิจัยนี้มีจุดมุ่งหมายที่จะสังเคราะห์เซ็นเซอร์ที่มีอนุพันธ์ของฟลูออเรสเซนต์และกรดโบโรนิก **F-oBOH** **F-mBOH** และ **F-pBOH** เพื่อใช้ตรวจวัดคอปเปอร์และไซยาไนด์ไอออนในขั้นต้นได้นำเซ็นเซอร์ทั้งสามตัวมาศึกษาการเกิดสารประกอบเชิงซ้อนกับแคดไอออนชนิดต่าง ๆ ใช้แอสซิโทไนไทร์เป็นตัวทำละลายโดยใช้เทคนิคยูวี-วิซิเบิล พบว่าแคดไอออนที่สามารถเกิดสารประกอบเชิงซ้อนกับเซ็นเซอร์ทั้งสามชนิดดีที่สุดคือคอปเปอร์ไอออน ทั้งนี้ได้ศึกษาความสามารถในการเกิดสารประกอบเชิงซ้อนระหว่างเซ็นเซอร์ **F-oBOH** **F-mBOH** และ **F-pBOH** กับคอปเปอร์ไอออนโดยใช้เทคนิคยูวี-วิซิเบิลไทเทรชัน ได้ค่าคงที่การจับ ($\log \beta$) เท่ากับ 6.67 8.87 และ 9.88 ตามลำดับ และได้ใช้เทคนิคฟลูออเรสเซนซ์ไทเทรชัน ได้ค่าคงที่การจับ ($\log \beta$) เท่ากับ 8.02 8.48 และ 11.53 ตามลำดับ นอกจากนี้พบว่าเซ็นเซอร์ทั้งสามตัวเกิดปฏิกิริยาไฮโดรไลซิสได้เมื่ออยู่ในน้ำ และผู้วิจัยจึงได้ออกแบบระบบเพื่อป้องกันการไฮโดรไลซิสของเซ็นเซอร์ **F-oBOH** โดยใช้โคออดิเนชันนาโนพาร์ติเคิล (**F-oBOH-AMP/Gd³⁺ CNPs**) พบว่า **F-oBOH-AMP/Gd³⁺ CNPs** <คอปเปอร์(II) มีความจำเพาะเจาะจงกับไซยาไนด์ไอออนเท่านั้น และมีค่าคงที่ในการเกิดสารประกอบเชิงซ้อนระหว่าง **F-oBOH-AMP/Gd³⁺ CNPs** <คอปเปอร์(II) และไซยาไนด์ เท่ากับ 3.97 จึงมีความสามารถในการมองเห็นการเปลี่ยนแปลงสีด้วยตาเปล่าของไซยาไนด์ไอออนและจากการคำนวณเท่ากับ 20 μM และ 4.03 μM ตามลำดับ นอกจากนี้พบว่าแอนไอออนชนิดต่าง ๆ สามารถรบกวนสารประกอบเชิงซ้อนของ **F-oBOH-AMP/Gd³⁺ CNPs** <คอปเปอร์(II) <ไซยาไนด์ ได้น้อยมาก

ภาควิชา.....เคมี.....ลายมือชื่อนิสิต.....
 สาขาวิชา.....เคมี.....ลายมือชื่อ อ.ที่ปรึกษาวิทยานิพนธ์หลัก.....
 ปีการศึกษา.....2553.....

5272561123 : MAJOR CHEMISTRY

KEYWORDS : FLUORESCHEIN / BORONIC ACID / COPPER / CYANIDE /
SENSOR / COORDINATION NANOPARTICLES / LANTHANIDE

SIRINAN KULCHAT: NEW BORONIC ACID/FLUORESCHEIN BASED
FLUORESCENT AND COLORIMETRIC SENSORS FOR COPPER
AND CYANIDE IONS. ADVISOR : ASST. PROF. BOOSAYARAT
TOMAPATANAGET, Ph.D., 101 pp.

A major aim of this research is to synthesize new sensors containing fluorescein and boronic acid moieties, **F-*o*BOH**, **F-*m*BOH**, and **F-*p*BOH**, for detection of copper and cyanide ions. Initially, the complexation studies of sensors with various cations in acetonitrile, evaluated by UV-vis spectrophotometry and naked-eyes detection, were found that **F-*o*BOH**, **F-*m*BOH**, and **F-*p*BOH** showed a high selectivity toward copper(II) ion. Then, the complexation abilities of three sensors with copper(II) ion were measured by using UV-vis and fluorescence titration techniques. The $\log\beta$ values evaluated by UV-vis titration of **F-*o*BOH**, **F-*m*BOH**, and **F-*p*BOH** were 6.67, 8.87, and 9.88, respectively; while, the $\log\beta$ values evaluated by fluorescence titration of **F-*o*BOH**, **F-*m*BOH**, and **F-*p*BOH** were 8.02, 8.48, and 11.53, respectively. In addition, we studied all of three sensors in aqueous media and discovered that sensors were hydrolyzed by water. Therefore, we designed the new strategy to prevent the hydrolysis approach by adapting coordination nanoparticles network (**F-*o*BOH-AMP/Gd³⁺** CNPs). It displayed the enhancement of fluorescent signal after adding copper ion following by cyanide ion. The $\log K$ value of **F-*o*BOH-AMP/Gd³⁺** CNPs \subset copper (II) with cyanide ion is 3.97. Additionally, the detection limit of **F-*o*BOH-AMP/Gd³⁺** CNPs \subset copper(II) with cyanide anion detected by naked-eyes and fluorescence technique was 20 μ M and 4.03 μ M, respectively. Furthermore, they possess a high selectivity for cyanide ion compared to other competitive anions.

Department : Chemistry Student's Signature _____
Field of Study : Chemistry Advisor's Signature _____
Academic Year : 2010 _____

ACKNOWLEDGEMENTS

I would initial like to thank to my master thesis supervisor, Assistant Professor Boosayarat Tomapatanaget, for her guidance throughout the master studying, and all the tremendous work involved in supervising me. In addition, she served as undergraduate research mentor to me to introduce me into a research setting. She has always expressed an enthusiastic approach to chemistry, and I owe any future successful to her influence. Moreover, I would like to thank Assist. Prof. Dr. Warinthorn Chavasiri, Assist. Prof. Dr. Soamwadee Chaianansutcharit, and Dr. Gamolwan Tumcharern for their interest, value suggestions, comments as committee members, and thesis examiners.

The supramolecular Chemistry Research Unit has been pivotal in complete my master, especially, Mr. Anusak Chaicham, who has been my best colleague and spent countless hours mulling over ideas about my research. Moreover, I would like to thank the members of the Supramolecular Chemistry Research Unit at the Department of Chemistry, Chulalongkorn University for all helps and their encouragement me. Moreover, I would like to thank Associate Professor Sanong Ekgasit and his student Mr. Prasert Sornprasit the member of Sensor Research Unit at Department of Chemistry, Chulalongkorn University for their assistance for Scanning Electron Microscopy (SEM) and Energy Dispersive X-Ray analysis experiments. In addition, I would like to acknowledge the Center for Petroleum, Petrochemicals, and Advanced Materials for their supporting.

I would like to express my deepest gratitude to my parents and family for their love, kindness, encouragement, and financial support throughout my life. Finally, I would like to fully thank the Junior Science Talent Project (JSTP) for financial support and inspiration for the scientific pathway.

CONTENTS

	Page
Abstract in Thai.....	IV
Abstract in English.....	V
Acknowledgements.....	VI
Contents.....	VII
List of Tables.....	XI
List of Figures.....	XIII
List of Schemes.....	XVIII
List of Abbreviations and Symbols.....	XIX
CHAPTER I INTRODUCTION.....	1
1.1 Supramolecular chemistry concept.....	1
1.2 Molecular recognition.....	2
1.3 The fundamental principle for cations and anions sensors.....	3
1.4 Absorption of UV-visible light.....	4
1.5 Phenomena of fluorescence.....	6
1.6 Determination of the stoichiometry of a complex by the method of continuous variation Job's method.....	7
1.7 The selectivity of chemosensors.....	9
1.8 Limit of detection.....	10
1.9 Nanoparticles.....	11
1.10 Energy Dispersive X-Ray Analysis (EDX).....	12
CHAPTER II LITERATURE REVIEWS.....	13
2.1 Literature reviews.....	13
2.1.1 Molecular chemosensors and chemodosimeters (ring-opening of spirocyclic system).....	13
2.1.2 Cyanide sensors.....	19
2.1.3 Self-assemble of supramolecular network.....	24
2.2 Objective and scope of this research.....	28
CHAPTER III EXPERIMENTAL SECTION.....	29
3.1 General procedures.....	29
3.1.1 Analytical instrument.....	29

	Page
3.1.2 Materials.....	29
3.2 Synthesis of boronic/fluorescein based sensors.....	30
3.2.1 Preparation of sensors F-oBOH , F-mBOH , and F-pBOH	30
3.2.1 Characterization of sensors F-oBOH , F-mBOH , and F-pBOH	31
3.3 Complexation Study of F-oBOH , F-mBOH , and F-pBOH in acetonitrile by UV-visible spectrophotometry technique.....	32
3.3.1 Complexation studies of F-oBOH , F-mBOH , and F-pBOH with various cations: copper, cadmium, nickel, silver, zinc, cobalt, and magnesium.....	32
3.3.2 Complexation studies of F-oBOH , F-mBOH , and F-pBOH with copper cation in acetonitrile by UV-visible spectrophotometry.....	35
3.4 Complexation Studies of F-oBOH , F-mBOH , and F-pBOH with copper cation in acetonitrile by fluorescence spectrophotometry.....	38
3.5 Determination of detection limit of F-oBOH , F-mBOH , and F-pBOH by fluorescence spectrophotometry.....	42
3.6 Study on the stability of sensor.....	42
3.6.1 The stability of F-oBOH in Tris buffer pH 7.0 by fluorescence Spectrophotometry.....	42
3.6.2 Study on the stability of F-oBOH , F-mBOH , and F-pBOH by ¹ H-NMR spectrophotometry.....	43
3.7 Preparation of F-oBOH doped nucleotide/lanthanide CNPs (F-oBOH-AMP/Gd³⁺ CNPs).....	43
3.8 Study on the stability of F-oBOH-AMP/Gd³⁺ CNPs.....	44
3.9 Complexation studies of F-oBOH-AMP/Gd³⁺ CNPs \subset copper(II) with various anions: fluoride, chloride, bromide, iodide, hydroxide, nitrate, perchlorate, benzoate, dihydrogenphosphate, thiocyanate, and cyanide.....	44
3.10 Job's plot study.....	46
3.10.1 Job's plot study of F-oBOH-AMP/Gd³⁺ CNPs \subset copper(II) with cyanide anion.....	46
3.10.2 Job's plot study of F-oBOH-AMP/Gd³⁺ CNPs \subset cyanide with copper(II) ion.....	47

3.11 Complexation studies of F-<i>o</i>BOH-AMP/Gd³⁺ CNPs \subset copper(II) with cyanide anion by fluorescence spectrophotometry.....	49
3.12 Determination of detection limit of F-<i>o</i>BOH-AMP/Gd³⁺ CNPs \subset copper(II) with cyanide anion.....	51
3.12.1 Fluorescence spectrophotometry: calculation method.....	51
3.12.2 Naked-eyes detection limit.....	51
3.13 Interference studies by fluorescence spectrophotometry.....	52
CHAPTER IV RESULTS AND DISCUSSION.....	55
4.1 Design concept of boronic acid/fluorescein based sensors.....	55
4.2 Synthesis and characterization of F-<i>o</i>BOH , F-<i>m</i>BOH , and F-<i>p</i>BOH	56
4.3 Complexation Study of F-<i>o</i>BOH , F-<i>m</i>BOH , and F-<i>p</i>BOH in acetonitrile by UV-visible spectrophotometry.....	57
4.3.1 Complexation studies of F-<i>o</i>BOH , F-<i>m</i>BOH , and F-<i>p</i>BOH with various cations: copper, cadmium, nickel, silver, zinc, cobalt, and magnesium.....	57
4.3.2 Complexation studies of F-<i>o</i>BOH , F-<i>m</i>BOH , and F-<i>p</i>BOH with copper cation in acetonitrile by UV-visible spectrophotometry...	59
4.4 Complexation Study of F-<i>o</i>BOH , F-<i>m</i>BOH , and F-<i>p</i>BOH in acetonitrile by fluorescence spectrophotometry.....	65
4.6 Determination of detection limit of F-<i>o</i>BOH , F-<i>m</i>BOH , and F-<i>p</i>BOH with copper(II) by fluorescence spectrophotometry.....	67
4.7 Study on the stability of sensors.....	69
4.8 Preparation of F-<i>o</i>BOH doped nucleotide/lanthanide CNPs (F-<i>o</i>BOH-AMP/Gd³⁺ CNPs).....	72
4.9 The stability study of F-<i>o</i>BOH-AMP/Gd³⁺ CNPs.....	73
4.10 Complexation studies of F-<i>o</i>BOH-AMP/Gd³⁺ CNPs \subset copper(II) with various anions: fluoride, chloride, bromide, iodide, hydroxide, nitrate, perchlorate, benzoate, dihydrogenphosphate, thiocyanate, and cyanide	74

4.11 Job's plot analyses for F-<i>o</i>BOH-AMP/Gd³⁺ CNPs⊂copper(II) with cyanide anion and F-<i>o</i>BOH-AMP/Gd³⁺ CNPs⊂cyanide with copper(II) by fluorescence spectrophotometry.....	77
4.12 Complexation studies of F-<i>o</i>BOH-AMP/Gd³⁺ CNPs⊂copper(II) with cyanide anion by fluorescence spectrophotometry.....	81
4.13 Determination of detection limit of F-<i>o</i>BOH-AMP/Gd³⁺ CNPs⊂copper(II) with cyanide anion.....	82
4.13.1 Fluorescence spectrophotometry: Calculation method.....	82
4.13.2 Naked-eyes detection limit.....	84
4.14 Interference studies of F-<i>o</i>BOH-AMP/Gd³⁺ CNPs⊂copper(II) by fluorescence spectrophotometry.....	85
CHAPTER V CONCLUSION.....	86
5.1 Conclusion.....	86
5.2 Future work.....	88
References.....	89
Appendix.....	95
Vita.....	101

LIST OF TABLES

Table	Page
3.1 Amounts of Cu^{2+} , Cd^{2+} , Ni^{2+} , Ag^+ , Zn^+ , Co^{2+} , Mg^{2+} as trifluoromethanesulfonate and nitrate salt were used in studies by UV-visible spectrophotometry.....	33
3.2 Amounts of cations solutions were used to prepare various cations: F-<i>o</i>BOH ratios.....	33
3.3 Amounts of cations solutions were used to prepare various cations: F-<i>m</i>BOH ratios.....	34
3.4 Amounts of cations solutions were used to prepare various cations: F-<i>p</i>BOH ratios.....	34
3.5 The concentration of Cu^{2+} cation was used in copper cationic complexation studies with F-<i>o</i>BOH and the ratios of F-<i>o</i>BOH:copper cation	35
3.6 The concentration of Cu^{2+} cation was used in copper cationic complexation studies with F-<i>m</i>BOH and the ratios of F-<i>m</i>BOH:copper cation	36
3.7 The concentration of Cu^{2+} cation was used in copper cationic complexation studies with F-<i>p</i>BOH and the ratios of F-<i>p</i>BOH:copper cation	37
3.8 The concentrations of stock solution of sensors and copper were used in complexation studies for fluorescence titration.....	39
3.9 The concentration of Cu^{2+} cation was used in copper cationic complexation studies with F-<i>o</i>BOH and the ratios of F-<i>o</i>BOH:copper cation for fluorescence titration	39
3.10 The concentration of Cu^{2+} cation was used in copper cationic complexation studies with F-<i>m</i>BOH and the ratios of F-<i>m</i>BOH:copper cation for fluorescence titration	40

Table	Page
3.11 The concentration of Cu^{2+} cation was used in copper cationic complexation studies with F-pBOH and the ratios of F-pBOH :copper cation for fluorescence titration.....	41
3.12 Amounts of F^- , Cl^- , Br^- , I^- , OH^- , NO_3^- , ClO_4^- , BzO^- , H_2PO_4^- , SCN^- , and CN^- ions used in these studies by fluorescence spectrophotometry.....	45
3.13 Amounts of anions solutions were used to prepare various anions: F-oBOH-AMP/Gd³⁺ ratios.....	46
3.14 Amounts of F-oBOH-AMP/Gd³⁺ CNPs, CN^- anion, Cu^{2+} cation, and HEPES pH 7.4 were used in Job's plot experiment.....	47
3.15 Amounts of F-oBOH-AMP/Gd³⁺ CNPs \subset CN^- and Cu^{2+} cation were used in Job's plot experiment.....	48
3.16 The concentration of CN^- anion used in cyanide anion complexation studies with F-oBOH-AMP/Gd³⁺ and the final ratios of F-oBOH-AMP/Gd³⁺ CNPs \subset Cu^{2+} :cyanide anion.....	50
3.17 The concentration of CN^- anion used in naked-eye detection limit.....	52
3.18 Amounts of F^- , Cl^- , Br^- , I^- , OH^- , NO_3^- , ClO_4^- , BzO^- , H_2PO_4^- , SCN^- , and CN^- as sodium and potassium salt used in interference studies with F-oBOH-AMP/Gd³⁺ CNPs \subset copper(II) by fluorescence Spectrophotometry.....	53
3.19 Amount of CN^- and anions used in interference studies with F-oBOH-AMP/Gd³⁺ CNPs \subset copper(II) by fluorescence spectrophotometry.....	54
4.1 The intensity of F-oBOH , F-mBOH , and F-pBOH ($5 \times 10^{-6}\text{M}$).....	67
4.2 The detection limit of F-oBOH , F-mBOH , and F-pBOH	68
4.3 The intensity of F-oBOH-AMP/Gd³⁺ CNPs \subset copper(II) ($1 \times 10^{-5}\text{M}$).....	83
4.4 Effect of interference anions on the determination of cyanide anion ($\text{C}_{\text{CN}} = 24.5 (\mu\text{g/mL})$).....	85

LIST OF FIGURES

Figure	Page
1.1 The development of Supermolecules.....	2
1.2 Chemosensors based on the binding site-signaling unit.....	4
1.3 Energy levels of molecular orbitals in formaldehyde (HOMO: highest Occupied Molecular Orbitals; LUMO: Lowest Unoccupied Molecular Orbitals) and possible electronic transition.....	5
1.4 Perrin-Jablonski diagram and illustration of the relative positions of absorption, fluorescence, and phosphorescence spectra.....	7
1.5 Job's plots for a 1:1 complex.....	9
2.1 a) The hydrolysis reaction of α -amino acid ester with copper ion b) The propose mechanism of chemodosimeter 4 react with copper ion and its hydrolysis reaction.....	13
2.2 The schematic explanation the response mechanism of probe 8 with mercury(II) ion.....	14
2.3 The explanation of the response of chemodosimeter 12 with mercury(II) ion and the color change by visual eyes detection from colorless to pink including the significantly of fluorescence changes.....	16
2.4 a) The schematic explanation the response mechanism of probe 14 with copper(II) ion b) Fluorescence emission change of probe 14 in 0.01M Tris-HCl buffer (pH 7.2) upon addition of metal ions.....	17
2.5 a) The schematic explanation the response mechanism of probe 18 with copper(II) ion b) UV-vis titration emission change of probe 18 in DMSO/water 4:6 upon gradually addition of copper(II).....	18
2.6 a) The schematic explanation the response mechanism of probe 20 with copper(II) ion b) Fluorescent spectra of probe 20 with various metal ions. c) A photo of naked-eye for probe 20 ; from second one from second one added with 200 μ M of Ca^{2+} , Cu^{2+} , Hg^{2+} , Zn^{2+} , Fe^{3+} , Ag^+ , Pb^{2+} (from left to right).....	19

Figure	Page
2.7 The cationic borane sensor 22 for detection of cyanide anion in water.....	20
2.8 a) Fluorescence emission of a solution of 23 (DMSO-water (95:5 v/v) upon addition of CN ⁻ (excitation at 480 nm). b) Plot of fluorescence intensity at 541 nm vs number of equivalents of CN ⁻ . c) The schematic explanation the mechanism of 23 with CN ⁻ ion d) Color changes of 23 in DMSO-water (95:5 v/v) in the presence of 1 equiv of the following anions: 1, CN ⁻ ; 2, AcO ⁻ ; 3, F ⁻ ; 4, Cl ⁻ ; 5, Br ⁻ ; 6, I ⁻ ; 7, H ₂ PO ₄ ⁻ ; 8, HSO ₄ ⁻ ; 9, SCN ⁻ ; 10, NO ₃ ⁻ ; 11, BzO ⁻ ; 12, N ₃ ⁻ ; 13, CH ₃ S; 14, ClO ₄ ⁻	21
2.9 The responding of chemosensor 26 for detection cyanide anion in water....	22
2.10 a) Molecular structures of cyanide. b) Complexation of DSPBA probes with aqueous free cyanide.....	23
2.11 The responding of chemosensor 28 for detection cyanide anion by an indirect strategy.....	24
2.12 The illustration of supramolecular nanowires self-assembled from ATP molecules and cationic cyanine dyes.....	25
2.13 A schematic illustration of nanoparticles formation through the self-assemble of AMP and Gd ³⁺	26
2.14 AuNPS in nucleotide/lanthanide nanoparticles. a) TEM image of AuNPs encapsulated by the supramolecular shell of GMP/Gd ³⁺ . b) HR-TEM image of a AuNps surrounded by the supramolecular shell of GMP/Gd ³⁺	26
2.15 a) Molecular structure of nucleotide and guest dyes 31 and 32 . b) SEM and c) TEM images of dye 31 -AMP/Gd ³⁺ CNPs with an average diameter of 30 nm.....	27
2.16 The sensor F-oBOH , F-mBOH , and F-pBOH	28
4.1 The UV-visible spectra change of a) F-oBOH , b) F-mBOH , and c) F-pBOH (3.0 x 10 ⁻⁵ M) in CH ₃ CN in the presence of excess amount of various cations.....	58
4.2 The UV-visible responses (A-A ₀ at 437 nm) of F-oBOH , F-mBOH , and F-pBOH (3.0 x 10 ⁻⁵ M) in CH ₃ CN in the presence of excess amount of various cations.....	59

Figure	Page
4.3 The UV-visible titration spectra of a) F-<i>o</i>BOH (2.5×10^{-5} M), c) F-<i>m</i>BOH (3.0×10^{-5} M), and e) F-<i>p</i>BOH (3.0×10^{-5} M) upon the gradual addition of copper(II) ion in CH ₃ CN and the compared experiment data and calculated data from UV-visible titration of b) F-<i>o</i>BOH , d) F-<i>m</i>BOH , and f) F-<i>p</i>BOH for calculation of the stability constant.....	61
4.4 The ESI-High Resolution Mass Spectroscopy (ESI-HRMS) of the complexation between F-<i>o</i>BOH and copper(II) ion.....	62
4.5 UV-vis spectra of a) F-<i>o</i>BOH (2.5×10^{-5} M) b) F-<i>m</i>BOH (2.5×10^{-5} M) and Cu ²⁺ (1.75×10^{-3} M) in CH ₃ CN in the presence of different amounts of cyanide anion.....	63
4.6 The color changes of F-<i>o</i>BOH (2.5×10^{-5} M) after adding and Cu ²⁺ (1.75×10^{-3} M) and follows adding CN ⁻ (2.5×10^{-4} M) in CH ₃ CN.....	64
4.7 The fluorescence titration spectra of a) F-<i>o</i>BOH , c) F-<i>m</i>BOH , and d) F-<i>p</i>BOH (5×10^{-6} M) upon gradual addition of copper(II) ion in CH ₃ CN and the compared experiment data and calculated data from fluorescence titration of b) F-<i>o</i>BOH , d) F-<i>m</i>BOH , and f) F-<i>p</i>BOH for calculation the stability constant ($\lambda_{\text{ex}}/\lambda_{\text{emiss}} = 437/475$ nm).....	66
4.8 Linear plot between intensity of a) F-<i>o</i>BOH b) F-<i>m</i>BOH c) F-<i>p</i>BOH and concentration of copper(II) ion.....	68
4.9 Fluorescence spectra of F-<i>o</i>BOH ($5 \mu\text{M}$) a) in the presence copper(II) ion ($5 \mu\text{M}$) b) The emission intensity at 518 nm in the presence copper(II) ($5 \mu\text{M}$) under various time in Tris-HCl 0.01 M pH 7.0 buffer solution (5% EtOH:water), ($\lambda_{\text{ex}} = 498$ nm).....	69
4.10 Comparing experiment of hydrolysis product of F-<i>o</i>BOH with F-<i>o</i>BOH , fluorescein, and 2-formylphenyl boronic acid.....	71
4.11 a) SEM image of F-<i>o</i>BOH-AMP/Gd³⁺ CNPs b) TEM image of F-<i>o</i>BOH-AMP/Gd³⁺ CNPs.....	73

Figure	Page
4.12 Fluorescence intensity at 515 nm for F-oBOH-AMP/Gd³⁺ CNPs⊂copper(II) under various time from 0-120 minutes. ($\lambda_{\text{ex}} = 492 \text{ nm}$).....	73
4.13 Fluorescence intensity of F-oBOH-AMP/Gd³⁺ CNPs⊂copper(II) at 515 nm in the presence of different anions (500 μ M) in HEPES (0.1M) pH 7.4 ($\lambda_{\text{ex}} = 492 \text{ nm}$).....	74
4.14 Fluorescence spectra of F-oBOH-AMP/Gd³⁺ CNPs in the presence of different amount of (a) copper(II) ion and (b) cyanide anion in HEPES buffer pH 7.4.....	75
4.15 Fluorescence spectra of F-oBOH-AMP/Gd³⁺ CNPs⊂copper(II) upon addition of cyanide anion in HEPES buffer pH 7.4.....	75
4.16 Photograph of Naked-eyes of (a) F-oBOH-AMP/Gd³⁺ CNPs in the presence of Cu ²⁺ 45 equiv and CN ⁻ 90 equiv (b) F-oBOH-AMP/Gd³⁺ CNPs in the presence of Cu ²⁺ 45 equiv (c) 5'-AMP/Gd ³⁺ CNPs in the presence of Cu ²⁺ 45 equiv and CN ⁻ 90 equiv (d) AMP/Gd ³⁺ CNPs in the presence of Cu ²⁺ 45 equiv and Luminescent of (e) F-oBOH-AMP/Gd³⁺ CNPs in the presence of Cu ²⁺ 45 equiv and CN ⁻ 90 equiv (f) F-oBOH-AMP/Gd³⁺ CNPs in the presence of Cu ²⁺ 45 equiv (g) AMP/Gd ³⁺ CNPs in the presence of Cu ²⁺ 45 equiv and CN ⁻ 90 equiv (h) AMP/Gd ³⁺ CNPs in the presence of Cu ²⁺ 45 equiv. Samples were illuminated by the 356 nm UV light.....	76
4.17 Job's plot analysis of fluorescence intensity for the complexation of the F-oBOH-AMP/Gd³⁺ CNPs⊂copper(II) and cyanide anion. The molar ratio of F-oBOH-AMP/Gd³⁺ CNPs⊂copper(II) CNPs to cyanide anion was varied: 2:8, 3:7, 4:6, 5:5, 6:4, 7:3, 8:2, 9:1.....	77
4.18 Job's plot analysis of fluorescence intensity for the complexation of the F-oBOH-AMP/Gd³⁺ CNPs⊂cyanide and copper(II). The molar ratio of F-oBOH-AMP/Gd³⁺ CNPs⊂cyanide and copper(II) was varied: 1:9, 3:7, 4:6, 5:5, 6:4, 7:3, 8:2, 9:1.....	78

Figure	Page
4.19 Energy dispersive X-ray (EDX) spectrum of F-oBOH-AMP/Gd³⁺ CNPs \subset copper(II) \subset cyanide anion. (Aluminium peak is from the supporting aluminium stub).....	80
4.20 Fluorescence titration spectra of F-oBOH-AMP/Gd³⁺ CNPs \subset copper(II) in HEPES (0.1M) pH 7.4 upon addition of CN ⁻ (0-80 equiv) at emission band at 515 nm. Inset: Binding isotherm between F-oBOH-AMP/Gd³⁺ CNPs \subset copper(II) and cyanide anion. ($\lambda_{\text{ex}}/\lambda_{\text{emis}} = 492/515 \text{ nm}$).....	81
4.21 Comparing experiment and calculated data from fluorescence titration curves of F-oBOH-AMP/Gd³⁺ CNPs \subset copper(II) and cyanide anion for calculation of stability constant ($\lambda_{\text{ex}}/\lambda_{\text{emis}} = 492/515 \text{ nm}$).....	82
4.22 Linear plot between intensity and concentration of cyanide anion.....	83
4.23 Naked-eyes of F-oBOH-AMP/Gd³⁺ CNPs \subset copper(II) in HEPES (0.1M) pH 7.4 in the presence of different concentrations of cyanide anion. From left to right (x10 μM): F-oBOH-AMP/Gd³⁺ , 0, 2.0, 4.0, 7.0, 10.0, 20.0 30.0, and 40.0.....	84

LIST OF SCHEMES

Schemes	Page
4.1 Synthesis pathway of F-<i>o</i>BOH , F-<i>m</i>BOH , and F-<i>p</i>BOH	56
4.2 Propose mechanism of F-<i>o</i>BOH complexation with copper(II) ion.....	63
4.3 Propose mechanism of F-<i>o</i>BOH complexation with copper(II) ion and cyanide anion.....	64
4.4 Proposed the hydrolysis mechanism of the F-<i>o</i>BOH and water followed by reaction with copper(II) to yield fluorescent fluorescein.....	70
4.5 A schematic illustration of nanoparticles formation through the self-assembly of F-<i>o</i>BOH , 5'AMP, and Gd ³⁺ ion (F-<i>o</i>BOH-AMP/Gd³⁺ CNPs).	72
4.6 The description of nanoparticles formation through the self-assembly of F-<i>o</i>BOH , AMP, and Gd ³⁺ and the proposed mechanism of F-<i>o</i>BOH-AMP/Gd³⁺ CNPs after adding copper(II) and cyanide anions.....	79

LIST OF ABBREVIATIONS AND SYMBOLS

^{13}C -NMR	Carbon nuclear magnetic resonance
^1H -NMR	Proton nuclear magnetic resonance
equiv.	Equivalent
g	Gram
Hz	Hertz
J	Coupling constant
mmol	Millimole
mL	Milliliter
μL	Microliter
δ	Chemical Shift
ppm	Part per million
s, d, t, m	Splitting patterns of ^1H -NMR (singlet, doublet, triplet, multiplet)
CNPs	Coordination Nanoparticles
EDX	Energy Dispersive X-ray Analysis
SEM	Scanning Electron Microscopy
TEM	Transmission Electron Microscopy
ESI-HRMS	Electrospray Ionization High Resolution Mass Spectroscopy

CHAPTER I

INTRODUCTION

1.1 Supramolecular Chemistry Concept

The concept and the definition of supramolecular chemistry or host guest chemistry were introduced in 1978 [1] as a development and generalization of previous works. Prof. Lehn invented the term, either a supermolecule or supramolecule is an organized, complex entity that is created from the association of two or more chemical species held together by intermolecular forces. Supermolecule structures are the result of not only additive but also cooperative interactions, including hydrogen bonding, hydrophobic interactions and coordination, and their properties are different from the sum of the properties of each individual component. Supramolecular chemistry is still a new branch, meaning that it can be rather difficult to define exactly what it encompasses. It is a chemistry subject that has improved so rapidly due to contributions from a variety of related fields.

As we know, supramolecular chemistry is a multidisciplinary field which impinges on various other disciplines, such as the traditional areas of organic and inorganic chemistry, needed to synthesize the precursors for a supermolecule, physical chemistry, to understand the properties of supramolecular system and computational modeling to understand complex supramolecular behavior.[2] In recent time, Ariga [3] categorized the supramolecular chemistry into three types: (i) the chemistry associated with a molecular recognizing a partner molecule (molecular recognition chemistry); (ii) the chemistry of molecules built to specific shapes; (iii) the chemistry of molecular assembly from numerous molecules. In addition, Figure 2.1 briefly explains the development of supermolecules in a recent time. Herein, we will describe the most fundamental of supramolecular chemistry by initially starting to explain the molecular recognition.

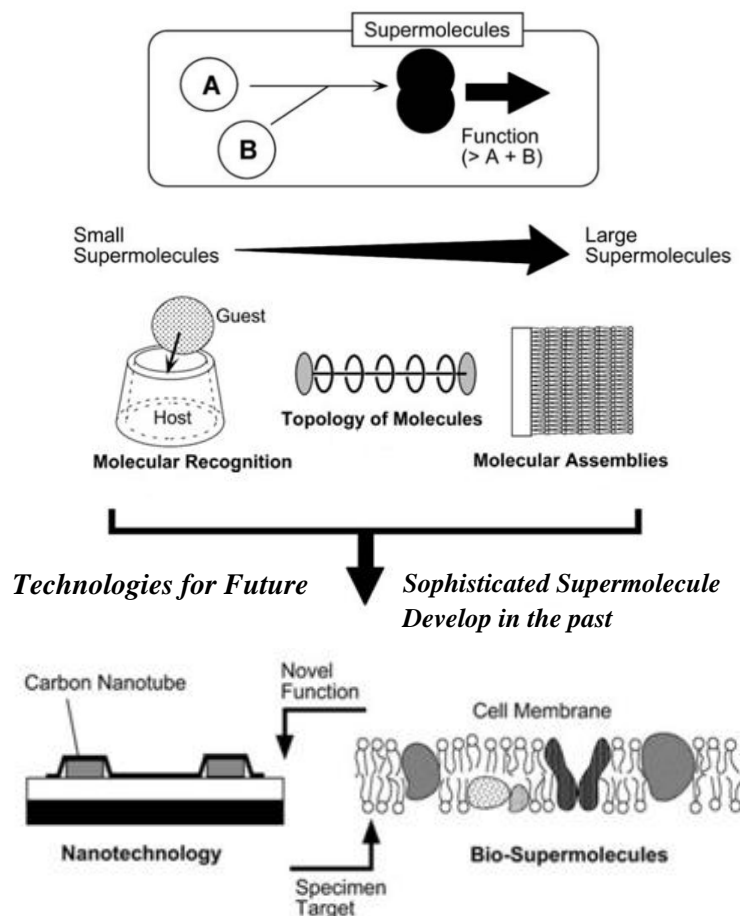


Figure 1.1 The development of Supermolecules [3]

1.2 Molecular Recognition [3]

In molecular recognition, a molecule selectively recognizes its partner via several molecular interactions. The first is electronic interactions that occur between charged molecules. An attractive force is observed between oppositely charged molecules, and a repulsive force between molecules with the identical type of charge. The second is hydrogen bonding that plays a critical role in biological environment. It occurs when the functional groups that are interacting are properly oriented such as the base-pairing of DNA strands. It represents a special kind of dipole-dipole interaction between a proton donor (D) and a proton acceptor (A). [4] The third is coordinated interaction that occurs between metal ions and electron-rich atoms and is of moderate strength. The fourth is van der Waals interaction that is weaker and less specific than those illustrated above but it is very important because it regularly applies to all kinds of molecule. Furthermore, in aqueous media the hydrophobic interaction has played important role. So the

hydrophobic molecule can aggregate in an aqueous medium such as the formation of a cell membrane from lipid-based component. This interaction is related to the hydration structure presents around hydrophobic molecules. The last one is π - π interaction that occurs between aromatic rings, and these sometimes provide important contributions to molecular recognition. When the aromatic rings face each other, the overlap of π -electron orbitals results in an energetic gain.

The effective recognition is accomplished through several combinations of the above-mentioned molecular interaction. When several types of molecular interaction work together, a cooperative enhancement in molecule association is often observed. Finding an appropriate combination of molecular interactions is the key to design efficient molecular recognition systems.

1.3 The fundamental principle for cations and anions sensors

Anions and cations play a fundamental role in a wide range of chemical and biological system. Researchers have been put strongly efforts to devote the development of receptors for both anionic and cationic species. [5] Receptors specifically designed for sensing purposes are generally defined as chemosensors. [6] The signals of chemosensor can be easily detected by human reception. Many chemosensors display changes in either color or fluorescence in the presence of guests by a reversible reaction. Figure 1.4 describes the chemosensor approach of the covalent attachment of signaling subunits and binding sites. The binding site binds guests and then the signaling unit is altered giving rise to several changes in the color (chromomeric chemosensor) or in its fluorescence behavior (fluorogenic chemosensor). This has been the most widely used in the improvement of chemosensors and will surely use to be a basic strategy to design chemosensors in the future development.

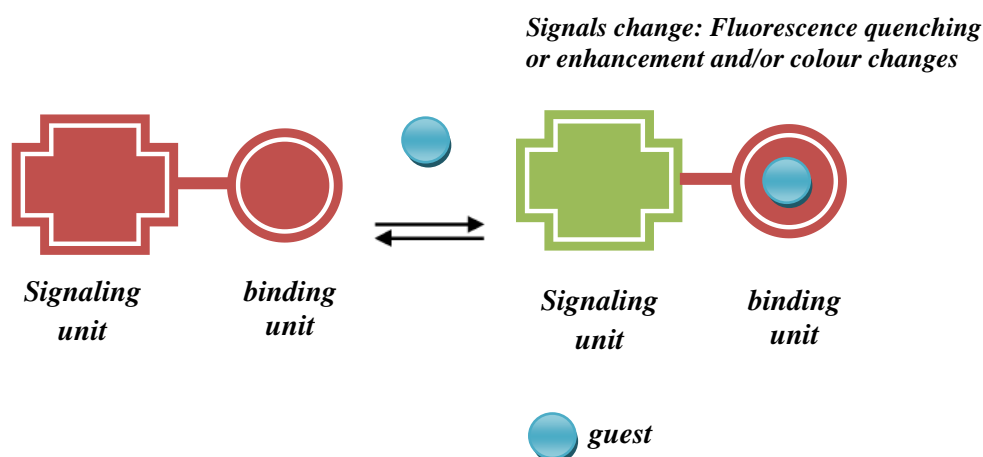


Figure 1.2 Chemosensors based on the binding site-signaling unit.

Fluorescent and colorimetric chemosensors for anions and cations have been developed so fast but those for important and toxic heavy ions such as Hg(II), Pb(II), and Cu(II) present challenges because these ions often act as fluorescence quenchers. Recently, researchers have developed the fluorescent chemodosimeters [7] because chemodosimeters provide an ideal way to design fluorescence “turn-on” probes for the quenching of the heavy metal ions. Furthermore, chemodosimeters are used to detect analyte through a highly selective and generally irreversible chemical reaction between the dosimeter molecule and the target analyte.

Chemodosimeters approach involves the use of reactions induced by a specific analyte such as an anion or cation or other molecules. These reactions result in a significant chemical transformation including both the breaking and formation of several covalent bonds.

1.4 Absorption of UV-visible light

An electronic transition contains the promotion of an electron from an orbital of a molecule in the ground state to an unoccupied orbital by absorption of a photon. The molecule is then said to be in an excited state. There are several types of molecular orbitals. The first principle orbital is a σ orbital generally performed from s atomic orbital, or from one s and one p atomic orbitals, or from two p atomic orbitals having a

collinear axis of symmetry. The bond performed is called a σ bond. A π orbital is performed from two p atomic orbitals overlapping and the resulting bond is called a π bond. A molecule may also consist of non-bonding electrons existed in heteroatoms such as oxygen or nitrogen. The corresponding molecular orbitals are called n orbitals. The transferring of a non-bonding electron to an antibonding orbital is possible and is denoted by $n \rightarrow \pi^*$. In addition, the energy of these electronic transitions is generally in the following order: $n \rightarrow \pi^* < \pi \rightarrow \pi^* < n \rightarrow \sigma^* < \sigma \rightarrow \pi^* < \sigma \rightarrow \sigma^*$. Figure 1.3 prescribes the energy levels of example molecule as formaldehyde with the possibility of all transitions.

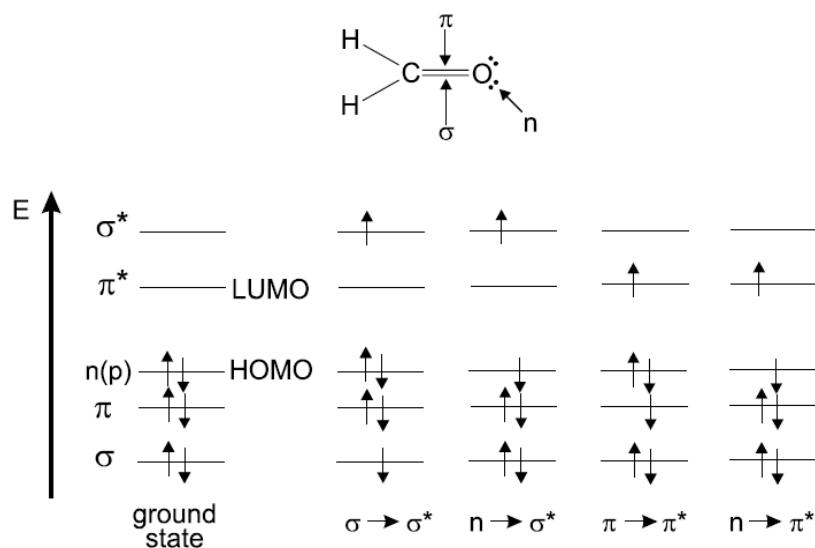


Figure 1.3 Energy levels of molecular orbitals in formaldehyde (HOMO: highest Occupied Molecular Orbitals; LUMO: Lowest Unoccupied Molecular Orbitals) and possible electronic transition. [8]

In absorption and fluorescence spectroscopy, two important categories of orbital are pondered: the Highest Occupied Molecular Orbitals (HOMO) and the Lowest Unoccupied Molecular Orbitals (LUMO). Both of these refer to the ground state of the molecule. For example, in formaldehyde, the HOMO is the n orbital and the LUMO is the π^* orbital.

1.5 Phenomena of fluorescence [9]

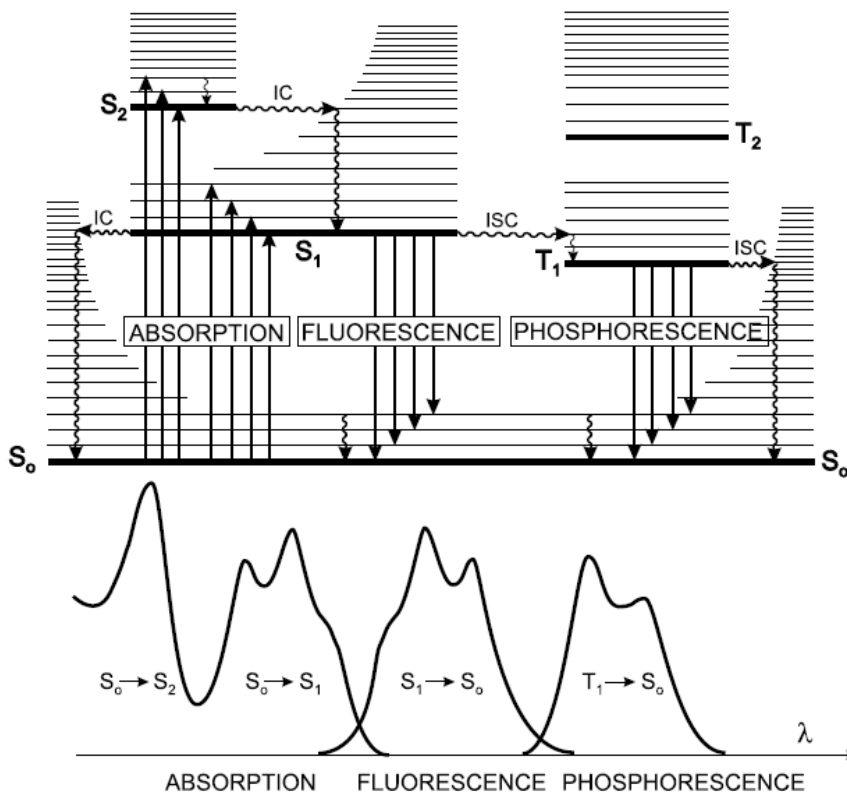
Luminescence is the emission of light from any compound and happens from electronically excited state. Luminescence is formally divided into two types; the fluorescence and the phosphorescence depending on the nature of the excited state.

Fluorescence is emission of light from singlet excited state, the electron in the excited orbital is paired to the second electron in the ground-state orbital. Thus, when electron returns to the ground state it is occurring so rapidly by emission of photon. The life time of fluorescence is too short estimated nearly nanoseconds. Phosphorescence is emission of light from triplet excited state, in which the electron in the excited orbital has the same spin orientation as the ground state electron. The emission rates are slow because the transmissions of electron to the ground state is forbidden, thus the phosphorescence life time is longer approximately milliseconds to seconds.

Fluorescence generally occurs from aromatic molecules. Various fluorophores are encountered in daily life. The green or red-orange glow sometimes seen in antifreeze is due to trace quantities of fluorescein or rhodamine, respectively. Polynuclear aromatic hydrocarbon, such as anthracene and perylene, are also fluorescent, and the emission from some species is utilized for environmental monitoring of oil pollution. Fluorescence spectral data are generally reported as emission spectra. A fluorescence emission spectrum is a plot of the fluorescence intensity versus wavelength (nanometers). Moreover, an important feature of fluorescence is high sensitivity to detection.

The processes that occur between the absorption and emission of light are usually prescribed by the Jablonski diagrams exhibited below. Jablonski diagrams[8] are often used to illustrate the light absorption and emission about varieties of molecular processes that can occur in excited states. A typical Jablonski diagram is shown in Figure 1.4. The singlet ground, first, and second electronic states are depicted by S_0 , S_1 , and S_2 , respectively. Following light absorption, several process usually occur. A fluorophore is usually excited to some higher vibrational level of either S_1 or S_2 . With a few rare exceptions, molecules in condensed phases immediately relax to the lowest vibrational level of S_1 . This process is called internal conversion and generally occurs within 10^{-12} s

or less. Since fluorescence lifetimes are typically near 10^{-8} s, internal conversion is generally complete prior to emission. Thus, fluorescence emission generally results from a thermally equilibrated excited state, that is, the lowest energy vibrational state of S_1 .



CHARACTERISTIC TIMES

absorption	10^{-15} s
vibrational relaxation	$10^{-12} - 10^{-10}$ s
lifetime of the excited state S_1	$10^{-10} - 10^{-7}$ s (fluorescence)
intersystem crossing	$10^{-10} - 10^{-8}$ s
internal conversion	$10^{-11} - 10^{-9}$ s
lifetime of the excited state T_1	$10^{-6} - 1$ s (phosphorescence)

Figure 1.4 Perrin-Jablonski diagram and illustration of the relative positions of absorption, fluorescence, and phosphorescence spectra. [8]

Molecule in the S_1 state can undergo a spin conversion to the first triplet state T_1 . Emission from T_1 is termed phosphorescence, and is generally shifted to longer wavelengths relative to the fluorescence. Conversion of S_1 to T_1 is defined as intersystem crossing. Transition from T_1 to the singlet ground state is forbidden, and as a result of the rates constants for triplet emission are several orders of magnitude smaller than those for fluorescence.

1.6 Determination of the stoichiometry of a complex by the method of continuous variations (Job's method) [8]

Information on the stoichiometry of a complex can also be obtained from the continuous variation method. To deliberate a complex M_mL_l formed according to the equilibrium



with

$$\beta_{ml} = \frac{[M_mL_l]}{[M]^m [L]^l} \quad 1.2$$

The principle of the method as follow: the fluorescence intensity Y is measured for a series of solutions consisting of the ligand and the cation such that *the sum of the total concentration of ligand and cation is constant*.

$$C_L + C_M = C = \text{constant}$$

The position of the maximum of Y is then related to the ration m/l . The complex product is equal to Y_0 and the value of Y is related to no cation added ($x=0$). When plotting the variations in fluorescence intensity versus x , it is convenient to subtract the fluorescence intensity that would be measured in the absence of cation at every concentration.

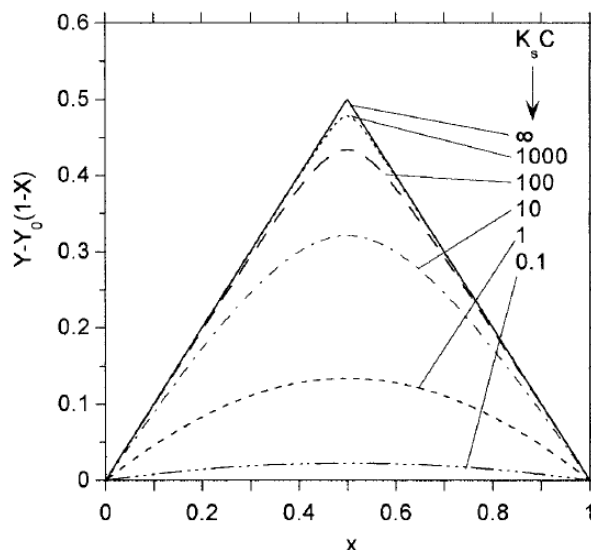


Figure 1.5 Job's plots for a 1:1 complex

1.7 The selectivity of chemosensors

A selectivity of a receptor is a preference of that receptor towards a guest. This is customarily estimated from a magnitude of a thermodynamic *stability constant* of a receptor-guest or, in more general terms, a ligand-metal complex. There are various methodologies to calculate the binding constant such as NMR spectroscopy, UV-visible and fluorescence spectrophotometry, and electrochemical techniques depending on the molecular design.

The stability constant [10] K_s which controls the equilibrium between the free ligand L and the complex ML with the metal may be obtained from the variation of either absorbance or fluorescence intensity at proper observation wavelengths.



It is easy to derive the following relation involving the absorbance A_0 of the free ligand and the absorbance A of the solution at a given wavelength where ϵ_L and ϵ_{ML} are the molar extinction coefficients of the ligand and the complex, respectively. The quantity $A_0/(A_0 - A)$ is plotted versus $[M]^{-1}$, and the stability constant is then given by the ratio of intercept/slope.

$$\frac{A_0}{A_0-A} = \frac{\varepsilon_L}{\varepsilon_L-\varepsilon_{ML}} \left(\frac{1}{K_s[M]} + 1 \right) \quad 1.4$$

The various methods for determining the stability constants from Fluorometric data were previously discussed [11]. The best of them uses the relation where Φ_L and Φ_{ML} are the quantum yields of the ligand and the complex, respectively. The quantity $I_F^0/(I_F-I_F^0)$ is plotted versus $[M]^{-1}$, and the stability constant is then given by the ratio of intercept/slope

$$\frac{I_F^0}{I_F^0-I_F} = \frac{\varepsilon_L\Phi_L}{\varepsilon_L\Phi_L-\varepsilon_{ML}\Phi_{ML}} \left(\frac{1}{K_s[M]} + 1 \right) \quad 1.5$$

1.8 Limit of Detection [12]

A limit of detection of an analyte generally defined as the concentration presents an instrument signal significantly distinct from the blank or background signal. This definition of the limit of detection is quite arbitrary and entirely open to an analyst to provide an alternative definition for a particular purpose. However, it is required to provide the definition whenever a detection limit is cited in a paper or a report.

This is an alternative definition that determines the detection limit as the analyte concentration giving a signal equal to the blank signal, y_B , plus three standard deviations of the blank, s_B

$$\text{Limit of detection} = y_B + 3s_B \quad 1.6$$

According to Eq. 1.6, the value of limit of detection, the calculated intercept of the calibration plot can be utilized instead of y_B .

1.9 Nanoparticles

A nanoparticle [13] is a microscopic particle with at least one dimension less than 100 nm. Currently, nanoparticles researches are an area of intense scientific research, because of their several of potential applications in biomedical, optical, and electronic fields. Nanoparticles are of great scientific interest as they are effectively a bridge between bulk materials and atomic or molecular structures. The properties of several conventional materials change upon forming of nanoparticles. Typically, nanoparticles have a greater surface area per weight than the larger particles. Therefore, nanoparticles have more reactive than other molecules. Nanoparticles are applied in many fields. The following lists introduce many of the uses under development in a recent time. [14]

1. Iron oxide nanoparticles can used to improve MRI images of cancer tumors.
2. Gold nanoparticles display many interesting electrical and optical properties. They can be used to be a variety of sensors such as using for detecting diseases as biosensors, improving the optical properties of materials, etc.
3. Magnetic nanoparticles that attach to cancer cells in the blood stream may allow the cancer cells to be removed before they establish new tumors.
4. Quantum Dots are crystalline nanoparticles that can be used to identify the location of cancer cells in the body.
5. Silver nanoparticles in fabric can kill bacteria making clothing odor-resistant.

In addition, nanoparticles characterization is necessary to establish understanding and control of nanoparticles synthesis and application. Characterization is done by using a variety of different techniques such as electron microscopy (SEM, TEM) atomic force microscopy (AFM), dynamic light scattering (DLS), X-ray photoelectron spectroscopy (XPS), powder X-ray diffraction (XRD), Fourier transform infrared spectroscopy (FTIR), and UV-vis spectrophotometry. [15]

1.10 Energy Dispersive X-Ray Analysis (EDX) [16]

The production of x-rays by a primary electron beam is the basis of qualitative and quantitative elemental analysis. Generally, the production of x-rays occurs in all electron-optical instruments, the scanning electron microscope (SEM) proves in performing x-ray microanalysis. Some of incident electrons excite the atoms of the specimen by removing electrons from their shells. Then the excited atom return to ground state by transition of electrons between outer and inner electron shells, therefore, the energy is emitted as x-rays. This energy is related to the atomic number of the atom, and is called the characteristic radiation.

Energy dispersive X-ray analysis (EDX) has the advantage of speed and sensitivity. When the x-rays are dispersed and detected, a spectrum is produced. The positions of the peaks are characteristic of the elements and additionally each element can generate for several peaks. It is necessary to identify and label each peak in the spectrum. Each line in the spectrum has the own meaning; K lines are corresponding to transitions into the first electron shell and used for elements whose atomic number are less than 42; L lines are corresponding to transition into the second shell and used for those atomic number above 42. M lines are corresponding to transition into the third shell and can also be used

CHAPTER II

LITERATURE REVIEWS

2.1 Literature reviews

2.1.1 Molecular Chemosensors and Chemodosimeters (Ring-opening of Spirocyclic System)

As mention in the previous chapter, chemosensors are molecules that can interact with the analyte to give measurable signals with a real-time response and based on coordination events. The reactions of chemosensors with the analyte and signal changes are reversible. According to a decade ago, Czarnik was the first person to invent a new approach in the field of optical sensing termed chemodosimetry[17]. Chemodosimeters are molecules that can interact with the analyte to give signal and the reaction between chemodosimeters and analyte are irreversible.

In 1997, He and his coworkers [18] reported the work utilizing a ring-opening reaction of rhodamine-B derivative fluorescent chemodosimeter **4** to detect copper ion in water. They applied the fundamental of that copper ion can support the hydrolysis of R-amino acid esters **1** at rates better than other metals (Figure 2.1 a). The rates of this reaction is complete within seconds, gaining the copper(II)- α -amino acid **3** as a product.

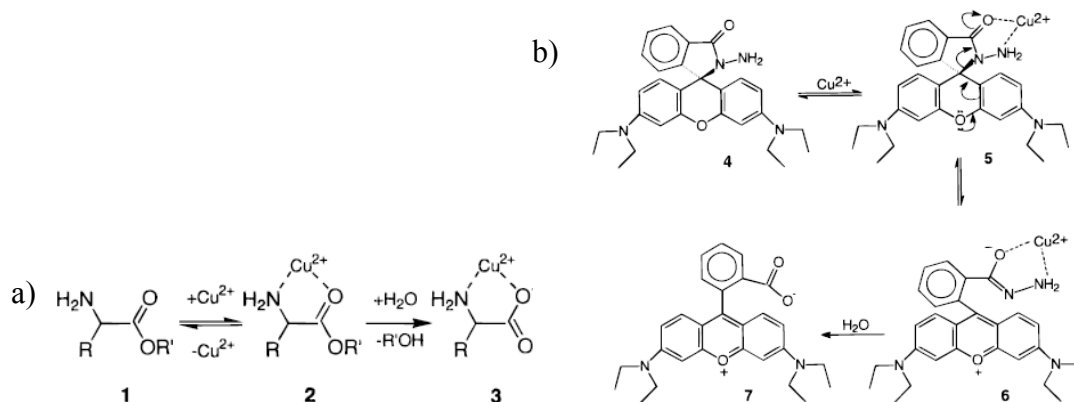


Figure 2.1 a) The hydrolysis reaction of α -amino acid ester with copper ion b) The propose mechanism of chemodosimeter **4** react with copper ion and its hydrolysis reaction.

The assumption of their group was the hydrazide of compound **4** would provide the binding site for copper by its behavior of α -amino. Initially, they investigated the powerful of this chemodosimeter by fluorescence spectrophotometry technique and observed that after adding copper to a colorless solution of **4** in acetonitrile, the pink color and fluorescence of Rhodamine B expressed obviously. While they studied compound **4** in water, it displayed analogue pathway mechanism to react with copper as shown in Figure 2.1b. They discovered that compound **4** could react with copper ion within 1 min and the reaction is faster than mercury ion that required 50 hours to complete the similar reaction.

Following this pioneering research, after an initial slow start, many exciting research papers on ring-opening reactions have been reported. In an effort to improve a technique to detect mercury(II), Tae and coworkers [19] designed a chemodosimeter **8** by combining the spirolactam ring-opening moiety and the mercury(II)-triggered 1,3,4-oxadiazole cyclization [20-21] of thiosemicarbazide.

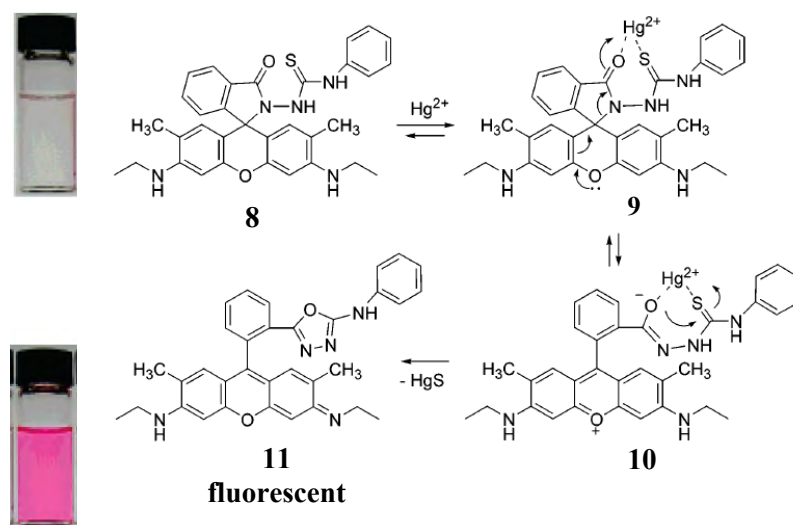


Figure 2.2 The schematic explanation of the responded mechanism of probe **8** with mercury(II) ion

Chemodosimeter **8** had been studied with mercury(II) in water-methanol (4/1 v/v) at pH 7. The fluorescence intensity was enhanced for 26-fold and the red-shift of emission maximum from 553 to 557 nm was observed after adding 1 equivalent of mercury(II). Figure 2.2 illustrated the reaction responsible for these changes and the reaction completed within less than a minute. Metal-ion selective manipulations of chemodosimeter **8** implies that the emission of **8** was unaffected by other cationic species: Cu(II), Pb(II), Cd(II), Ni(II), Co(II), Fe(II), Mn(II), Mg(II), Ca(II), Ba(II), Li(I), K(I), Na(I), Rh(III), and Cr(II). In addition, chemodosimeter **8** showed the limit of detection of <2 ppb, below the Environmental Protection Agency (EPA) drinking water limits for mercury(II). The interaction of mercury(II) with **8** induced the color solution changed from colorless to pink and easy to observe by naked-eyes, indicating the ring-opening of rhodamine-6G.

In 2007, Kim and co-workers [22] synthesized the fluorescent and colorimetric chemodosimeter **12**. The result showed that mercury(II) induced the *N* atom of the spirolactam to attack the C atom of the thiourea. Then, mercury(II) promoted ring opening of spirolactam of the rhodamine part followed by removal of HgS and the formation of intramolecular guanylation. Furthermore, they put an effort to study the interference of **12** by mixing other cationic species; Fe(II), Co(II), Ni(II), Cu(II), Zn(II), Pb(II), Cd(II), Ca(II), Mg(II), K(I), and Na(I) into the solution and **12** did not interfere by other ions. This indicate that chemodosimeter **12** was very selectively for only Hg(II). The introduction of mercury(II) caused an emission color change from blue to yellow and visible by the naked-eyes. For the absorption, a new band appeared at 532 nm, inducing a color change from colorless to pink upon addition of mercury (II) into the solution of **12**. Figure 2.3 described the color change of **12** and structural change upon introduction of the mercury(II) into the solution of **12**.

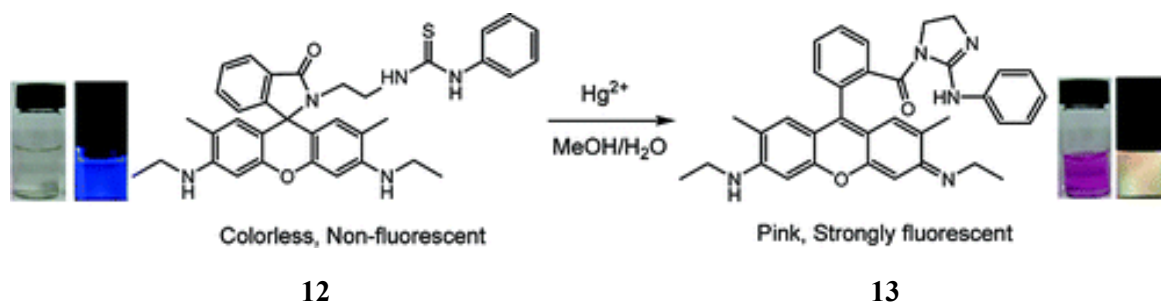


Figure 2.3 The explanation of the response of chemodosimeter **12** with mercury(II) ion and the color change by visual-eyed detection from colorless to pink including the significantly of fluorescence changes.

Among the heavy metal ions, Cu(II) is of particular interest which plays various important functions such as a catalytic cofactor for a variety of metalloenzymes, a feature in electron-transfer proteins of photosynthesis and respiration, in the metabolism system. Interestingly, acute copper deficiency may express especially in newborn infants and cause insufficient oxygen utilization in the brain and therefore permanent damage. [23] Nonetheless, it also exhibits toxicity to biological systems under excessive amounts which are known to cause neurodegenerative diseases such Alzheimer's and Wilson's [24] diseases. As mentioned in most of reports, fluorescence "turn-off" probes can result in false-positive results caused by other quenchers in real samples and, thus, are unpopular for practical. However, the reports of Cu(II) fluorescence chemosensors, the binding of the Cu(II) causes a quenching of the fluorescence emission and the signal tends to turn off because of its paramagnetic nature. [25-26] Luckily, chemodosimeters and some special chemosensors play a different function from general chemosensors and can provide an ideal way to design fluorescence "turn on" probes for paramagnetic metal ions such as copper(II).

Recently, Chen and Ma [27] have been designed chemodosimeter **14** contained spiro form of fluorescein hydrazide bearing a cleavable active amide bond which can be promoted hydrolysis by Cu(II) in aqueous solution. It exhibited the highly turn-on fluorescence when reacted with copper in aqueous solution causing the release of the fluorophore (fluorescein) and thereby the turn-on fluorescence intensity. Additionally, the

propose mechanism shown in Figure 2.4a that was similar to the mechanism of hydrolytic cleavage of α -amino acid amide bond. Moreover, other metal ions did not response to this probe. The ability of this probe selective with copper worked in the range of 0.1 – 10 μ M. They also applied this probe to use in real time application in biological fluids such as human serum and cerebrospinal fluid.

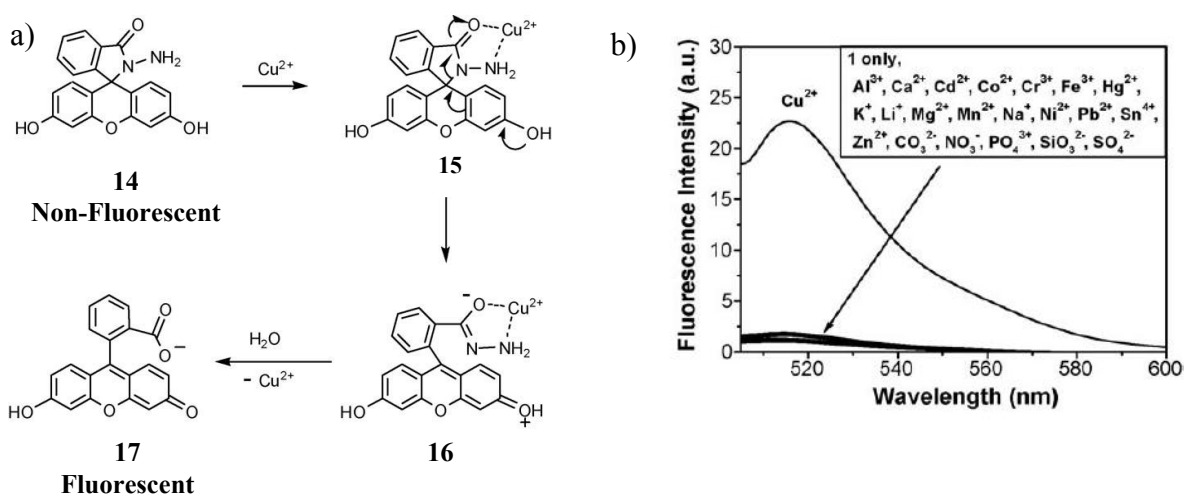


Figure 2.4 a) The schematic explanation the response mechanism of probe **14** with copper(II) ion b) Fluorescence emission change of probe **14** in 0.01M Tris-HCl buffer (pH 7.2) upon addition of metal ions.

Li and coworker [28] synthesized fluorescein-based colorimetric chemodosimeter **18** for detecting copper(II) in aqueous solution. The solution of **18** was changed from colorless to deep yellow upon addition of copper(II) in micro molar level. Compound **18** was a naked-eyes chemosensor for detection of copper(II) upon chelation of copper(II) and subsequently changed to a strong yellow color in the form of ring opening of spirolactam structure (Figure 2.5).

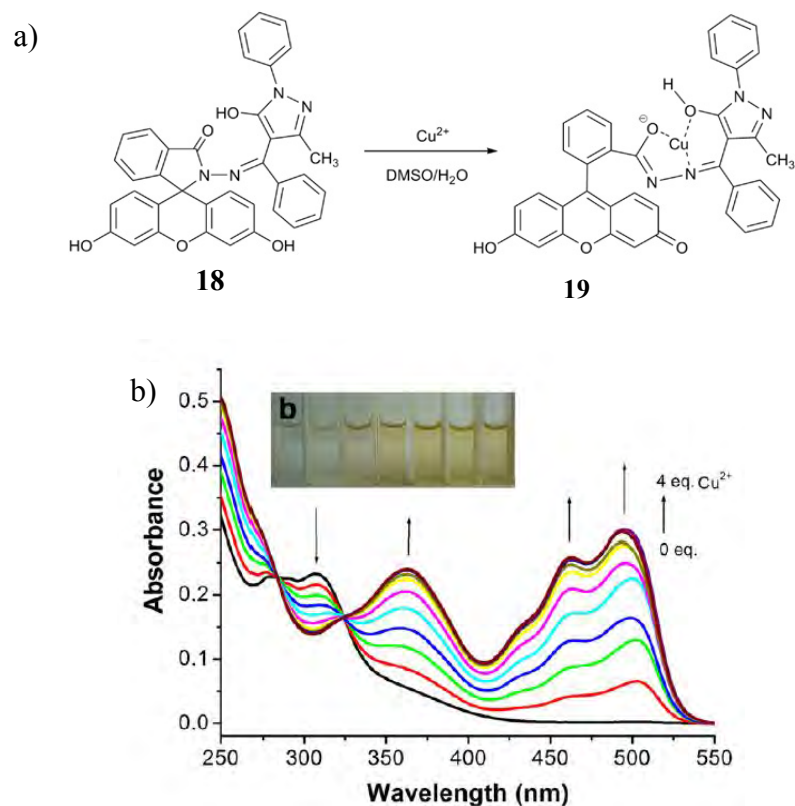


Figure 2.5 a) The schematic explanation the response mechanism of probe **18** with copper(II) ion b) UV-vis titration emission change of probe **18** in DMSO/water 4:6 upon gradually addition of copper(II).

Zhou and coworker [29] created a ratiometric fluorescent probe for copper (II) containing rhodamine as fluorophore onto the pyrene moiety. The ratiometric fluorescent measurements monitor changes in the ratio of the intensities of the emission at two wavelengths. The probe **20** was nonfluorescent and colorless, whereas the spiro lactam ring opening by copper (II) gave rise to strong fluorescence emission and a pink color depicted in Figure 2.6b and 2.6c. The probe **20** was used to investigate its selectivity among several metal ions shown that it was very selectively toward only copper(II). The proposed mechanism for probe **20** was explained in Figure 2.6a.

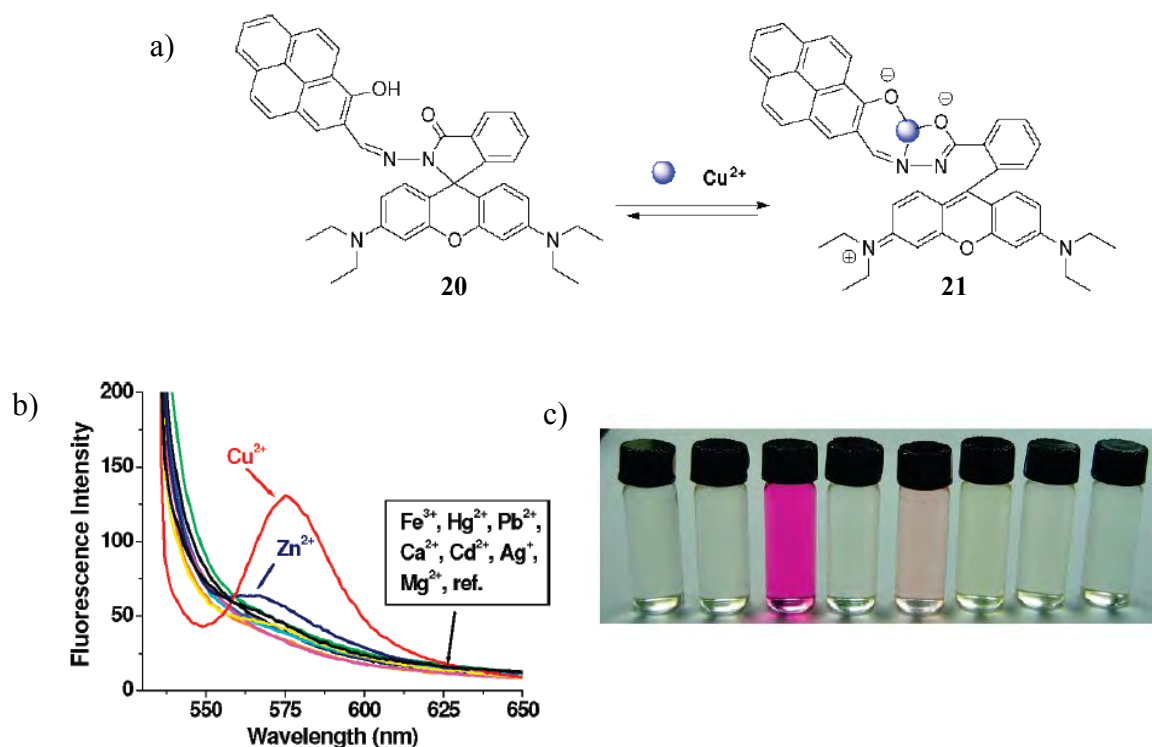


Figure 2.6 a) The schematic explanation the response mechanism of probe **20** with copper(II) ion b) Fluorescent spectra of probe **20** with various metal ions. c) A photo of naked-eye for probe **20**; from second one from second one added with $200 \mu\text{M}$ of Ca^{2+} , Cu^{2+} , Hg^{2+} , Zn^{2+} , Fe^{3+} , Ag^{+} , Pb^{2+} (from left to right).

Moreover, they also examined the fluorescence energy transfer (FRET) the result explicated that the FRET was not observed in this research because of the fluorescence of pyrene was decreased upon addition of copper (II). Moreover, they discovered that the reaction between probe **20** was reversible by adding EDTA into the complexation of probe **20** with copper (II).

2.1.2 Cyanide Sensor

Cyanide anion is severely poisonous to living creatures. Besides, it restrains the terminal step of cellular respiratory system by hampering the irreversible coordination of the mainly metal centers in the active site of cytochrome c oxidase. [30] Nevertheless, the wide applications of cyanide salts have remained prevalent, such as industrially in gold mining, electroplating, metallurgy, and the synthesis of nylon and other synthetic fibers and resins.[31-32] However, unintentionally releasing of cyanide into environment and

human may be occurred from dietary, industrial, surrounding, and other sources. Due to its toxicity and beneficial parts of cyanide anion inspired researchers to put a strongly interested in development sensors for detection of cyanide anion.

In 2007, Gabbai and Hudnall [33] reported cationic borane sensor **22** for detection of cyanide anion in water. They applied the fundamental of that triarylboranes can interact with cyanide to form the corresponding cyanoborate complex and act as stable species in water. They hypothesized that cationic borane can complex with cyanide ion in water because of its coulombic receptor-anion attraction. Herein, they also optimized sensor **22** by using DFT methods. The results implied that the positive charge in cationic boranes increases lewis acidity property of sensor **22**. Sensor **22** was also studied in organic solvent to form cyanoborate/ammonium zwitterions $\mathbf{22} \rightleftharpoons \mathbf{22} \cdot \text{CN}^-$. Moreover, it was performed in aqueous solution by using water/DMSO 60:40 vol (HEPES 6 mM, pH 7) to complex with cyanide anion and given the binding constant equal to $3.9 \times 10^8 \text{ M}^{-1}$. In addition, sensor **22** showed a negligible response in the presence of other common anions including Cl^- , Br^- , NO_3^- , AcO^- , H_2PO_4^- , and HSO_4^- .

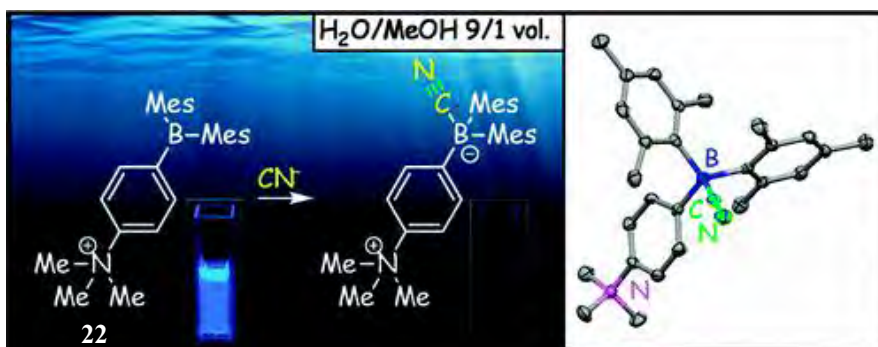


Figure 2.7 The cationic borane sensor **22** for detection of cyanide anion in water. [33]

Tae and Yang [34] synthesized a new selective chemosensor **23** to detect cyanide in water in micromolar level. They used the fundamental knowledge to design this chemosensor that cyanide can act as a strongly nucleophile and form stable complex with other metal ions. They took an advantage of the nucleophilic addition reaction of cyanide at the 9-position of N-methylacridinium ion. [35]

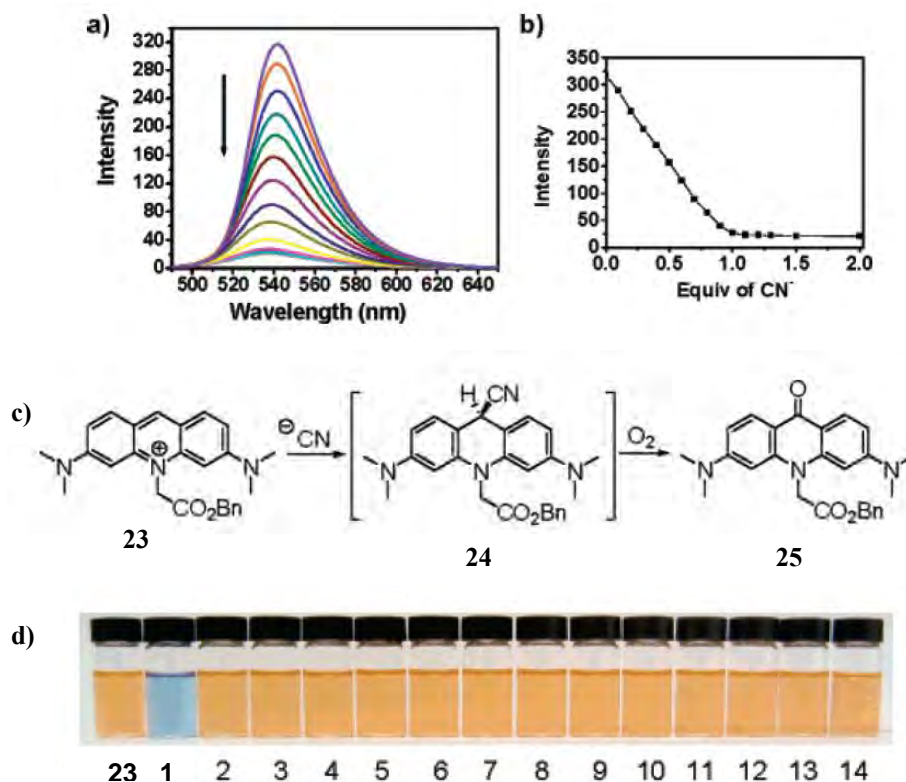


Figure 2.8 a) Fluorescence emission of a solution of **23** (DMSO-water (95:5 v/v) upon addition of CN^- (excitation at 480 nm). b) Plot of fluorescence intensity at 541 nm vs number of equivalents of CN^- . c) The schematic explanation the mechanism of **23** with CN^- ion d) Color changes of **23** in DMSO-water (95:5 v/v) in the presence of 1 equiv of the following anions: 1, CN^- ; 2, AcO^- ; 3, F^- ; 4, Cl^- ; 5, Br^- ; 6, I^- ; 7, H_2PO_4^- ; 8, HSO_4^- ; 9, SCN^- ; 10, NO_3^- ; 11, BzO^- ; 12, N_3^- ; 13, CH_3S^- ; 14, ClO_4^- .

Considering, the fluorescent experiments of chemosensor **23** as showed in Figure 2.8 a; upon addition of 1 equivalent of cyanide, the fluorescence intensity decreased related to an increasing of cyanide concentration. They found that **23** reacted irreversibly with CN^- in a 1:1 stoichiometric ratio. They also evaluated the cyanide-selective nature of acridinium salt **23** that **23** acted as a selective chemosensor toward only cyanide ion illustrated in Figure 2.8 d and can be observed by naked-eyes detection. In addition, the detection limit of this chemosensor with cyanide was $2.0 \mu\text{M}$ corresponding to the minimum level in drinking water announced by WHO.

Tomapatanaget [36] and coworkers put considerable attention to study on synthesizing and designing chemosensor **26** for cyanide anion. This chemosensor relied on the basis of acceptor-donor-acceptor (A-D-A) system and acted as an internal charge transfer process composed of naphthoquinone connecting to boronic acid with imidazole as a spacer. The naphthoquinone and imidazole moieties are a major A-D system performing a large dipole moment changes upon excitation by light. In addition, the boron part can be changed to be an electron rich boron center by the substitution of cyanide anion.

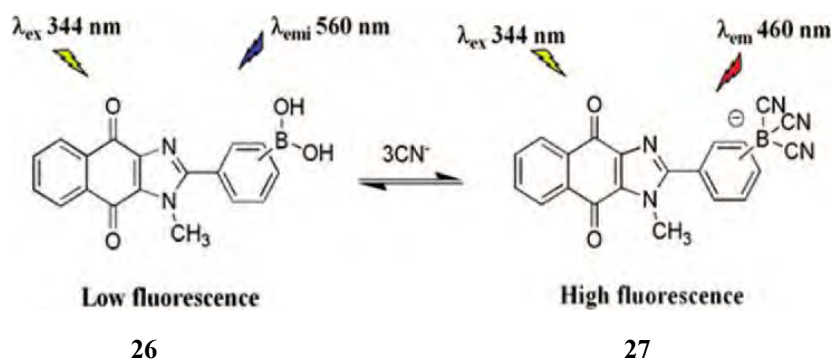


Figure 2.9 The responding of chemosensor **26** for detection cyanide anion in water.

Chemosensor **26** had been synthesized for three isomers named as **26a**, **26b**, and **26c** for ortho, meta, and para isomers, respectively. Initially, they study the complexation with cyanide anion for all of three sensors; the results showed that the most reactive isomer with cyanide was **26b**. Meanwhile, in the presence of a high concentration of cyanide (500 μM), pH of the solution was changed from pH 7.4 to 11 because OH^- could be produced. Therefore, they solved this problem by applying **26b** to a CTAB micellar system and found that the pH of solution remained at pH 7.0 in concomitant with appearing of a strong fluorescence intensity at 460 upon addition of cyanide 50 μM . This band at 460 nm displayed a large blue shift of 100 nm. This emission band was assigned to the internal charge transfer (ICT) state occurred upon addition of cyanide anion due to the poor acceptability on the boron after cyanide substitution.

Geddes and coworker [37] described a powerful set of new fluorescent probes (**DSPBA**: shown in Figure 2.10) which can detect cyanide anion in the wide range of cyanide concentration of 1-30 μM in the presence of a high background of physiological interference. The sensing of these chemosensors was based on the ability of boronic acid to complex cyanide by cyanide anions substitution at the boron moiety and altered boron from rich electron to poor electron acceptability. The properties of these sensors have an intramolecular charge transfer (ICT) from the amino group to the electron-deficient quaternary nitrogen center in the absence of cyanide. However, in the presence of cyanide, the ICT process was reduced affording an increasing and wavelength shift in fluorescence spectrum.

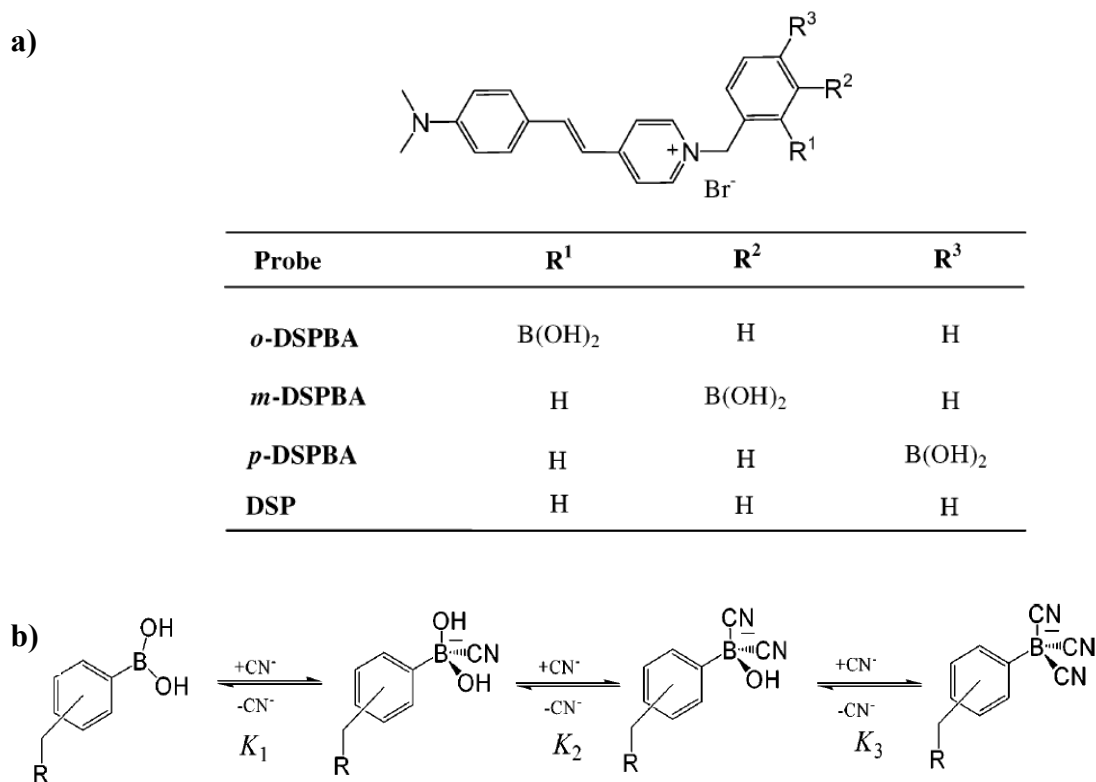


Figure 2.10 a) Molecular structures of cyanide. b) Complexation of **DSPBA** probes with aqueous free cyanide.

Interestingly, they discovered that *o*-DSPBA exhibited a much better response to cyanide than the other two isomers because *o*-DSPBA had the shortest distance and expressed the most effective electrostatic interaction of the positively charged quaternary nitrogen center with the electron-rich boron atom upon cyanide complexation.

Qin and coworkers [38] reported conjugated polymer-based fluorescent chemosensor relied on the principle of cyanide anion can form stable complexes with transition metals. They prepared chemosensor **28** composed of imidazole-functionalized polyfluorene which could bind with copper ion based on the fluorescence switch off. Then, after the addition of cyanide anions, the quenched fluorescence of polyfluorene by copper(II) could recover. This chemosensor **28** lead selectively and sensitivity toward cyanide anion as low as 0.31 ppm by an indirect strategy, making a good candidate for potential application of human safeguard.

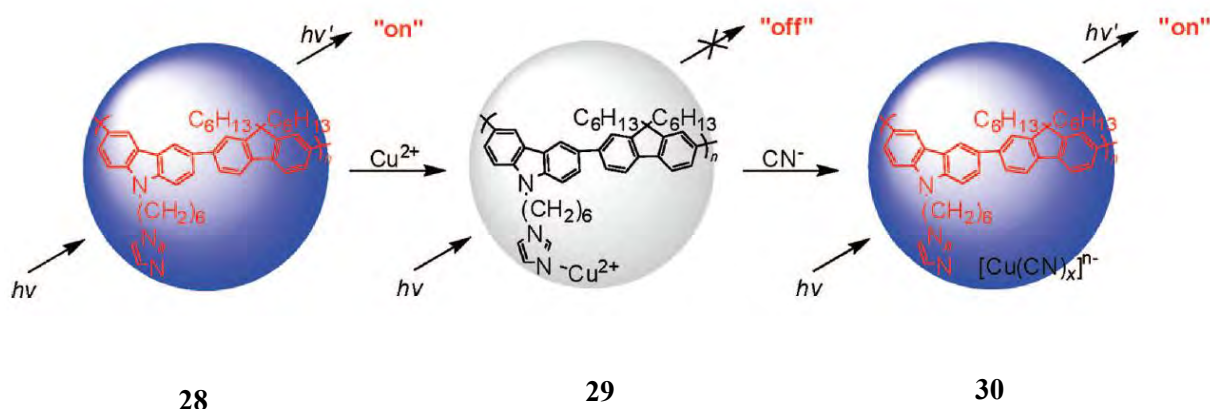


Figure 2.11 The responding of chemosensor **28** for detection cyanide anion by an indirect strategy.

2.1.3 Self-assemble of supramolecular network

Kimizuka and coworkers [39] firstly reported the self-assembly of adenosine 5'-triphosphate (ATP) and dichloro-substituted thiocarbocyanine dyes to form the supramolecular nanowires. ATP is a major energy component in the biological systems. Recently, many researchers have designed the synthetic host-guest receptor for ATP but no reports were concerned on the development of ATP-direct artificial self-assemble.

They brought the cyanine dyes which were good cationic chromophores and their color changes from pink to orange upon the addition of ATP. They confirmed the forming of nanostructure morphology by transmission electron microscopy (TEM) defined the core size width of 10 nm and lengths of micrometers. Moreover, this self-assembly was thermally reversible shown the briefly illustration in Figure 2.12.



Figure 2.12 The illustration of supramolecular nanowires self-assembled from ATP molecules and cationic cyanine dyes.

In 2009, they studied on the properties of self-adaptive supramolecular networks [40] in water from nucleotides and lanthanide ions prescribed in Figure 2.13. They utilized nucleotides as one of the candidates in this system because of their biocompatible properties. Additionally, nucleotides are composing of nucleobases and phosphates group deserved as bidentate ligands. Herein, they selected lanthanide ions to be the partners because of the large coordination numbers which are suitable for forming the several size and shape of materials. Moreover, lanthanide ions have the significant characteristics such as luminescent, magnetic, and catalytic properties. In this research, they reported that nucleotide/lanthanide nanoparticles showed a magnetic improvement properties using as MRI contrasting agents for the chelation of paramagnetic Gd^{3+} ion.

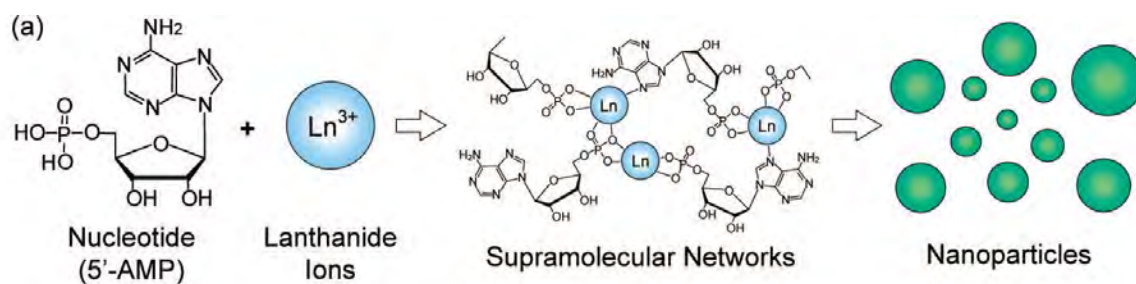


Figure 2.13 A schematic illustration of nanoparticles formation through the self-assembly of AMP and Gd^{3+} .

It was found that the nanoparticles formation can perform on several lanthanide ions; Sc^{3+} , Y^{3+} , La^{3+} , Ce^{3+} , Pr^{3+} , Nd^{3+} , Sm^{3+} , Eu^{3+} , Gd^{3+} , Tb^{3+} , Dy^{3+} , Ho^{3+} , Er^{3+} , Yb^{3+} , and Lu^{3+} , and their sizes were dependent on the chemical structure of nucleotides. Interestingly, the dyes were employed as guest molecules to incorporate in this molecular network and found that only anionic dyes could form with other partners. Herein, gold nanoparticles (AuNPs) were lead to be nanosized guest and performed with GMP molecules. The transmission electron microscopy revealed that AuNPs were encapsulated by the amorphous shell of supramolecular network (shown in Figure 2.14).

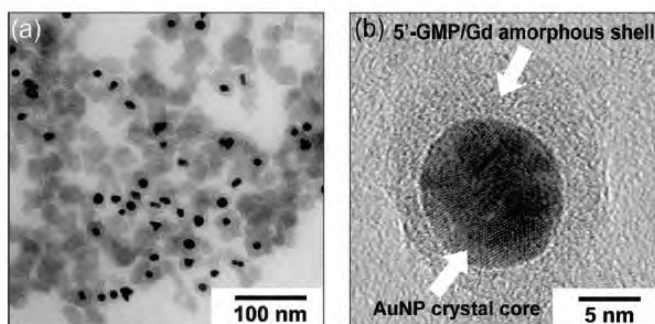


Figure 2.14 AuNPs in nucleotide/lanthanide nanoparticles. a) TEM image of AuNPs encapsulated by the supramolecular shell of GMP/ Gd^{3+} . b) HR-TEM image of a AuNPs surrounded by the supramolecular shell of GMP/ Gd^{3+} .

They further investigated the binding of several types of proteins and the results showed that only anionic protein such as Ferritin, BSA, PNA, and ConA were shown effectively incorporation with nanoparticles because of the coordination of carboxylic group of proteins.

Moreover in the same period, Kimizuka [41] expanded his research to explore the fundamental properties of coordination networks. Herein, they illustrated the properties of polymeric coordination shells from nucleotides and lanthanide ions. Anionic dyes **31-32** were effectively formed with AMP/Gd³⁺ using the coordination of carboxylate groups to Gd³⁺ ions. The UV-Vis spectrum of **31**-AMP/Gd³⁺ CNPs revealed a small red shift relative to that observed for **31** in pure water. Dye **31** also showed the enhancement of fluorescence after incorporation into AMP/Gd³⁺ implied that the conformational rotation of dye **31** in AMP/Gd³⁺ is restricted by the surrounding coordination networks.

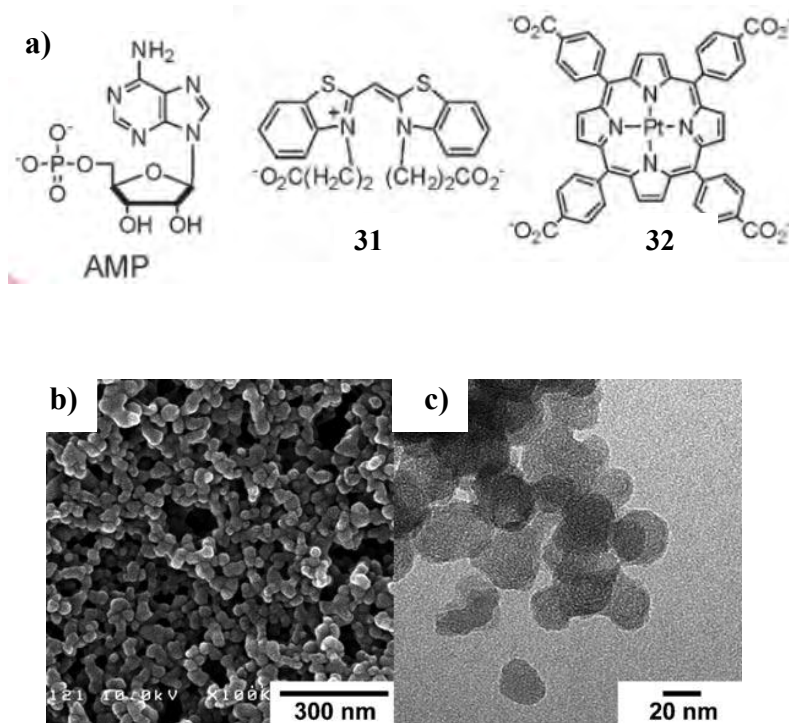


Figure 2.15 a) Molecular structure of nucleotide and guest dyes **31** and **32**. b) SEM and c) TEM images of dye **31**-AMP/Gd³⁺ CNPs with an average diameter of 30 nm.

Moreover, they studied the barrier properties by investigating the permeation of oxygen through coordination networks. They used dye **32** to be a guest molecule because it can be deactivated fluorescence intensity when oxygen molecule existed in system. The oxygen molecule cannot collide with **32** in aqueous **32-AMP/Gd³⁺** CNPs referring that the dense coordination network shells provided barrier to protect oxygen molecules.

2.2 Objectives and scope of this research

2.2.1 To design and synthesized the new fluorescence sensors containing fluorescein linked to boronic acid for detection of copper and cyanide ions.

2.2.2 To investigate the mechanism between all of three sensors with copper and cyanide ions using various spectroscopy techniques such as UV-vis and fluorescence spectrophotometry and ESI high resolution mass spectroscopy.

2.2.3 To study the sensing purpose in aqueous solution by designing the new strategy to protect the hydrolysis of sensor **F-*o*BOH** by self-assembly coordination nanoparticles.

2.2.4 To examine the binding properties of **F-*o*BOH** incorporated in coordination nanoparticles toward cyanide anion in aqueous system.

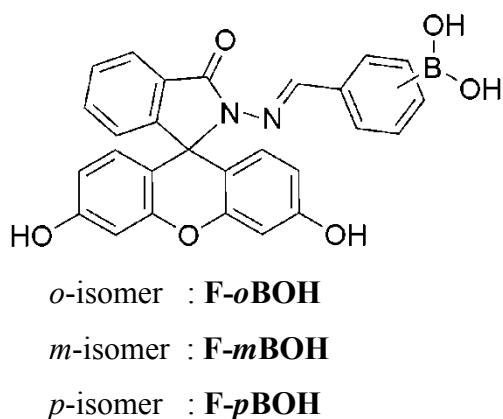


Figure 2.16 The sensors **F-*o*BOH**, **F-*m*BOH**, and **F-*p*BOH**

CHAPTER III

EXPERIMENTAL SECTION

3.1 General procedures

3.1.1 Analytical instrument

Nuclear magnetic resonance (NMR) spectra were recorded on a Varian 400 and Bruker DRX 400 MHz nuclear resonance spectrometers. All of samples were dissolved in deuterated DMSO. The chemical shifts were recorded in part per million (ppm) using a residue proton solvents as internal interference. Elemental analysis was carried out on CHNS/O analyzer (Perkin Elmers PE 2400 series II) by ignition combustion gas chromatography separated by frontal analysis and qualitative detected by thermal conductivity detector. High resolution mass spectra were determined on Bruker Daltonics DataAnalysis 3.3 with an electrospray ion source using methanol as a solvent. Absorption spectra were measured by a Varian Cary 50 UV-vis spectrophotometer. Fluorescence spectra were performed on a Varian eclipse spectrofluorometer by personal computer data processing unit. The light source is Cary Eclipse a pulsed xenon lamp and a detector is a photomultiplier tube. Scanning electron microscopy (SEM) and energy dispersive X-ray (EDX) analysis were performed on a JEOL JSM-6510A with a high resolution of 3.0 nm at 30 kV. Samples were grounded using aluminum stub. Transmission electron microscopy (TEM) was performed on a JEOL JEM 2010 with the field emission gun operated at 200 kV.

3.1.2 Materials

Unless otherwise specified, the solvents and all materials were reagent grades purchased from Fluka, BDH, Aldrich, Carlo erba, Merck or Lab Scan and use without further purification. Commercial grade solvents such as acetone, dichloromethane, hexane, methanol, and ethyl acetate were purified by distillation before using.

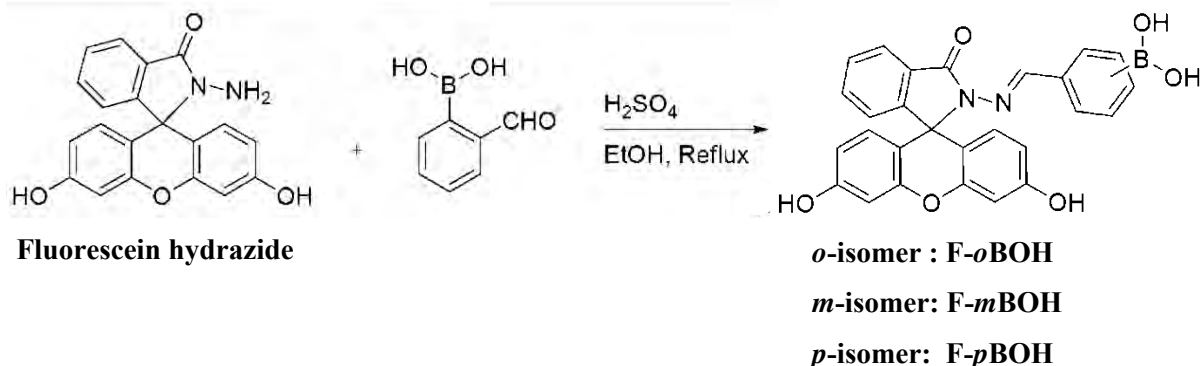
Thin layer chromatography (TLC) was performed on silica gel plates (Kieselgel 60, F₂₅₄, 1 mm). Compounds on TLC plates were detected by the UV-light. Ethanol, methanol, acetonitrile used in UV-visible and fluorescence measurement (AR grade, Lab

Scan) were used without drying. All synthesized compounds were characterized by $^1\text{H-NMR}$, $^{13}\text{C-NMR}$ spectroscopy, mass spectroscopy and elemental analysis.

Adaptive Coordination nanoparticles were characterized by Scanning Electron Microscopy (SEM), Transmission Electron Microscopy (TEM), and Energy Dispersive X-ray analysis (EDX).

3.2 Synthesis of boronic/fluorescein based sensors

3.2.1 Preparation of sensors **F-*o*BOH**, **F-*m*BOH**, and **F-*p*BOH**



Initially, to prepare the spiro form fluorescein hydrazide by treatment of fluorescein with hydrazine hydrate (yield 60%) [42]. In a 100 mL two-necked round bottom flask equipped with a magnetic bar and a reflux condenser, a solution of fluorescein hydrazide (0.173 g, 0.5 mmol) was stirred for 5 min in ethanol (20 mL). Formylphenylboronic acid (0.075 g, 0.5 mmol) in ethanol (30 mL) was added dropwise into the mixture and followed by adding approximately 6 drops of sulfuric acid thereafter the reaction was refluxed overnight under nitrogen atmosphere. Upon completion of the reaction, the solvent was removed under vacuum to obtain a crude product. The crude product was dissolved in ethyl acetate and extracted with water. The organic layer was dried over anhydrous sodium sulfate and evaporated to dryness under reduced pressure. The desired products were obtained after recrystallization in hexane/ethyl acetate (**F-*o*BOH** as a white solid 85%, **F-*m*BOH** as pale yellow solid 92%, and **F-*p*BOH** as pale yellow solid 90%)

3.2.2 Characterization of sensors F-*o*BOH, F-*m*BOH, and F-*p*BOH

Characterization data for F-*o*BOH

¹H-NMR (400 MHz, DMSO-*d*₆): δ (in ppm)=9.854 (s, -ArOH, 2H), 9.584 (s, -N=CH, 1H), 8.170 (s, -BOH, 2H), 7.891 ($J=7.2$ Hz, d, -ArH, 1H), 7.609 ($J=8.0$ Hz, dd, -ArH, 2H), 7.755 (m, -ArH, 1H), 7.492 (m, -ArH, 1H), 7.292 ($J=3.2$ Hz, dd, -ArH, 2H), 7.117 ($J=7.2$ Hz, d, -ArH, 1H), 6.644 (s, -ArH, 2H), 6.463 (m, -ArH, 4H).

¹³C NMR (100 MHz, DMSO-*d*₆): δ (in ppm)= 163.446, 158.321, 152.267, 151.063, 150.315, 137.796, 133.748, 129.204, 128.948, 128.836, 127.814, 123.753, 122.987, 112.948, 110.213, 102.447, 65.447;

ESI-HRMS: m/z Calcd for [M+CH₃OH+H₃O]⁺ = 529.1777, found 529.1542.

Elemental analysis:

Anal. Calcd for C₂₇H₁₉BN₂O₆·1.25H₂O: C, 64.76; H, 4.33; N, 5.59.

Found: C, 64.88; H, 4.04; N, 5.87.

Characterization data for F-*m*BOH

¹H-NMR (400 MHz, DMSO-*d*₆): δ (in ppm)=9.925 (s, -ArOH, 2H), 8.784 (s, -N=CH, 1H), 8.129 (s, -BOH, 2H), 7.918 ($J=7.2$ Hz, d, -ArH, 1H), 7.757 ($J=7.2$ Hz, d, -ArH, 2H), 7.600 (m, -ArH, 2H), 7.474 ($J=8.4$ Hz, d, -ArH, 1H), 7.317 ($J=7.2$ Hz, t, -ArH, 1H), 7.101 ($J=7.6$ Hz, d, -ArH, 1H), 6.666 ($J=1.6$ Hz, d, -ArH, 2H), 6.516 (m, -ArH, 2H), 6.461 (m, -ArH, 2H).

¹³C NMR (100 MHz, DMSO-*d*₆): δ (in ppm)= 163.349, 158.192, 151.597, 150.475, 148.373, 135.726, 133.617, 133.298, 132.947, 128.648, 128.081, 127.509, 126.966, 123.249, 122.816, 111.991, 109.549, 102.163, 64.623;

ESI-HRMS: m/z Calcd for [M+CH₃OH+H₃O]⁺ = 529.1777, found 529.1552.

Characterization data for F-*p*BOH

¹H-NMR (400 MHz, DMSO-*d*₆): δ (in ppm)=9.924 (s, -ArOH, 2H), 8.952 (s, -N=CH, 1H), 8.110 (s, -BOH, 2H), 7.922 ($J=7.6$ Hz, d, -ArH, 1H), 7.739 ($J=7.6$ Hz, d, -ArH, 2H), 7.620 (m, -ArH, 2H), 7.368 ($J=8.0$ Hz, d, -ArH, 2H), 7.132 ($J=7.2$ Hz, d, -ArH, 1H), 6.645 (s, -ArH, 2H), 6.476 (m, -ArH, 4H).

¹³C NMR (100 MHz, DMSO-*d*₆): δ (in ppm)= 163.805, 158.718, 152.314, 150.587, 148.989, 135.898, 134.737, 134.186, 129.264, 129.017, 128.112, 125.832, 123.927, 123.357, 112.465, 110.237, 102.604, 65.413;

ESI-HRMS: m/z Calcd for $[M+CH_3OH+H_3O]^+ = 529.1777$, found 529.1481.

3.3 Complexation Study of F-*o*BOH, F-*m*BOH, and F-*p*BOH in acetonitrile by UV-visible spectrophotometry technique

3.3.1 Complexation studies of F-*o*BOH, F-*m*BOH, and F-*p*BOH with various cations: copper, cadmium, nickel, silver, zinc, cobalt, and magnesium

Typically, a solution of 1×10^{-3} M of a F-*o*BOH, F-*m*BOH, and F-*p*BOH in 0.01 M tetrabutyl ammonium hexafluorophosphate in dried acetonitrile was prepared. A stock solution of 0.01 M of cation (Cu^{2+} , Cd^{2+} , Ni^{2+} , Ag^+ , Zn^+ , Co^{2+} , and Mg^{2+} as trifluoromethanesulfonate and nitrate salt) in dried acetonitrile was prepared in 5 mL volumetric flask (shown in Table 3.1).

Table 3.1 Amounts of Cu^{2+} , Cd^{2+} , Ni^{2+} , Ag^+ , Zn^+ , Co^{2+} , Mg^{2+} as trifluoromethanesulfonate and nitrate salt were used in studies by UV-visible spectrophotometry.

cation	molecular weight (gmol^{-1})	Weight(mg)	mL
$\text{Cu}(\text{CF}_3\text{SO}_3)_2$	361.68	0.0181	5
$\text{Cd}(\text{NO}_3)_2 \cdot 4\text{H}_2\text{O}$	308.47	0.0154	5
$\text{Ni}(\text{NO}_3)_2 \cdot 6\text{H}_2\text{O}$	290.81	0.0145	5
AgNO_3	169.87	0.0085	5
$\text{Zn}(\text{NO}_3)_2 \cdot 6\text{H}_2\text{O}$	297.49	0.0149	5
$\text{Co}(\text{NO}_3)_2 \cdot 6\text{H}_2\text{O}$	291.04	0.0146	5
$\text{Mg}(\text{NO}_3)_2 \cdot 6\text{H}_2\text{O}$	256.41	0.0128	5

Absorption spectra of **F-*o*BOH**, **F-*m*BOH**, and **F-*p*BOH** with cation complexes were recorded from 200 – 600 nm at ambient temperature. The solution of cation was added directly to 2.00 mL of 3.0×10^{-5} M **F-*o*BOH**, **F-*m*BOH**, and **F-*p*BOH** in a 1-cm quartz cuvette by micropipette and stirred for 5 min. Absorption spectra were recorded after each addition.

Table 3.2 Amounts of cations solutions were used to prepare various cations:**F-*o*BOH** ratios.

cation	[cation]M	Cation added (μL)	cation: F-<i>o</i>BOH ratios
$\text{Cu}(\text{CF}_3\text{SO}_3)_2$	2.10×10^{-3} M	420	70:1
$\text{Cd}(\text{NO}_3)_2 \cdot 4\text{H}_2\text{O}$	2.10×10^{-3} M	420	70:1
$\text{Ni}(\text{NO}_3)_2 \cdot 6\text{H}_2\text{O}$	2.10×10^{-3} M	420	70:1
AgNO_3	2.10×10^{-3} M	420	70:1
$\text{Zn}(\text{NO}_3)_2 \cdot 6\text{H}_2\text{O}$	2.10×10^{-3} M	420	70:1
$\text{Co}(\text{NO}_3)_2 \cdot 6\text{H}_2\text{O}$	2.10×10^{-3} M	420	70:1
$\text{Mg}(\text{NO}_3)_2 \cdot 6\text{H}_2\text{O}$	2.10×10^{-3} M	420	70:1

Table 3.3 Amounts of cations solutions were used to prepare various cations:**F-*m*BOH** ratios.

cation	[cation]M	cation added (μL)	cation:F-<i>m</i>BOH ratios
Cu(CF ₃ SO ₃) ₂	2.10 x 10 ⁻³ M	420	70:1
Cd(NO ₃) ₂ ·4H ₂ O	2.10 x 10 ⁻³ M	420	70:1
Ni(NO ₃) ₂ ·6H ₂ O	2.10 x 10 ⁻³ M	420	70:1
AgNO ₃	2.10 x 10 ⁻³ M	420	70:1
Zn(NO ₃) ₂ ·6H ₂ O	2.10 x 10 ⁻³ M	420	70:1
Co(NO ₃) ₂ ·6H ₂ O	2.10 x 10 ⁻³ M	420	70:1
Mg(NO ₃) ₂ ·6H ₂ O	2.10 x 10 ⁻³ M	420	70:1

Table 3.4 Amounts of cations solutions were used to prepare various cations:**F-*p*BOH** ratios.

cation	[cation]M	cation added (μL)	cation:F-<i>p</i>BOH ratios
Cu(CF ₃ SO ₃) ₂	1.50 x 10 ⁻³ M	300	50:1
Cd(NO ₃) ₂ ·4H ₂ O	1.50 x 10 ⁻³ M	300	50:1
Ni(NO ₃) ₂ ·6H ₂ O	1.50 x 10 ⁻³ M	300	50:1
AgNO ₃	1.50 x 10 ⁻³ M	300	50:1
Zn(NO ₃) ₂ ·6H ₂ O	1.50 x 10 ⁻³ M	300	50:1
Co(NO ₃) ₂ ·6H ₂ O	1.50 x 10 ⁻³ M	300	50:1
Mg(NO ₃) ₂ ·6H ₂ O	1.50 x 10 ⁻³ M	300	50:1

3.3.2 Complexation studies of **F-*o*BOH**, **F-*m*BOH**, and **F-*p*BOH** with copper cation in acetonitrile by UV-visible spectrophotometry

Typically, 0.01 M solution of tetrabutyl ammonium hexafluorophosphate ([Bu₄N][PF₆]) (0.194 g) in 50 mL of acetonitrile was prepared. Stock solution of 1×10^{-3} M solution of **F-*o*BOH** (4.8 mg), **F-*m*BOH** (4.8 mg), and **F-*p*BOH** (4.8 mg) in 0.01 M tetrabutyl ammonium hexafluorophosphate in acetonitrile was prepared in a 10 mL volumetric flask. A solution of 5×10^{-3} M of copper trifluoromethanesulfonate in 0.01 M tetrabutyl ammonium hexafluorophosphate in acetonitrile was prepared in a 10 mL volumetric flask.

UV-vis spectra of **F-*o*BOH**, **F-*m*BOH**, and **F-*p*BOH** with copper complexes were recorded from 200-800 nm at ambient temperature. The solution of copper cations was added directly to 2.00 mL of 2.5×10^{-3} M of **F-*o*BOH**, **F-*m*BOH**, and **F-*p*BOH** in a 1-cm quartz cuvette by micropipette and stirred for 2 min. UV-vis spectra were monitored after each addition of cation to gain the ratios of 0:1 to 80:1 for **F-*o*BOH**, 0:1 to 55:1 for **F-*m*BOH** and 0:1 to 36:1 for **F-*p*BOH** shown in Table 3.5, 3.6, and 3.7, respectively.

Table 3.5 The concentration of Cu²⁺ cation was used in copper cationic complexation studies with **F-*o*BOH** and the ratios of **F-*o*BOH**:copper cation.

Point	Cu ²⁺ / F- <i>o</i> BOH	[F- <i>o</i> BOH] (M)	[Cu ²⁺] (M)	V of Cu ²⁺ (mL)	V total (mL)
1	0	2.50×10^{-5}	0	0.00	2.00
2	2	2.48×10^{-5}	5.00×10^{-5}	0.02	2.02
3	4	2.45×10^{-5}	1.00×10^{-4}	0.04	2.04
4	6	2.43×10^{-5}	1.50×10^{-4}	0.06	2.06
5	8	2.40×10^{-5}	2.00×10^{-4}	0.08	2.08
6	10	2.38×10^{-5}	2.50×10^{-4}	0.10	2.10
7	12	2.36×10^{-5}	3.00×10^{-4}	0.12	2.12
8	14	2.34×10^{-5}	3.50×10^{-4}	0.14	2.14
9	16	2.31×10^{-5}	4.00×10^{-4}	0.16	2.16
10	18	2.29×10^{-5}	4.50×10^{-4}	0.18	2.18

Point	$\text{Cu}^{2+}/$ $\text{F-}o\text{BOH}$	$[\text{F-}o\text{BOH}]$ (M)	$[\text{Cu}^{2+}]$ (M)	V of Cu^{2+} (mL)	V total (mL)
11	20	2.27×10^{-5}	5.00×10^{-4}	0.20	2.20
12	22	2.25×10^{-5}	5.50×10^{-4}	0.22	2.22
13	24	2.23×10^{-5}	6.00×10^{-4}	0.24	2.24
14	26	2.21×10^{-5}	6.50×10^{-4}	0.26	2.26
15	28	2.19×10^{-5}	7.00×10^{-4}	0.28	2.28
16	30	2.17×10^{-5}	7.50×10^{-4}	0.30	2.30
17	32	2.16×10^{-5}	8.00×10^{-4}	0.32	2.32
18	34	2.14×10^{-5}	8.50×10^{-4}	0.34	2.34
19	36	2.12×10^{-5}	9.00×10^{-4}	0.36	2.36
20	40	2.08×10^{-5}	1.00×10^{-4}	0.40	2.40
21	45	2.04×10^{-5}	1.13×10^{-4}	0.45	2.45
22	50	2.00×10^{-5}	1.25×10^{-4}	0.50	2.50
23	55	1.96×10^{-5}	1.38×10^{-4}	0.55	2.55
24	60	1.92×10^{-5}	1.50×10^{-4}	0.60	2.60
25	65	1.89×10^{-5}	1.63×10^{-4}	0.65	2.65
26	70	1.85×10^{-5}	1.75×10^{-4}	0.70	2.70
27	75	1.82×10^{-5}	1.88×10^{-4}	0.75	2.75
28	80	1.79×10^{-5}	2.00×10^{-4}	0.80	2.80

Table 3.6 The concentration of Cu^{2+} cation was used in copper cationic complexation studies with **F-*m*BOH** and the ratios of **F-*m*BOH**:copper cation.

Point	$\text{Cu}^{2+}/$ $\text{F-}m\text{BOH}$	$[\text{F-}m\text{BOH}]$ (M)	$[\text{Cu}^{2+}]$ (M)	V of Cu^{2+} (mL)	V total (mL)
1	0	3×10^{-5}	0	0.00	2.000
2	0.2	2.96×10^{-5}	6.00×10^{-6}	0.024	2.024
3	0.4	2.93×10^{-5}	1.20×10^{-5}	0.048	2.048
4	0.6	2.90×10^{-5}	1.80×10^{-5}	0.072	2.072
5	0.8	2.86×10^{-5}	2.40×10^{-5}	0.096	2.096
6	1.0	2.83×10^{-5}	3.00×10^{-5}	0.120	2.120
7	1.2	2.80×10^{-5}	3.60×10^{-5}	0.144	2.144

Point	$\text{Cu}^{2+}/$ $\text{F-}m\text{BOH}$	$[\text{F-}m\text{BOH}]$ (M)	$[\text{Cu}^{2+}]$ (M)	V of Cu^{2+} (mL)	V total (mL)
8	1.4	2.77×10^{-5}	4.20×10^{-5}	0.168	2.168
9	1.6	2.74×10^{-5}	4.80×10^{-5}	0.192	2.192
10	1.8	2.71×10^{-5}	5.40×10^{-5}	0.216	2.216
11	2.0	2.68×10^{-5}	6.00×10^{-5}	0.240	2.240
12	2.2	2.65×10^{-5}	6.60×10^{-5}	0.264	2.264
13	2.4	2.62×10^{-5}	7.20×10^{-5}	0.288	2.288
14	2.6	2.60×10^{-5}	7.80×10^{-5}	0.312	2.312
15	2.8	2.57×10^{-5}	8.40×10^{-5}	0.336	2.336
16	3.0	2.54×10^{-5}	9.00×10^{-5}	0.360	2.360
17	3.4	2.49×10^{-5}	1.02×10^{-4}	0.408	2.408
18	3.8	2.44×10^{-5}	1.14×10^{-4}	0.456	2.456
19	4.2	2.40×10^{-5}	1.26×10^{-4}	0.504	2.504
20	4.8	2.33×10^{-5}	1.44×10^{-4}	0.576	2.576
21	5.2	2.29×10^{-5}	1.56×10^{-4}	0.624	2.624
22	6.0	2.21×10^{-5}	1.80×10^{-4}	0.720	2.720
23	7.0	2.11×10^{-5}	2.10×10^{-4}	0.840	2.840
24	8.0	2.03×10^{-5}	2.40E-04	0.960	2.960
25	10.0	1.88×10^{-5}	3.00E-04	1.200	3.200

Table 3.7 The concentration of Cu^{2+} cation was used in copper cationic complexation studies with **F-*p*BOH** and the ratios of **F-*p*BOH**:copper cation.

Point	$\text{Cu}^{2+}/$ $\text{F-}p\text{BOH}$	$[\text{F-}p\text{BOH}]$ (M)	$[\text{Cu}^{2+}]$ (M)	V of Cu^{2+} (mL)	V total (mL)
1	0.0	3×10^{-5}	0	0.00	2.000
2	0.2	2.96×10^{-5}	6.00×10^{-6}	0.024	2.024
3	0.4	2.93×10^{-5}	1.20×10^{-5}	0.048	2.048
4	0.6	2.90×10^{-5}	1.80×10^{-5}	0.072	2.072
5	0.8	2.86×10^{-5}	2.40×10^{-5}	0.096	2.096
6	1.0	2.83×10^{-5}	3.00×10^{-5}	0.120	2.120
7	1.5	2.75×10^{-5}	4.50×10^{-5}	0.180	2.180

Point	Cu ²⁺ / F- <i>p</i> BOH	[F- <i>p</i> BOH] (M)	[Cu ²⁺] (M)	V of Cu ²⁺ (mL)	V total (mL)
8	2.0	2.68 x 10 ⁻⁵	6.00 x 10 ⁻⁵	0.240	2.240
9	2.5	2.61 x 10 ⁻⁵	7.50 x 10 ⁻⁵	0.300	2.300
10	3.0	2.54 x 10 ⁻⁵	9.00 x 10 ⁻⁵	0.360	2.360
11	3.5	2.48 x 10 ⁻⁵	1.05 x 10 ⁻⁴	0.420	2.420
12	4.0	2.42 x 10 ⁻⁵	1.20 x 10 ⁻⁴	0.480	2.480
13	5.0	2.31 x 10 ⁻⁵	1.50 x 10 ⁻⁴	0.600	2.600
14	6.0	2.21 x 10 ⁻⁵	1.80 x 10 ⁻⁴	0.720	2.720
15	7.0	2.11 x 10 ⁻⁵	2.10 x 10 ⁻⁴	0.840	2.840
16	8.0	2.03 x 10 ⁻⁵	2.40 x 10 ⁻⁴	0.960	2.960

3.4 Complexation Studies of F-*o*BOH, F-*m*BOH, and F-*p*BOH with copper cation in acetonitrile by fluorescence spectrophotometry

Typically, 0.01 M solution of tetrabutyl ammonium hexafluorophosphate ([Bu₄N][PF₆]) in 50 mL of acetonitrile was prepared. Stock solution of **F-*o*BOH**, **F-*m*BOH**, and **F-*p*BOH** in 0.01 M tetrabutyl ammonium hexafluorophosphate in acetonitrile was prepared in a 10 mL volumetric flask as shown in Table 3.8. The solution of copper cations was added directly to 2.00 mL of 5 x 10⁻⁶ M of **F-*o*BOH**, **F-*m*BOH**, and **F-*p*BOH** in a 1-cm quartz cuvette by micropipette and stirred for 2 min. Fluorescence spectra were monitored after each addition as shown in Table 3.9, Table 3.10, and Table 3.11, under the following condition

Condition for fluorescence spectrophotometry:

Start: 445 nm

End: 700 nm

Excitation: 437 nm

Excitation Slit: 10.0

Emission Slit: 5.0

Table 3.8 The concentrations of stock solution of sensors and copper were used in complexation studies for fluorescence titration

sensors	Stock solution	
	[sensor] (M)	[Cu ²⁺] (M)
F-<i>o</i>BOH	1 x 10 ⁻⁴	1 x 10 ⁻³
F-<i>m</i>BOH	1 x 10 ⁻⁴	5 x 10 ⁻³
F-<i>p</i>BOH	1 x 10 ⁻⁴	1 x 10 ⁻⁴

Table 3.9 The concentration of Cu²⁺ cation was used in copper cationic complexation studies with **F-*o*BOH** and the ratios of **F-*o*BOH**:copper cation for fluorescence titration.

Point	Cu ²⁺ / F- <i>o</i> BOH	[F- <i>o</i> BOH] (M)	[Cu ²⁺] (M)	V of Cu ²⁺ (mL)	V total (mL)
1	0	5.00 x 10 ⁻⁶	0	0.00	2.00
2	3	4.93 x 10 ⁻⁶	1.48 x 10 ⁻⁵	0.03	2.03
3	6	4.85 x 10 ⁻⁶	2.91 x 10 ⁻⁵	0.06	2.06
4	8	4.81 x 10 ⁻⁶	3.85 x 10 ⁻⁵	0.08	2.08
5	10	4.76 x 10 ⁻⁶	4.76 x 10 ⁻⁵	0.10	2.10
6	12	4.72 x 10 ⁻⁶	5.66 x 10 ⁻⁵	0.12	2.12
7	14	4.67 x 10 ⁻⁶	6.54 x 10 ⁻⁵	0.14	2.14
8	16	4.63 x 10 ⁻⁶	7.41 x 10 ⁻⁵	0.16	2.16
9	18	4.59 x 10 ⁻⁶	8.26 x 10 ⁻⁵	0.18	2.18
10	20	4.55 x 10 ⁻⁶	9.09 x 10 ⁻⁵	0.20	2.20
11	22	4.50 x 10 ⁻⁶	9.91 x 10 ⁻⁵	0.22	2.22
12	26	4.42 x 10 ⁻⁶	1.15 x 10 ⁻⁴	0.26	2.26
13	30	4.35 x 10 ⁻⁶	1.30 x 10 ⁻⁴	0.30	2.30
14	34	4.27 x 10 ⁻⁶	1.45 x 10 ⁻⁴	0.34	2.34
15	38	4.20 x 10 ⁻⁶	1.60 x 10 ⁻⁴	0.38	2.38
16	42	4.13 x 10 ⁻⁶	1.74 x 10 ⁻⁴	0.42	2.42
17	46	4.07 x 10 ⁻⁶	1.87 x 10 ⁻⁴	0.46	2.46

Point	$\text{Cu}^{2+}/$ $\text{F-}o\text{BOH}$	$[\text{F-}o\text{BOH}]$ (M)	$[\text{Cu}^{2+}]$ (M)	V of Cu^{2+} (mL)	V total (mL)
18	50	4.00×10^{-6}	2.00×10^{-4}	0.50	2.50
19	54	3.94×10^{-6}	2.13×10^{-4}	0.54	2.54
20	58	3.88×10^{-6}	2.25×10^{-4}	0.58	2.58
21	62	3.82×10^{-6}	2.37×10^{-4}	0.62	2.62
22	66	3.76×10^{-6}	2.48×10^{-4}	0.66	2.66
23	70	3.70×10^{-6}	2.59×10^{-4}	0.70	2.70
24	74	3.65×10^{-6}	2.70×10^{-4}	0.74	2.74
25	78	3.60×10^{-6}	2.81×10^{-4}	0.78	2.78

Table 3.10 The concentration of Cu^{2+} cation was used in copper cationic complexation studies with **F-*m*BOH** and the ratios of **F-*m*BOH**:copper cation for fluorescence titration.

Point	$\text{Cu}^{2+}/$ $\text{F-}m\text{BOH}$	$[\text{F-}m\text{BOH}]$ (M)	$[\text{Cu}^{2+}]$ (M)	V of Cu^{2+} (mL)	V total (mL)
1	0	5.00×10^{-6}	0	0.00	2.00
2	5	4.98×10^{-6}	2.49×10^{-5}	0.01	2.01
3	10	4.95×10^{-6}	4.95×10^{-5}	0.02	2.02
4	15	4.93×10^{-6}	7.39×10^{-5}	0.03	2.03
5	20	4.90×10^{-6}	9.80×10^{-5}	0.04	2.04
6	25	4.88×10^{-6}	1.22×10^{-4}	0.05	2.05
7	30	4.85×10^{-6}	1.46×10^{-4}	0.06	2.06
8	35	4.83×10^{-6}	1.69×10^{-4}	0.07	2.07
9	40	4.81×10^{-6}	1.92×10^{-4}	0.08	2.08
10	45	4.78×10^{-6}	2.15×10^{-4}	0.09	2.09
11	50	4.76×10^{-6}	2.38×10^{-4}	0.10	2.10
12	55	4.74×10^{-6}	2.61×10^{-4}	0.11	2.11
13	60	4.72×10^{-6}	2.83×10^{-4}	0.12	2.12
14	70	4.67×10^{-6}	3.27×10^{-4}	0.14	2.14
15	80	4.63×10^{-6}	3.70×10^{-4}	0.16	2.16

Point	$\text{Cu}^{2+}/$ $\text{F-}m\text{BOH}$	$[\text{F-}m\text{BOH}]$ (M)	$[\text{Cu}^{2+}]$ (M)	V of Cu^{2+} (mL)	V total (mL)
16	90	4.59×10^{-6}	4.13×10^{-4}	0.18	2.18
17	100	4.55×10^{-6}	4.55×10^{-4}	0.20	2.20

Table 3.11 The concentration of Cu^{2+} cation was used in copper cationic complexation studies with **F-*p*BOH** and the ratios of **F-*p*BOH**:copper cation for fluorescence titration.

Point	$\text{Cu}^{2+}/$ $\text{F-}p\text{BOH}$	$[\text{F-}p\text{BOH}]$ (M)	$[\text{Cu}^{2+}]$ (M)	V of Cu^{2+} (mL)	V total (mL)
1	0	5.00×10^{-6}	0	0.00	2.00
2	0.05	4.98×10^{-6}	2.49×10^{-7}	0.01	2.01
3	0.10	4.95×10^{-6}	4.95×10^{-7}	0.02	2.02
4	0.15	4.93×10^{-6}	7.39×10^{-7}	0.03	2.03
5	0.20	4.90×10^{-6}	9.80×10^{-7}	0.04	2.04
6	0.25	4.88×10^{-6}	1.22×10^{-6}	0.05	2.05
7	0.30	4.85×10^{-6}	1.46×10^{-6}	0.06	2.06
8	0.35	4.83×10^{-6}	1.69×10^{-6}	0.07	2.07
9	0.40	4.81×10^{-6}	1.92×10^{-6}	0.08	2.08
10	0.45	4.78×10^{-6}	2.15×10^{-6}	0.09	2.09
11	0.50	4.76×10^{-6}	2.38×10^{-6}	0.10	2.10
12	0.55	4.74×10^{-6}	2.61×10^{-6}	0.11	2.11
13	0.60	4.72×10^{-6}	2.83×10^{-6}	0.12	2.12
14	0.65	4.69×10^{-6}	3.05×10^{-6}	0.13	2.13
15	0.70	4.67×10^{-6}	3.27×10^{-6}	0.14	2.14
16	0.75	4.65×10^{-6}	3.49×10^{-6}	0.15	2.15

3.5 Determination of detection limit of **F-*o*BOH**, **F-*m*BOH**, and **F-*p*BOH** by Fluorescence spectrophotometry

Typically, 0.01 M solution of tetrabutyl ammonium hexafluorophosphate ([Bu₄N][PF₆]) in 50 mL of acetonitrile was prepared. Stock solution of 1×10^{-4} M of **F-*o*BOH**, **F-*m*BOH**, and **F-*p*BOH** in 0.01 M tetrabutyl ammonium hexafluorophosphate in acetonitrile was prepared in a 10 mL volumetric flask. Fluorescence spectra of **F-*o*BOH**, **F-*m*BOH**, and **F-*p*BOH** (final concentration at 5×10^{-6} M) were monitored for 10 times under the following condition.

Condition for fluorescence spectrophotometry:

Start: 500 nm

End: 700 nm

Excitation: 492 nm

Excitation Slit: 10.0

Emission Slit: 5.0

3.6 Study on the stability of sensor

3.6.1 The stability of **F-*o*BOH** in Tris buffer pH 7.0 by fluorescence spectrophotometry

Typically, stock solution of **F-*o*BOH** was prepared in analytical grade ethanol at concentration of 1×10^{-4} M. Stock solution of copper was prepared in MilliQ water at the concentration of 5×10^{-3} M. The solution of **F-*o*BOH** and Tris buffer solution pH 7.0 was mixed together with copper solution to give a final concentration of **F-*o*BOH** at 5×10^{-6} M and copper at 5×10^{-6} M (the ratio of ethanol and Tris buffer was 5:95). Fluorescence spectra were recorded under the following condition by varying time from 0 to 180 minutes.

Condition for fluorescence spectrophotometry:

Start: 500 nm

End: 700 nm

Excitation: 492 nm

Excitation Slit: 5.0

Emission Slit: 5.0

3.6.2 Study on the stability of F-*o*BOH, F-*m*BOH, and F-*p*BOH by ¹H-NMR spectrophotometry

The solution of **F-*o*BOH**, **F-*m*BOH**, and **F-*p*BOH** was prepared in ethanol and Tris buffer pH 8.5 (the ratio of ethanol:buffer solution is 5:95) at concentration 1×10^{-3} M in volumetric flask 5.00. The mixture of **F-*o*BOH**, **F-*m*BOH**, and **F-*p*BOH** stirred at room temperature for 7 days, 2 days and 2 days, respectively.

The mixtures were evaporated under vacuum to remove the remaining solvent. The crude mixtures were dissolved in n-butanol saturated with water and the solution was separated in two layer. The organic layer was collected and dried by vacuum. Finally, the corresponding solution of sensors was prepared for ¹H-NMR experiment by dissolving the sensors in DMSO-*d*₆.

3.7 Preparation of F-*o*BOH doped nucleotide/lanthanide CNPs (F-*o*BOH-AMP/Gd³⁺ CNPs)

Coordination nanoparticles were prepared by mixing aqueous mixture of AMP (10 mM, 1.0 mL) and **F-*o*BOH** (0.2 mM, 0.5 mL) and followed by adding the ethanol solution of Gd(NO₃)₃ (10 mM, 0.5 mL) into this mixture at room temperature. Finally, the volume of solution was adjusted to be 10 mL by 0.1 M HEPES buffer pH 7.4. Immediately, the colorless precipitate nanoparticles were observed. After stirring the mixture for 1h, the resultant aqueous suspensions were washed with milliQ water several times and gathered by ultracentrifugation. Accordingly, the coordination nanoparticles were dispersed in water by sonication. The prepared sensors were examined for SEM, EDX and TEM measurements

3.8 Study on the stability of F-*o*BOH-AMP/Gd³⁺ CNPs

Typically, stock solution of 1×10^{-5} M of F-*o*BOH-AMP/Gd³⁺ CNPs was prepared in volumetric flask (10 mL) following the method mentioned in the topic of 3.7. Stock solution of copper was prepared in MilliQ water at the concentration of 5×10^{-3} M. The solution of copper cation was added directly to 2.00 mL of 1×10^{-5} M F-*o*BOH-AMP/Gd³⁺ CNPs in a 1-cm quartz cuvette by micropipette and stirred. Fluorescence spectra were monitored from 1 to 120 minutes under the following condition.

Condition for fluorescence spectrophotometry:

Start: 500 nm

End: 700 nm

Excitation: 492 nm

Excitation Slit: 5.0

Emission Slit: 5.0

3.9 Complexation studies of F-*o*BOH-AMP/Gd³⁺ CNPs-copper(II) with various anions: fluoride, chloride, bromide, iodide, hydroxide, nitrate, perchlorate, benzoate, dihydrogenphosphate, thiocyanate, and cyanide

Typically, 0.1 M solution of HEPES buffer (pH 7.4) was prepared in MilliQ water with sodium chloride as supporting electrolyte. Stock solution of 1×10^{-5} M of F-*o*BOH-AMP/Gd³⁺ CNPs was prepared in volumetric flask (25 mL) following the method mentioned in the topic of 3.7. Solution of anion (F⁻, Cl⁻, Br⁻, I⁻, OH⁻, NO₃⁻, ClO₄⁻, BzO⁻, H₂PO₄⁻, SCN⁻, and CN⁻) in HEPES (pH 7.4) solution was prepared in 5 mL and 10 mL volumetric flask (shown in Table 3.12).

Table 3.12 Amounts of F⁻, Cl⁻, Br⁻, I⁻, OH⁻, NO₃⁻, ClO₄⁻, BzO⁻, H₂PO₄⁻, SCN⁻, and CN⁻ ions used in these studies by fluorescence spectrophotometry.

anion	molecular weight (gmol ⁻¹)	Weight(mg)	mL
KF	58.10	2.20	5
NaCl	58.44	9.90	5
NaBr	102.90	5.90	5
NaI	149.89	6.30	5
NaOH	40.00	9.29	10
NaNO ₃	85.01	2.80	5
NaClO ₄	140.46	3.41	10
NaBzO	144.11	5.20	10
KH ₂ PO ₄	136.09	4.30	5
KSCN	97.18	7.60	5
NaCN	49.00	0.98	10

Fluorescence spectra of **F-oBOH-AMP/Gd³⁺** and anion complexes were monitored under the following condition.

Condition for fluorescence spectrophotometry:

Start: 500 nm

End: 700 nm

Excitation: 492 nm

Excitation Slit: 5.0

Emission Slit: 5.0

The solution of anion (shown in Table 3.13) was added directly into 2.00 mL of 1x10⁻⁵ M of **F-oBOH-AMP/Gd³⁺** in a 1-cm quartz cuvette by micropipette and stirred for 2 minutes. Emission spectra were recorded after each addition. Table 3.13 exhibits **F-oBOH-AMP/Gd³⁺**:anion ratios utilized in the experiments.

Table 3.13 Amounts of anions solutions were used to prepare various anions: **F-*o*BOH-AMP/Gd³⁺** ratios

Anion	[anion](mM)	Anion(μ L)	F- <i>o</i> BOH-AMP/Gd ³⁺ : anion ratio
KF	7.60	132	1:50
NaCl	33.90	29	1:50
NaBr	11.50	87	1:50
NaI	8.40	119	1:50
NaOH	23.23	40	1:50
NaNO ₃	6.60	152	1:50
NaClO ₄	2.43	412	1:50
NaBzO	3.60	278	1:50
KH ₂ PO ₄	6.30	159	1:50
KSCN	15.60	64	1:50
NaCN	2.0	500	1:50

3.10 Job's plot study

3.10.1 Job's plot study of F-*o*BOH-AMP/Gd³⁺ CNPs \subset copper(II) with cyanide anion

Typically, 0.1 M solution of HEPES buffer (pH 7.4) was prepared in MilliQ water with sodium chloride as supporting electrolyte. Stock solution of 1×10^{-5} M **F-*o*BOH-AMP/Gd³⁺** CNPs was prepared in volumetric flask (25 mL) following the method which mentioned in the topic of 3.7. A solution of 2.15×10^{-3} M copper(II) nitrate was prepared in MilliQ water in a 10 mL volumetric flask. A solution of 5.4×10^{-6} M sodium cyanide was prepared in a solution of HEPES buffer (pH 7.4) in a 10 mL volumetric flask by pipette 27 μ L of 2.0×10^{-3} M sodium cyanide solution using micropipette.

Fluorescence spectra of **F-*o*BOH-AMP/Gd³⁺** CNPs with copper and cyanide complexes were monitored from 500 – 700 nm upon with excitation at 492 nm at ambient temperature. Firstly, the solution of copper cations was added directly to 2.00 mL **F-*o*BOH-AMP/Gd³⁺** CNPs in a 1-cm quartz cuvette by micropipette and stirred for a

minute. Then, the solution of cyanide anions was added immediately to a solution of **F-*o*BOH-AMP/Gd³⁺** CNPs mixed with copper cation. Fluorescence spectra were recorded after each experiment. Table 3.14 showed $[CN^-]/([CN^-] + [CNPs])$ ratios utilized in the manipulation.

Table 3.14 Amounts of **F-*o*BOH-AMP/Gd³⁺** CNPs, CN^- anion, Cu^{2+} cation, and HEPES pH 7.4 were used in Job's plot experiment.

Ratio	CNPs (μ L)	Cu^{2+} (μ L)	CN^- (μ L)	V of HEPES(μ L)	V total (μ L)
0	1000	63	0	1938	3000
0.1	900	56	185	1859	3000
0.2	800	50	370	1780	3000
0.3	700	44	556	1701	3000
0.4	600	38	741	1622	3000
0.5	500	31	926	1543	3000
0.6	400	25	1111	1464	3000
0.7	300	19	1296	1385	3000
0.8	200	13	1481	1306	3000
0.9	100	6	1667	1227	3000
1.0	0	0	1852	1148	3000

3.10.2 Job's plot study of **F-*o*BOH-AMP/Gd³⁺** CNPs \subset cyanide with copper(II) ion

Typically, 0.1 M solution of HEPES buffer (pH 7.4) was prepared in MilliQ water with sodium chloride as supporting electrolyte. Stock solution of 1×10^{-5} M **F-*o*BOH-AMP/Gd³⁺** CNPs was prepared in volumetric flask (25 mL) following the method which mentioned in the topic of 3.7. A solution of 1.0×10^{-5} M copper(II) nitrate was prepared in MilliQ water in a 10 mL volumetric flask. A solution of 0.01M sodium cyanide was prepared in a solution of HEPES buffer (pH 7.4) in a 10 mL volumetric flask.

Firstly, **F-*o*BOH-AMP/Gd³⁺** CNPs was doped with cyanide anion by pipette 1.00 mL of 0.01 M sodium cyanide in to the solution of **F-*o*BOH-AMP/Gd³⁺** CNPs and keep

stirring for 24 hours. The complexation of **F-*o*BOH-AMP/Gd³⁺** CNPs_⊂cyanide was obtained by using ultracentrifugation to collect the nanoparticles then washed the **F-*o*BOH-AMP/Gd³⁺** CNPs_⊂cyanide with HEPES 0.1 M pH 7.4 for 2 times. After, **F-*o*BOH-AMP/Gd³⁺** CNPs_⊂cyanide was redispersed in HEPES 0.1 M pH 7.4 and then used for Job's plot method to determine the ratio of **F-*o*BOH-AMP/Gd³⁺** CNPs_⊂cyanide with copper(II) ion

Fluorescence spectra of **F-*o*BOH-AMP/Gd³⁺** CNPs_⊂cyanide and copper complexes were monitored from 500 – 700 nm upon with excitation at 492 nm at ambient temperature. Table 3.15 showed the amount of **F-*o*BOH-AMP/Gd³⁺** CNPs_⊂CN⁻, Cu²⁺, and the ratios of [Cu²⁺]/([Cu²⁺] + [CNPs]) utilized in the manipulation.

Table 3.15 Amounts of **F-*o*BOH-AMP/Gd³⁺** CNPs_⊂CN⁻ and Cu²⁺ cation were used in Job's plot experiment.

Ratio	CNPs_⊂CN⁻ (mL)	Cu²⁺ (mL)	V total (mL)
0.1	1.8	0.2	2.0
0.2	1.6	0.4	2.0
0.3	1.4	0.6	2.0
0.4	1.2	0.8	2.0
0.5	1.0	1.0	2.0
0.6	0.8	1.2	2.0
0.7	0.6	1.4	2.0
0.8	0.4	1.6	2.0
0.9	0.2	1.8	2.0

3.11 Complexation studies of F-*o*BOH-AMP/Gd³⁺ CNPs with copper(II) with cyanide anion by fluorescence spectrophotometry

Typically, 0.1 M solution of HEPES buffer (pH 7.4) was prepared in MilliQ water with sodium chloride as supporting electrolyte. Stock solution of 1×10^{-5} M F-*o*BOH-AMP/Gd³⁺ CNPs was prepared in volumetric flask (10 mL) following the method mentioned in the topic of 3.7. A solution of 2.15×10^{-3} M copper(II) nitrate was prepared in MilliQ water in a 10 mL volumetric flask. A solution of 2×10^{-3} M of sodium cyanide was prepared in a solution of HEPES buffer (pH 7.4) in a 10 mL volumetric flask.

Initially, the solution of copper cations (47 μ L) was added directly to 2.00 mL of 1×10^{-5} M F-*o*BOH-AMP/Gd³⁺ CNPs in a 1-cm quartz cuvette by micropipette and stirred for a minute. Then, the solution of cyanide anions was added immediately in a portion to a solution of F-*o*BOH-AMP/Gd³⁺ CNPs mixed with copper cation (shown in Table 3.16). Fluorescence spectra were recorded after each addition of cyanide to F-*o*BOH-AMP/Gd³⁺ CNPs in the ratios of 1:0 to 1:80. Fluorescence spectra of F-*o*BOH-AMP/Gd³⁺ CNPs with copper and cyanide complexes were recorded under the following condition.

Condition for fluorescence spectrophotometry:

Start: 500 nm

End: 700 nm

Excitation: 492 nm

Excitation Slit: 5.0

Emission Slit: 5.0

Table 3.16 The concentration of CN^- anion used in cyanide anion complexation studies with $\text{F-}o\text{BOH-AMP/Gd}^{3+}\text{Cu}^{2+}$ and the final ratios of $\text{F-}o\text{BOH-AMP/Gd}^{3+}\text{CNPs}\text{Cu}^{2+}$:cyanide anion.

Point	CN^- / $\text{CNPs}\text{Cu}^{2+}$	$[\text{CNPs}]$ (M)	$[\text{CN}^-]$ (M)	V of CN^- (mL)	V total (mL)
1	0	1×10^{-5}	0	0.00	2.00
2	1	9.95×10^{-6}	1.00×10^{-5}	0.01	2.01
3	3	9.85×10^{-6}	3.00×10^{-5}	0.03	2.03
4	5	9.76×10^{-6}	5.00×10^{-5}	0.05	2.05
5	7	9.66×10^{-6}	7.00×10^{-5}	0.07	2.07
6	9	9.57×10^{-6}	9.00×10^{-5}	0.09	2.09
7	11	9.48×10^{-6}	1.10×10^{-4}	0.11	2.11
8	13	9.39×10^{-6}	1.30×10^{-4}	0.13	2.13
9	15	9.30×10^{-6}	1.50×10^{-4}	0.15	2.15
10	17	9.22×10^{-6}	1.70×10^{-4}	0.17	2.17
11	19	9.13×10^{-6}	1.90×10^{-4}	0.19	2.19
12	22	9.01×10^{-6}	2.20×10^{-4}	0.22	2.22
13	25	8.89×10^{-6}	2.50×10^{-4}	0.25	2.25
14	28	8.77×10^{-6}	2.80×10^{-4}	0.28	2.28
15	31	8.66×10^{-6}	3.10×10^{-4}	0.31	2.31
16	34	8.55×10^{-6}	3.40×10^{-4}	0.34	2.34
17	37	8.44×10^{-6}	3.70×10^{-4}	0.37	2.37
18	40	8.33×10^{-6}	4.00×10^{-4}	0.40	2.40
19	43	8.23×10^{-6}	4.30×10^{-4}	0.43	2.43
20	46	8.13×10^{-6}	4.60×10^{-4}	0.46	2.46
21	49	8.03×10^{-6}	4.90×10^{-4}	0.49	2.49
22	52	7.94×10^{-6}	5.20×10^{-4}	0.52	2.52
23	55	7.84×10^{-6}	5.50×10^{-4}	0.55	2.55
24	60	7.69×10^{-6}	6.00×10^{-4}	0.60	2.60
25	66	7.52×10^{-6}	6.60×10^{-4}	0.66	2.66
26	80	7.14×10^{-6}	8.00×10^{-4}	0.80	2.80

3.12 Determination of detection limit of F-*o*BOH-AMP/Gd³⁺ CNPs-copper(II) with cyanide anion

3.12.1 Fluorescence spectrophotometry: calculation method

Typically, 0.1 M solution of HEPES buffer (pH 7.4) was prepared in milliQ water with sodium chloride as supporting electrolyte. Stock solution of 1×10^{-5} M of F-*o*BOH-AMP/Gd³⁺ CNPs was prepared in volumetric flask (25 mL) following the method which mentioned in the topic of 3.7. A solution of 2.15×10^{-3} M copper(II) nitrate was prepared in MilliQ water in a 10 mL volumetric flask. Fluorescence spectra of F-*o*BOH-AMP/Gd³⁺ CNPs with copper (final concentration at 5×10^{-5} M) complexes were monitored for 10 times under the following condition.

Condition for fluorescence spectrophotometry:

Start: 500 nm

End: 700 nm

Excitation: 492 nm

Excitation Slit: 5.0

Emission Slit: 5.0

3.12.2 Naked-eyes detection limit

Typically, 0.1 M solution of HEPES buffer (pH 7.4) was prepared in MilliQ water with sodium chloride as supporting electrolyte. Stock solution of 1×10^{-5} M of F-*o*BOH-AMP/Gd³⁺ CNPs was prepared in volumetric flask (25 mL) following the method mentioned in the topic of 3.7. A solution of 2.15×10^{-3} M copper(II) nitrate was prepared in milliQ water in a 10 mL volumetric flask. A solution of 2×10^{-3} M sodium cyanide was prepared in a solution of HEPES buffer (pH 7.4) in a 10 mL volumetric flask.

Initially, the solution of copper cations (47 μ L) was added directly to 2.00 mL of 1×10^{-5} M F-*o*BOH-AMP/Gd³⁺ CNPs in a 1-cm quartz cuvette by micropipette and stirred for a minute. Then, the solution of cyanide anions was added immediately in a portion to a solution of F-*o*BOH-AMP/Gd³⁺ CNPs mixed with copper cation (shown in Table 3.17).

Table 3.17 The concentration of CN⁻ anion used in naked-eye detection limit.

vial	CNPs (μL)	Cu ²⁺ (μL)	CN ⁻ (μL)
1	2000	0	0
2	2000	47	0
3	2000	47	20
4	2000	47	40
5	2000	47	70
6	2000	47	100
7	2000	47	200
8	2000	47	300
9	2000	47	400

3.13 Interference studies by fluorescence spectrophotometry

Typically, 0.1 M HEPES pH 7.4 was prepared in all interference studies. Solution of 1×10^{-5} M **F-*o*BOH-AMP/Gd³⁺** CNPs was prepared in a 50 mL volumetric flask. The solution of guest was prepared in volume metric flask (shown in Table 3.17). The **F-*o*BOH-AMP/Gd³⁺** CNPs solution (2 mL), Cu²⁺ (1×10^{-5} M), CN⁻ (5×10^{-4} M), and foreign (the amount of foreign anion shown in Table 3.18 and 3.19.) were pipetted into the cuvette. The emission spectra were recorded under the following condition.

Condition for fluorescence spectrophotometry:

Start: 500 nm

End: 700 nm

Excitation: 492 nm

Excitation Slit: 5.0

Emission Slit: 5.0

Procedure for evaluation of relative error:

1. To record the emission intensity of free ligand **F-*o*BOH-AMP/Gd³⁺** CNPs with Cu²⁺ (5×10^{-5} M)

2. To record the emission intensity of complexation between **F-oBOH-AMP/Gd³⁺** CNPs with Cu²⁺ (5 x 10⁻⁵ M) and CN⁻

3. To record the emission of complexation **F-oBOH-AMP/Gd³⁺** CNPs with Cu²⁺ (5 x 10⁻⁵ M) + CN after adding the foreign guest.

The value of relative error was calculated by $[(\Delta F_1 - \Delta F_2) / \Delta F_1] \times 100$, where ΔF_1 is the fluorescence decrement of emission intensity of complexation of **F-oBOH-AMP/Gd³⁺** CNPs with Cu²⁺ and CN⁻ compared to **F-oBOH-AMP/Gd³⁺** CNPs with Cu²⁺, and ΔF_2 is the fluorescence decrement of emission intensity of complexation of **F-oBOH-AMP/Gd³⁺** CNPs with Cu²⁺ and CN⁻ + foreign guest compared to **F-oBOH-AMP/Gd³⁺** CNPs with Cu²⁺

Table 3.18 Amounts of F⁻, Cl⁻, Br⁻, I⁻, OH⁻, NO₃⁻, ClO₄⁻, BzO⁻, H₂PO₄⁻, SCN⁻, and CN⁻ as sodium and potassium salt used in interference studies with **F-oBOH-AMP/Gd³⁺** CNPs \subset copper(II) by fluorescence spectrophotometry

compound	molecular weight (gmol ⁻¹)	Concentration (M)	Weight (g)	mL
CNPs	-	1x 10 ⁻⁵	-	25
KF	58.10	0.05	0.0291	10
NaCl	58.44	2.00	0.5840	5
NaBr	102.90	2.00	1.0290	5
NaI	149.89	0.50	0.3747	5
NaOH	40.00	0.05	0.0200	10
NaNO ₃	85.01	2.00	0.8501	5
NaClO ₄	140.46	2.00	2.8092	10
NaBzO	144.11	0.50	0.7206	10
KH ₂ PO ₄	136.09	2.00	1.3609	5
KSCN	97.18	0.50	0.2430	5
NaCN	49.00	0.05	0.0245	10
Cu(NO ₃) ₂ ·3H ₂ O	241.60	0.005	0.0121	10

Table 3.19 Amount of CN^- and anions used in interference studies with **F-*o*BOH-AMP/Gd³⁺** CNPs@copper(II) by fluorescence spectrophotometry.

Anion	[anion](M)	Anion(μL)	Foreign anion:cyanide ratio
KF	2.50×10^{-4}	10	5:1
NaCl	5.00×10^{-2}	50	1000:1
NaBr	5.00×10^{-2}	50	1000:1
NaI	5.00×10^{-3}	20	100:1
NaOH	5.00×10^{-4}	20	10:1
NaNO_3	5.00×10^{-2}	50	1000:1
NaClO_4	5.00×10^{-2}	50	1000:1
NaBzO	5.00×10^{-3}	20	100:1
KSCN	5.00×10^{-3}	20	100:1
KH_2PO_4	n.d. ^a	n.d. ^a	n.d. ^a

^acannot be determined

CHAPTER IV

RESULTS AND DISCUSSION

4.1 Design concept of boronic acid/fluorescein based sensors

Our research group has considerable paid attention on the design, development of new colorimetric sensors, and synthesis of the molecular sensors for cations and anions. Recently, molecular recognition has been performed at the actual heart of sensor chemistry. The process itself includes the interaction between two substances, often defined as a host and guest, a lock and a key or a receptor, sensor and a substrate chemistry. [43] Importantly, recognition events take place through non-covalent interactions comprising hydrogen bonding, ion-dipole interactions, electrostatic interactions, cation- π interactions and π - π stacking interaction. [44] Therefore, the recognition is not just defined as a binding event but also acquired selectivity between the host and guest.

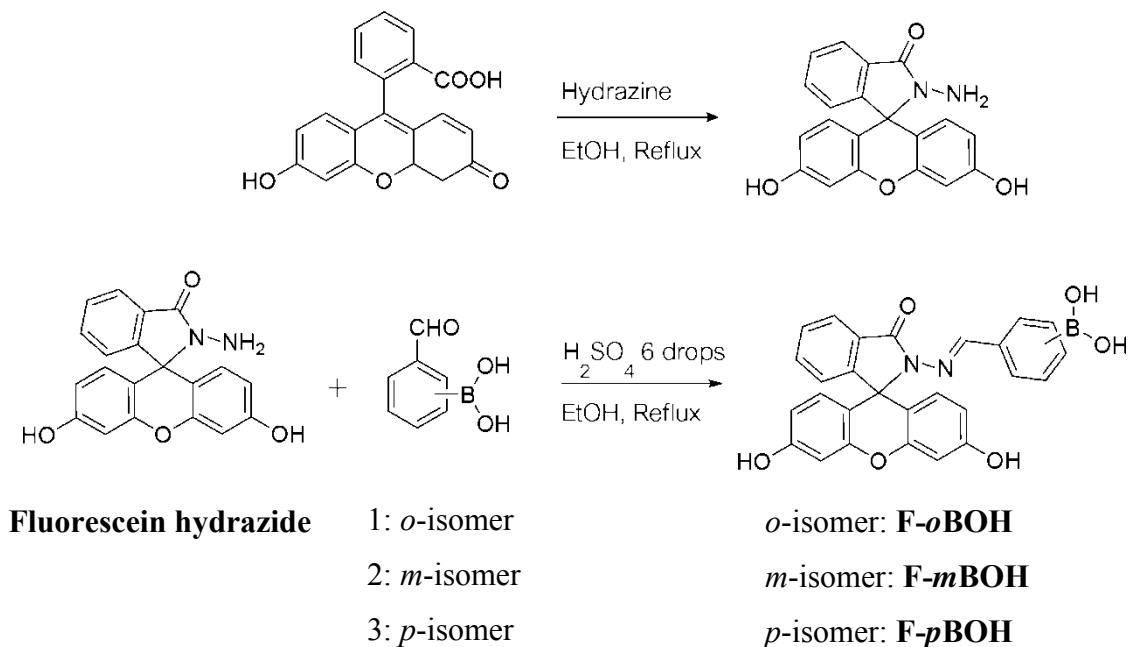
Fluorescein or rhodamine spirolactam derivatives are nonfluorescent and colorless, whereas ring-opening of the corresponding spirolactam enhances in strong fluorescence emission. Recently, a spirolactam ring to ring-opening can be utilized for the detection of metal ions including Hg^{2+} [45], Pb^{2+} [46], Fe^{3+} [47] and Cu^{2+} . [48] Moreover, boronic acid moiety is readily demonstrated to have high affinity for compound which composes of diol groups such as saccharide and carbohydrate, consequently, it has been used as carbohydrate sensors. In addition, Swamy [49] illustrated the utilization of boronic acid-linked fluorescent chemosensors in which the ring-opening process of rhodamine to detect copper ion but there is no precedent exist for the use of boronic acid connected with fluorescein or rhodamine to detect cyanide ion directly.

From the reasons mentioned above, we have concentrated on designing the sensors contained both fluorescein and boronic acid moieties. Three sensors with different isomers were synthesized by linking fluorescein hydrazide and 2-formylphenyl boronic acid using the Schiff base reaction pathway illustrated in the scheme 4.1. All of

three sensors consist of copper and cyanide binding sites. We, then, studied the complexation of sensors with copper and cyanide ion in organic solvent using acetonitrile by UV-vis and fluorescence spectrophotometry techniques. Since the sensors contain hydrazone part which can be hydrolyzed by water, therefore, we designed the system to protect the hydrolysis phenomenon by applying adaptive coordination nanoparticles. The complexation of coordination nanoparticles using several techniques such as UV-vis and fluorescence spectrophotometry, and energy dispersive X-ray (EDX) spectroscopy were also studied.

4.2 Synthesis and characterization of F-*o*BOH, F-*m*BOH, and F-*p*BOH

Fluorescein hydrazide was selected as a sensory unit due to the different photophysical property of the spirolactam form. The closed form of spirolactam is non-fluorescence while that in opened form shows a strong fluorescence and distinct color change. [22, 46, 50, 51] The synthesis pathway of sensors **F-*o*BOH**, **F-*m*BOH**, and **F-*p*BOH** was illustrated in Scheme 4.1.



Scheme 4.1 Synthesis pathway of **F-*o*BOH**, **F-*m*BOH**, and **F-*p*BOH**

Spiro form fluorescein hydrazone can be synthesized by the reaction of fluorescein with hydrazine hydrate. [42] Then, the fluorescein hydrazone was reacted with formylphenylboronic acid using a small amount of sulfuric acid as a catalyst in ethanol under nitrogen atmosphere. The desired product was purified by crystallization applying ethylacetate and hexane as solvents. The $^1\text{H-NMR}$ spectrum of the desired products of **F-*o*BOH**, **F-*m*BOH**, and **F-*p*BOH** was assigned a singlet signal of imine proton ($\text{N}=\text{CH}$) at 9.584, 8.784, and 8.952, respectively. In addition, the $^1\text{H-NMR}$ data of **F-*o*BOH**, **F-*m*BOH**, and **F-*p*BOH** explicated the boronic acid protons ($\text{B}(\text{OH})_2$) at 8.170, 8.129, and 8.110, respectively. The range of aromatic protons (8-6 ppm) of compound **F-*o*BOH** exhibited a significant difference from fluorescein hydrazone. Furthermore, the $^{13}\text{C-NMR}$ spectra of **F-*o*BOH**, **F-*m*BOH**, and **F-*p*BOH** described a characteristic peak of spirolactam carbon at 65.447, 64.623, and 65.413, respectively. The electrospray high resolution mass spectra confirmed the structure of **F-*o*BOH**, **F-*m*BOH**, and **F-*p*BOH** including methanol and hydronium ion showing the intense peak at m/z 529.1542, 529.1552, and 529.1481, respectively. According to all results, the obtained products have a structure corresponding to the structure of **F-*o*BOH**, **F-*m*BOH**, and **F-*p*BOH**.

4.3 Complexation Study of **F-*o*BOH**, **F-*m*BOH**, and **F-*p*BOH** in acetonitrile by UV-visible spectrophotometry

4.3.1 Complexation studies of **F-*o*BOH**, **F-*m*BOH**, and **F-*p*BOH** with various cations: copper, cadmium, nickel, silver, zinc, cobalt, and magnesium

The spirolactam structure of fluorescein ring [22, 46, 50, 51] was a good characteristic to express a strong fluorescence and an obvious color change as a result of cation inducing the ring opening of the spirolactam ring. Initially, we evaluated the complexation abilities of **F-*o*BOH**, **F-*m*BOH**, and **F-*p*BOH** consisted of spirolactam moiety with various cations including Cu^{2+} , Cd^{2+} , Ni^{2+} , Ag^+ , Zn^+ , Co^{2+} , Mg^{2+} in acetonitrile using tetrabutylammonium hexafluorophosphate as supporting electrolyte measured by UV-Vis spectrophotometry technique. In the presence of excess amount of cations, absorption spectra of the sensors in the range of 250 – 600 nm were monitored to explore the selectivity of the sensors.

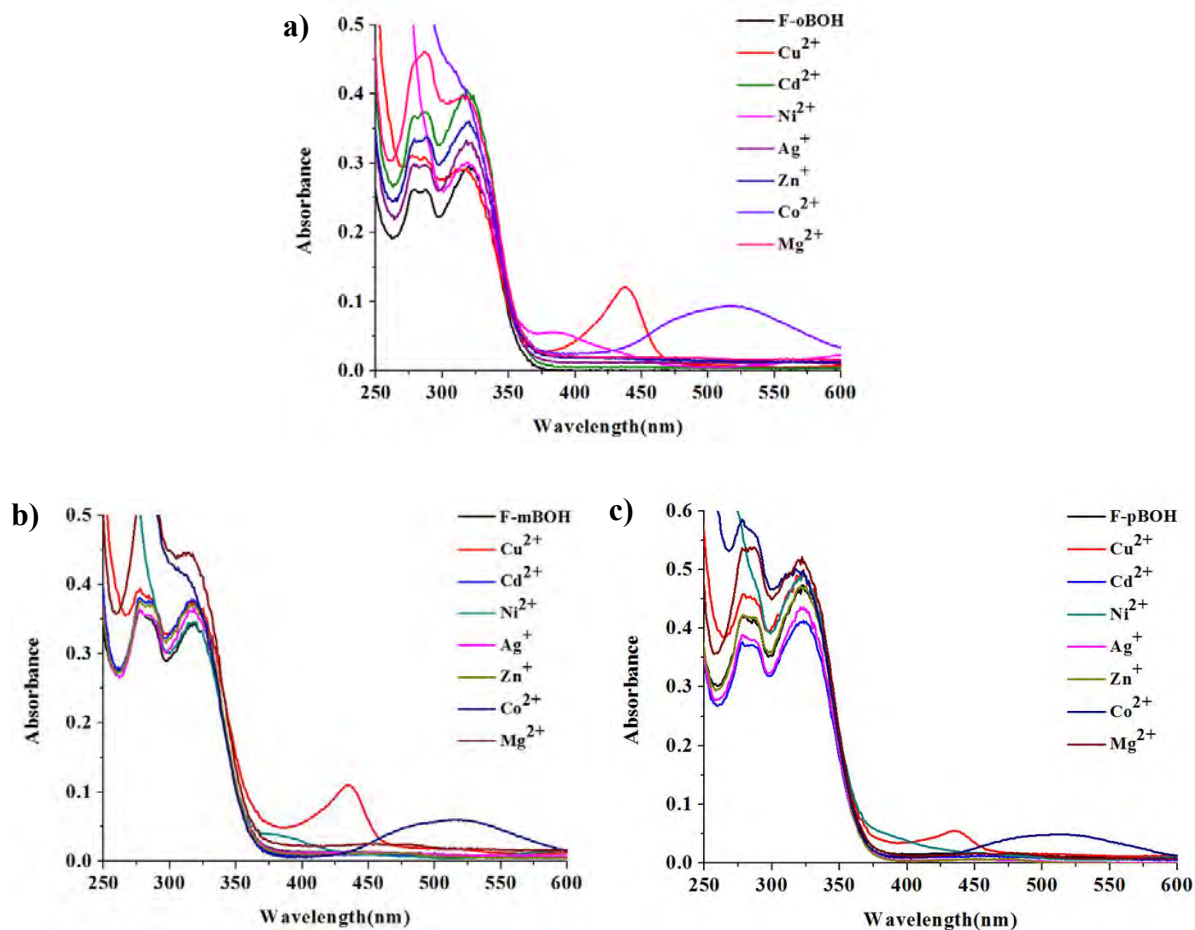


Figure 4.1 The UV-visible spectra change of a) **F-oBOH**, b) **F-mBOH**, and c) **F-pBOH** (3.0×10^{-5} M) in CH₃CN in the presence of excess amount of various cations.

As shown in Figure 4.1, the observation of absorption band at 437 nm upon the addition of copper ion in all sensors is indicative of the opened forms of spirolactam ring of **F-oBOH**, **F-mBOH**, and **F-pBOH**. The small changes of the absorption spectra of **F-oBOH**, **F-mBOH**, and **F-pBOH** were observed in the case of Cd²⁺, Ni²⁺, Ag⁺, Zn⁺, Co²⁺, and Mg²⁺ (shown in Figure 4.1 and 4.2). This suggested that copper(II) ion can induce selectively a ring opening of spirolactam ring.

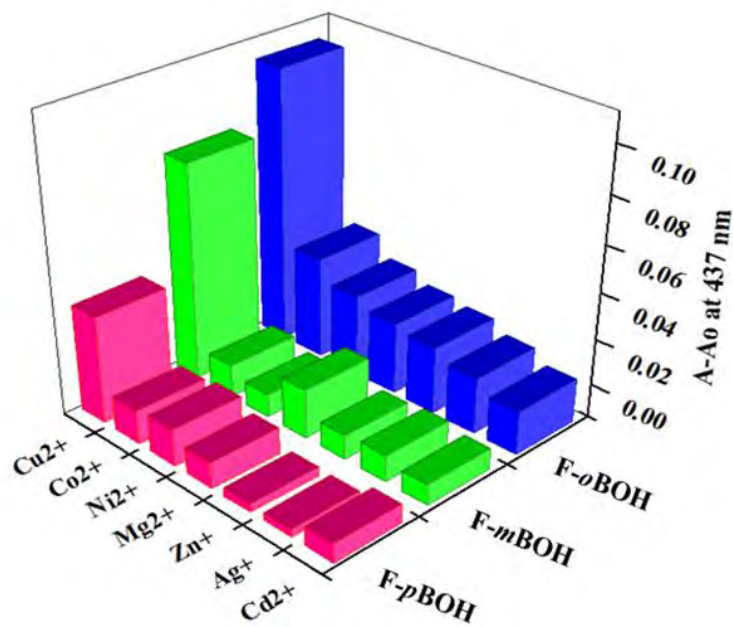


Figure 4.2 The UV-visible responses ($A-A_0$ at 437 nm) of **F-oBOH**, **F-mBOH**, and **F-pBOH** (3.0×10^{-5} M) in CH_3CN in the presence of excess amount of various cations

4.3.2 Complexation studies of **F-oBOH**, **F-mBOH**, and **F-pBOH** with copper cation in acetonitrile by UV-visible spectrophotometry

To verify the sensitivity of each sensor, UV-visible titrations of sensors were investigated in acetonitrile using tetrabutylammonium hexafluorophosphate as supporting electrolyte. Prior to UV-visible measurement, the solution mixture of the sensor and copper(II) ion was stirred for 2 minutes. The absorption intensities at 437 nm of the complexation of **F-oBOH**, **F-mBOH**, and **F-pBOH** with copper(II) ion increased as a function of cyanide concentration as shown in Figure 4.3a, 4.3c, and 4.3e, respectively. The UV-visible titration was measured at least twice. The $\log \beta$ value of **F-oBOH** with copper(II) ion was 6.67 calculated by Spectfit 32 program showing the best fit curve in Figure 4.7b. Moreover, the $\log \beta$ values of **F-mBOH** and **F-pBOH** with copper(II) ion were 8.87 and 9.88, respectively, calculated by equation 4.1 showing the best fit curve in Figure 4.3d and 4.3f.

$$A = \frac{(A_0 + A_{lim}\beta[guest]^2)}{(1 + \beta[guest]^2)} \quad (4.1)$$

- A = Absorption Intensity of a particular concentration of guest
 A_0 = Initial absorption intensity
 A_{lim} = Limiting (final) absorption intensity
 β = Stability constant of the receptor with the guest
 $[guest]$ = Concentration of guest

The $\log \beta$ values of sensors with copper(II) was followed the trend of **F-*p*BOH** > **F-*m*BOH** > **F-*o*BOH**. This sequence was due to the coordination of copper(II) ion with sensors at a boronic acid and a spirolactam ring. The copper(II) ion can bind with **F-*p*BOH** at the hydroxy group of boronic acid much easier than those of **F-*m*BOH** and **F-*o*BOH**, respectively indicated by the highest value of $\log \beta$ of **F-*p*BOH** with copper(II). Moreover, in the presence of copper(II) ion, the colorless solution of **F-*o*BOH**, **F-*m*BOH**, and **F-*p*BOH** changed to strong yellow color within 3 min, 10 min, and 120 min, respectively. Because, the copper(II) ion can induce the spirolactam ring to be open form of **F-*o*BOH** easier than those of **F-*m*BOH** and **F-*p*BOH** as corresponding to the clearly appearance of the opening spirolactam signal at 437 nm of **F-*o*BOH**. This suggests that the hydroxy group of **F-*o*BOH** of boronic acid can chelate with copper(II) ion and induces spirolactam to be open form more quickly than **F-*m*BOH** and **F-*p*BOH**.

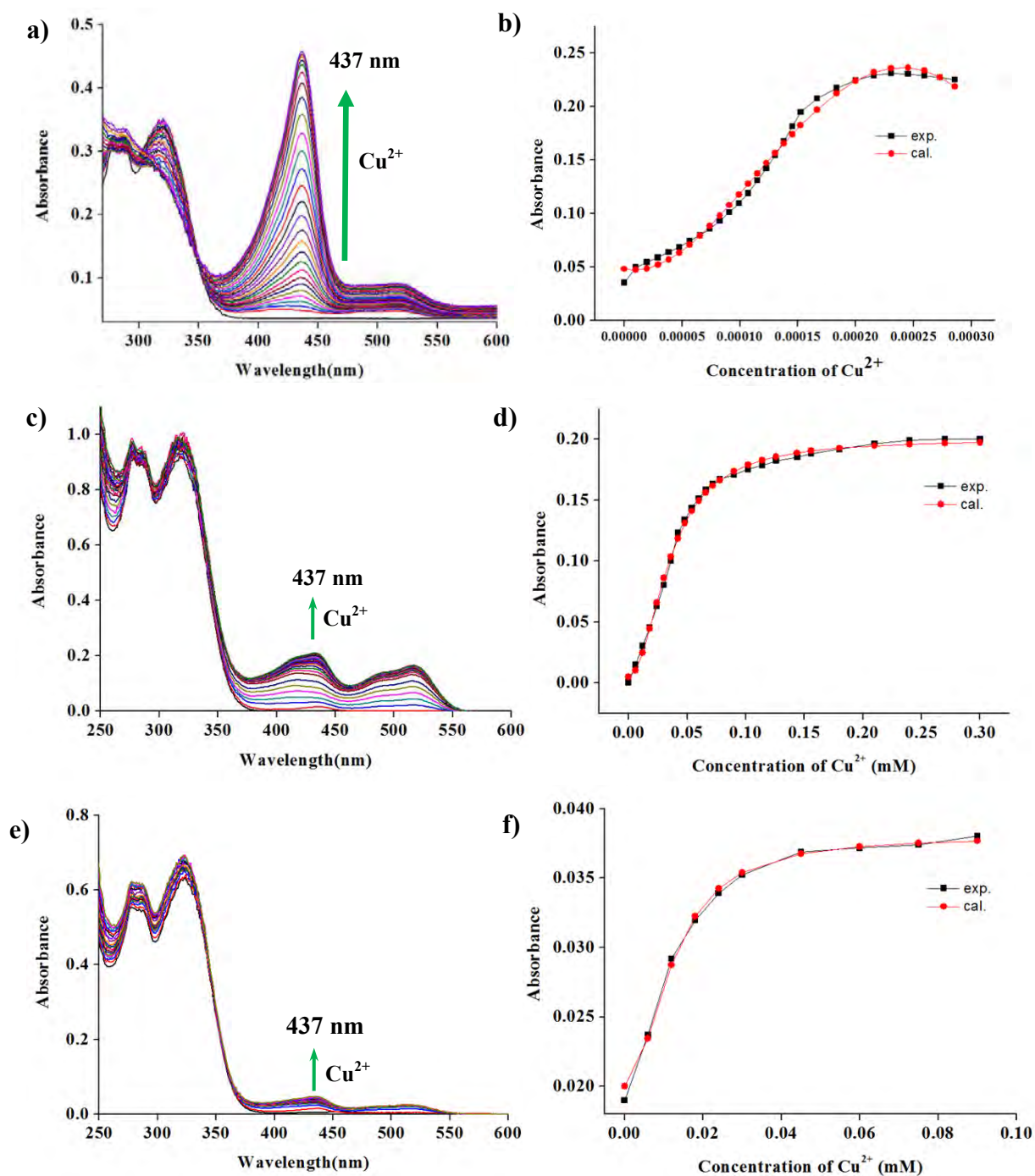


Figure 4.3 The UV-visible titration spectra of a) **F-oBOH** (2.5×10^{-5} M), c) **F-mBOH** (3.0×10^{-5} M), and e) **F-pBOH** (3.0×10^{-5} M) upon the gradual addition of copper(II) ion in CH₃CN and the compared experiment data and calculated data from UV-visible titration of b) **F-oBOH**, d) **F-mBOH**, and f) **F-pBOH** for calculation of the stability constant.

Herein, the structures of sensors contain two binding sites for copper(II) ion including a boronic part and a spirolactam ring. The association constant of sensors with copper(II) ion were determined by fitting the data of titration curves to a 1:2 binding model using the specfit 32 program and equation 4.1. In addition, sensor **F-oBOH** was selected to study the stoichiometry of sensors with copper(II) ion using the ESI-HRMS spectroscopy showing the intense peak of $[\mathbf{F-oBOH}+2\text{Cu}^{2+}+\text{MeOH}]$ at m/z of 629.5241 as shown in Figure 4.4. It strongly indicated that the stoichiometry of **F-oBOH** with copper(II) ion was 1:2 and corresponded to the binding of copper(II) ion at the spirolactam and boronic acid position shown in scheme 4.2.

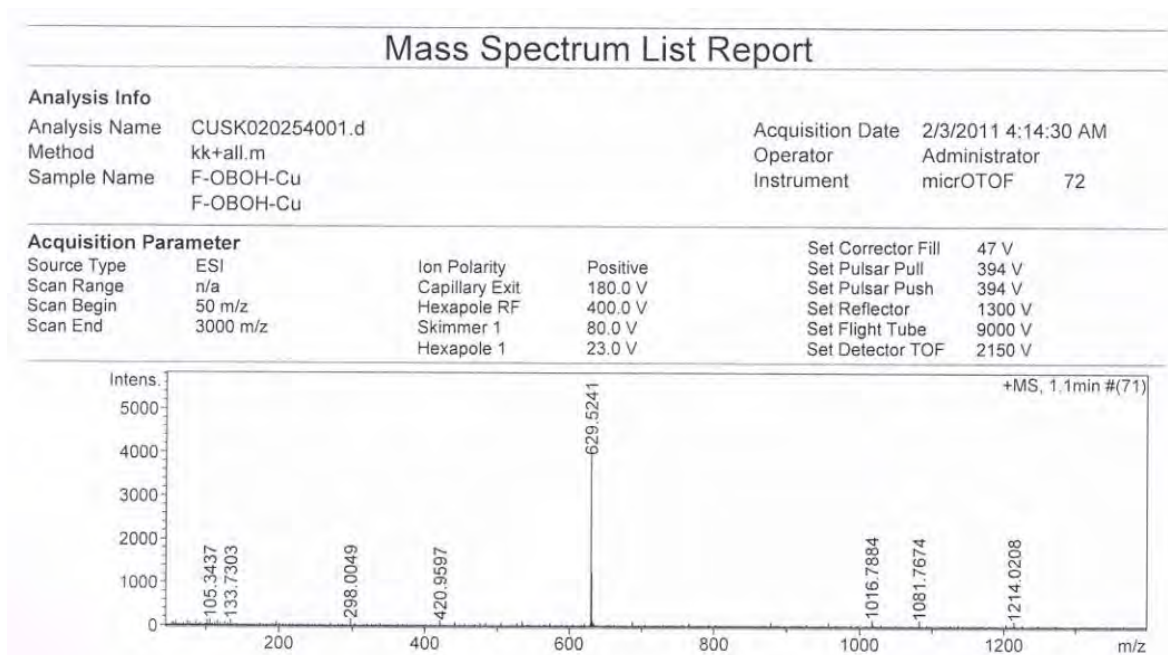
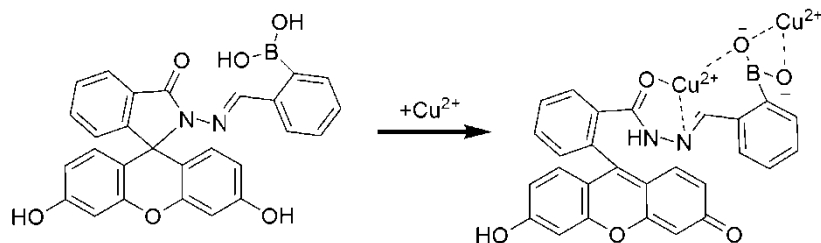


Figure 4.4 The ESI-High Resolution Mass Spectroscopy (ESI-HRMS) of the complexation between **F-oBOH** and copper(II) ion



Scheme 4.2 Purpose mechanism of **F-oBOH** complexation with copper(II) ion

Interestingly, our sensors have a boronic moiety which is an electron deficiency boron center that can alternate to be an electron rich by cyanide substitution on the boron atom. To study the cyanide complexation of **F-oBOH**–copper(II), the concentration of copper(II) ion of 1.75×10^{-3} M was used to study the cyanide complexation. Upon the addition of cyanide anion, the absorption band at 437 nm of **F-oBOH**–copper(II) decreased and turned to the original spectrum of **F-oBOH**. It suggested that cyanide anion can remove copper(II) ion from the binding site.

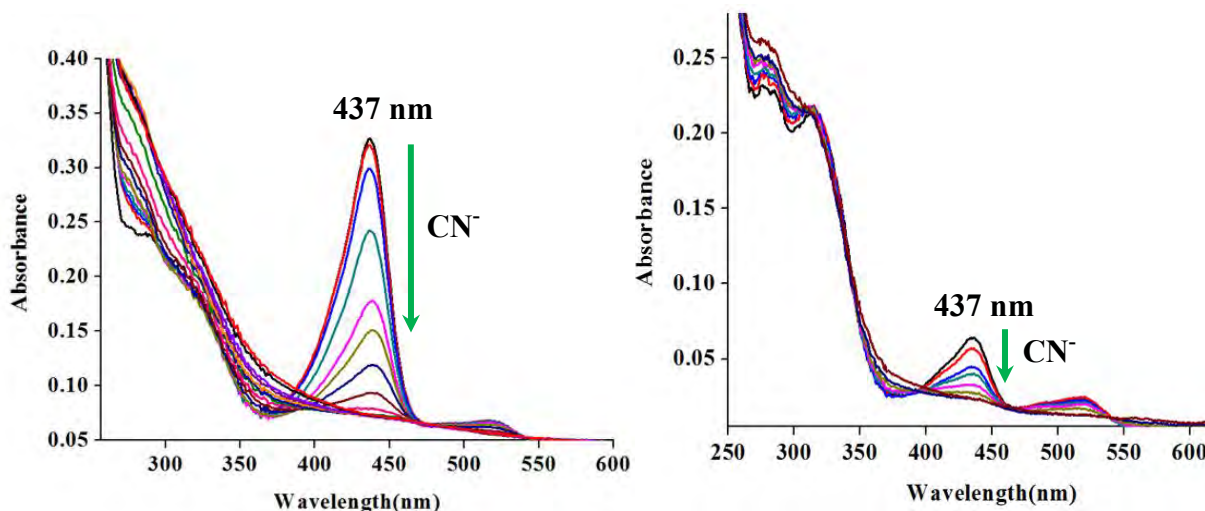


Figure 4.5 UV-vis spectra of a) **F-oBOH** (2.5×10^{-5} M) b) **F-mBOH** (2.5×10^{-5} M) and Cu^{2+} (1.75×10^{-3} M) in CH_3CN in the presence of different amounts of cyanide anion.

In deeply, the absorption spectrum in the region of 250-325 nm (corresponding to the boron part of **F-oBOH**) is unidentical with the original spectrum of **F-oBOH** (Figure 4.5). It suggested that the cyanide anion can coordinate at the boron center and the bound copper(II) ion at hydroxy group of boronic acid could not be taken off by the remaining cyanide ion. The binding mechanism was proposed in scheme 4.3. Furthermore, the observation of the color changes from strong yellow to colorless is consistent with the resultant as shown in Figure 4.6.

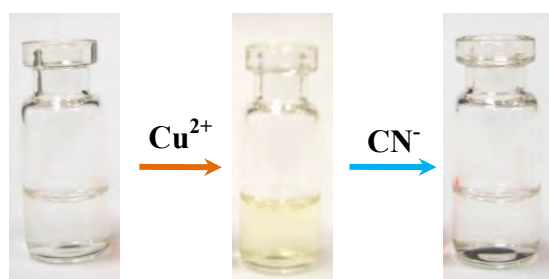
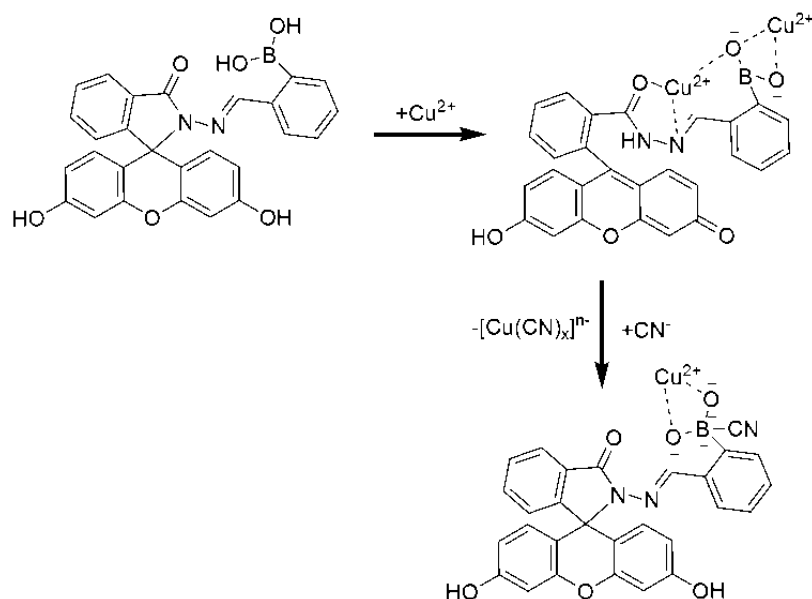


Figure 4.6 The color changes of **F-oBOH** (2.5×10^{-5} M) after adding and Cu^{2+} (1.75×10^{-3} M) and follows adding CN^- (2.5×10^{-4} M) in CH_3CN .



Scheme 4.3 Proposed mechanism of **F-oBOH** complexation with copper(II) ion and cyanide anion

4.4 Complexation Study of **F-oBOH**, **F-mBOH**, and **F-pBOH** in acetonitrile by fluorescence spectrophotometry

To verify the sensitivity of each sensor, fluorescence titrations of sensors were examined in acetonitrile using tetrabutylammonium hexafluorophosphate as the supporting electrolyte. Prior to fluorescence measurement, the solution mixture of the sensor and copper ion was stirred for 2 minutes. The fluorescence intensity of the complexation of **F-oBOH**, **F-mBOH**, and **F-pBOH** with copper(II) ion at 475 nm increased significantly as a function of cyanide concentration shown in Figure 4.7a, 4.7c, and 4.7e, respectively. The fluorescence titration was carried out at least twice. The $\log \beta$ values of **F-oBOH** and copper(II) ion are 8.02 calculated by Specfit 32 program showing the best fit curve in Figure 4.7b. Moreover, the $\log \beta$ values of **F-mBOH** and **F-pBOH** are 8.48 and 11.53 calculated by equation 4.2 showing the best fit curve in Figure 4.7d and 4.7f, respectively.

$$I = \frac{(I_0 + I_{lim}\beta[guest]^2)}{(1 + \beta[guest]^2)} \quad (4.2)$$

I = Intensity of a particular concentration of guest

I_0 = Initial intensity

I_{lim} = Limiting (final) intensity

β = Stability constant of the receptor with the guest

[guest] = concentration of guest

The $\log \beta$ values of **F-oBOH** < **F-mBOH** < **F-pBOH** were observed by both fluorescence and UV-vis techniques. However, the $\log \beta$ values obtained by fluorescence titration are much higher than those obtained by UV-visible titration.

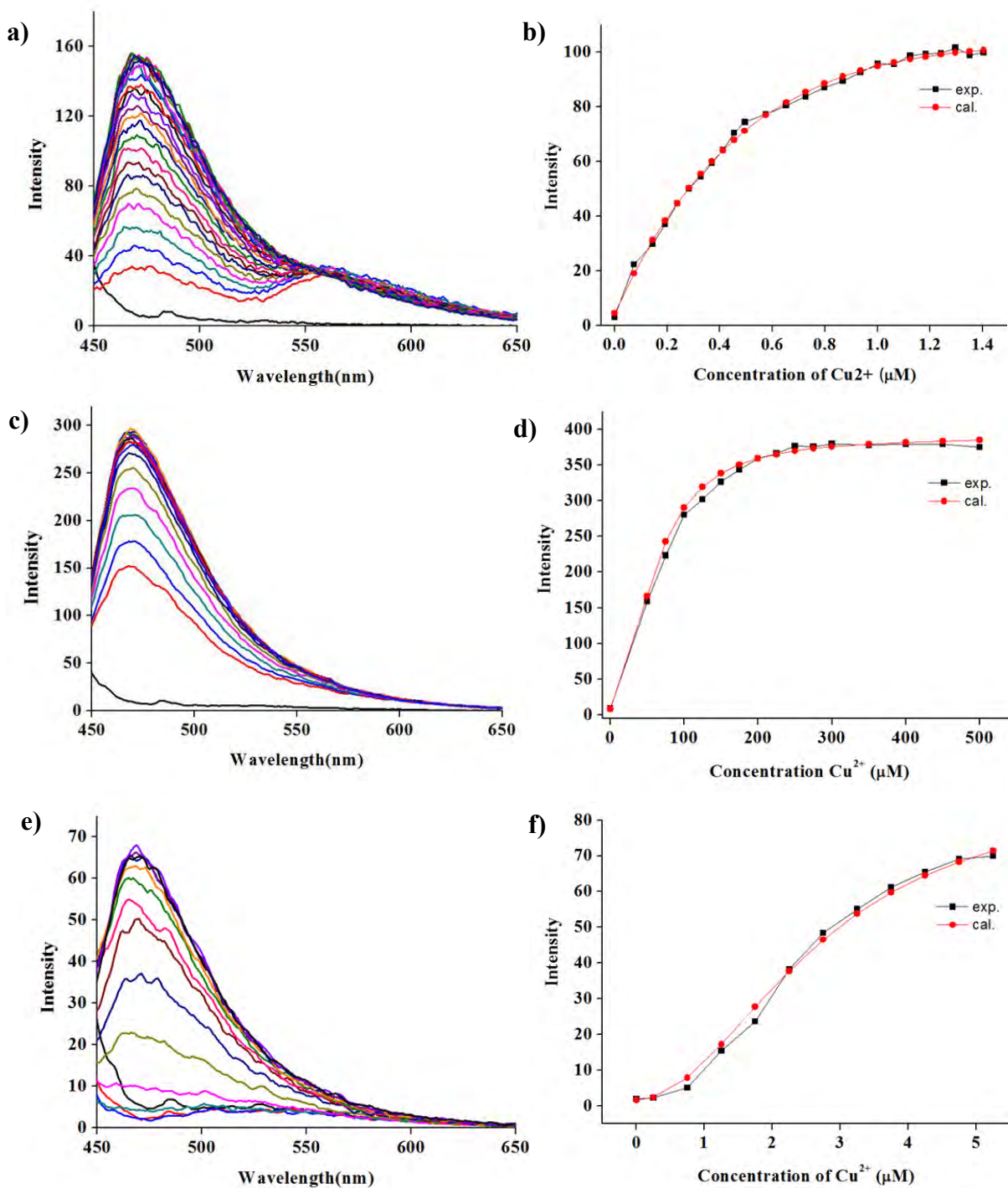


Figure 4.7 The fluorescence titration spectra of a) **F-*o*BOH**, c) **F-*m*BOH**, and d) **F-*p*BOH** (5×10^{-6} M) upon gradual addition of copper(II) ion in CH_3CN and the compared experiment data and calculated data from fluorescence titration of b) **F-*o*BOH**, d) **F-*m*BOH**, and f) **F-*p*BOH** for calculation of the stability constant. ($\lambda_{\text{ex}}/\lambda_{\text{emiss}} = 437/475$ nm)

4.6 Determination of detection limit of **F-*o*BOH**, **F-*m*BOH**, and **F-*p*BOH** with copper(II) ion by fluorescence spectrophotometry

The detection limit of **F-*o*BOH**, **F-*m*BOH**, and **F-*p*BOH** was evaluated by fluorescence spectroscopy. The 10 samples of **F-*o*BOH**, **F-*m*BOH**, and **F-*p*BOH** (5×10^{-6} M) were prepared and the intensity were measured (Table 4.1).

Table 4.1 The intensity of **F-*o*BOH**, **F-*m*BOH**, and **F-*p*BOH** (5×10^{-6} M)

Point	Intensity		
	F-<i>o</i>BOH	F-<i>m</i>BOH	F-<i>p</i>BOH
1	15.4194	12.0011	9.5410
2	16.3047	10.5800	10.1878
3	15.1501	9.2396	6.3245
4	16.5699	9.9443	7.2172
5	14.7407	11.0948	6.6163
6	14.0937	11.8388	6.9950
7	14.2172	11.1580	7.3621
8	16.5390	10.9071	8.3547
9	16.3850	9.5410	9.1373
10	15.0809	10.1878	9.0106
Standard Deviation	0.9507	0.9247	1.3457

The standard deviation of intensity of **F-*o*BOH**, **F-*m*BOH**, and **F-*p*BOH** is shown in Table 4.1. In addition, the linear relationships of **F-*o*BOH**, **F-*m*BOH**, and **F-*p*BOH** were plotted between the concentration of copper(II) ion and emission intensity at 475 nm shown in Figure 4.8 and the linear correlation, R^2 , listed in Table 4.2.

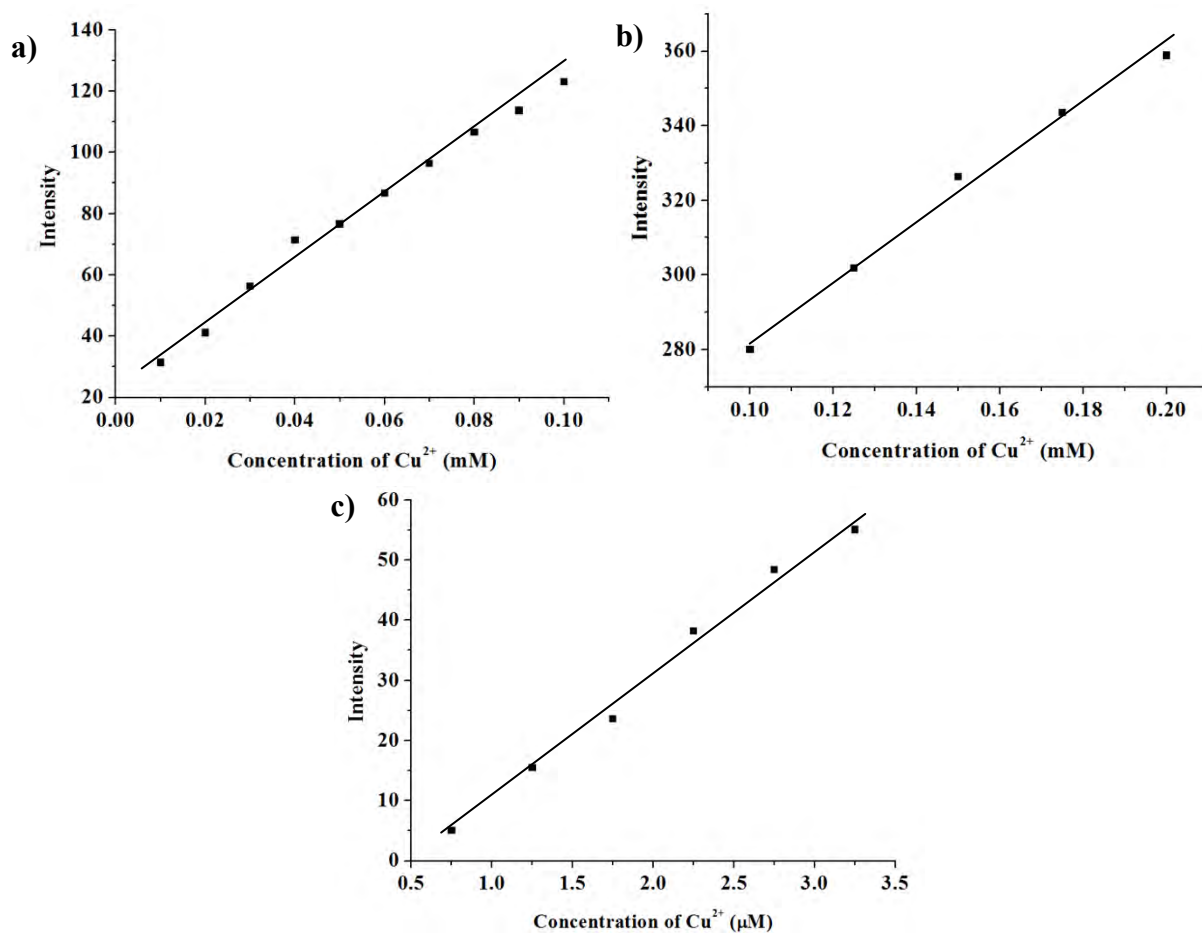


Figure 4.8 Linear plot between intensity of a) *F-oBOH* b) *F-mBOH* c) *F-pBOH* and concentration of copper(II) ion

The detection limit of three sensors was calculated as three times of the standard deviation of the background noise and shown in Table 4.2.

Table 4.2 The detection limit of *F-oBOH*, *F-mBOH*, and *F-pBOH*

Compound	Equation	R ²	Standard Deviation	Detection Limit
<i>F-oBOH</i>	$y = 1 \times 10^6 x + 24.634$	0.9902	0.9507	2.85 μM
<i>F-mBOH</i>	$y = 797492x + 202.47$	0.9912	0.9247	3.48 μM
<i>F-pBOH</i>	$y = 2 \times 10^7 - 10.617$	0.9915	1.3457	1.34 μM

The detection limit indicated that copper(II) ion interact with the hydroxy group of boronic acid at para position better than the meta and ortho position. Moreover, the results also imply that sensors can detect copper(II) ion in the micro molar range.

4.7 Study on the stability of F-*o*BOH

With the aim of developing new chemosensors which can lead to utilize in aqueous solution, therefore, these sensors in aqueous system were investigated. According to the reporting of Hyman [52], the fluorescein connected to boronate ester cannot bind significantly with any metals due to its instability by hydrolysis in aqueous solution. In this research, **F-*o*BOH** also consists of the metal binding site and is unstable in aqueous media. The hydrolysis process of **F-*o*BOH** in the presence of copper(II) ion was investigated by using fluorescence spectrophotometry technique. According to the fluorescence spectra of **F-*o*BOH** + copper(II) under various time, the fluorescence intensity at 518 nm increased upon the increment of time from 0-180 minutes (shown in Figure 4.9 a, b). This observation is indication of the unstable complex of **F-*o*BOH** with copper(II) ion in aqueous solution at pH 7.0 as shown in scheme 4.4.

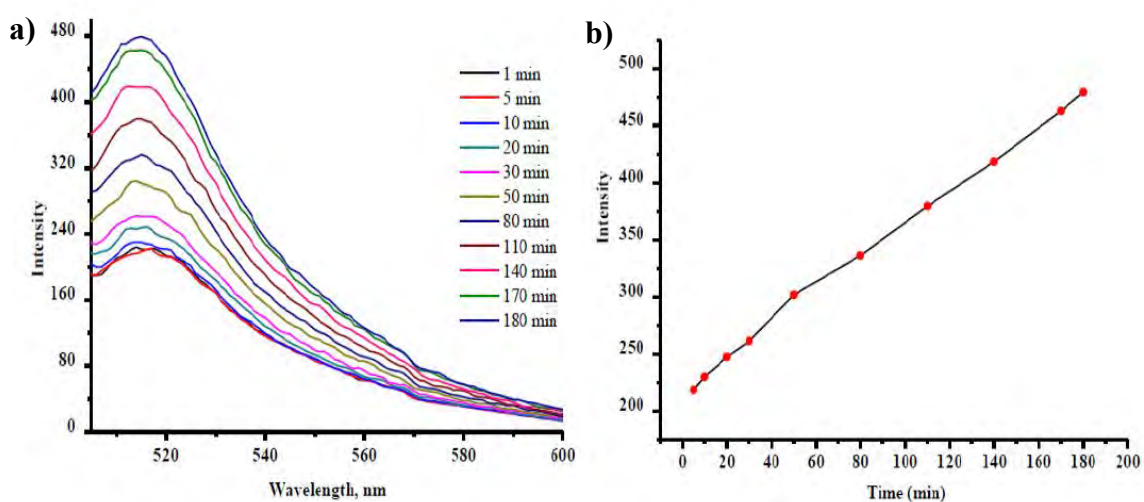
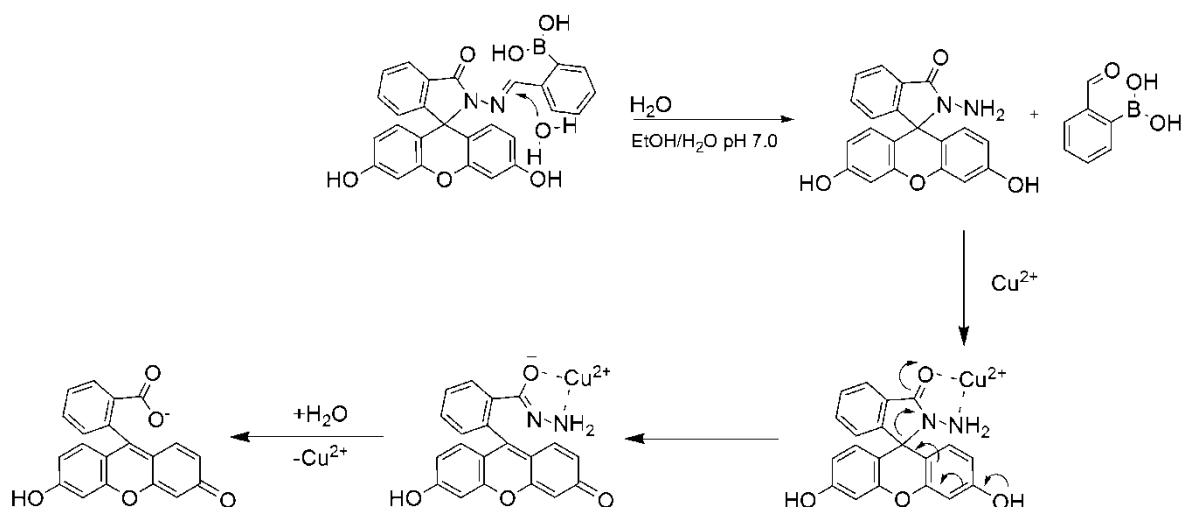


Figure 4.9 Fluorescence spectra of **F-*o*BOH** (5 μM) a) in the presence copper(II) ion (5 μM) b) The emission intensity at 518 nm in the presence copper(II) (5 μM) under various time in Tris-HCl 0.01 M pH 7.0 buffer solution (5% EtOH:water), ($\lambda_{\text{ex}} = 498 \text{ nm}$)



Scheme 4.4 Proposed the hydrolysis mechanism of the **F-oBOH** and water followed by reaction with copper(II) to yield fluorescent fluorescein.

With attempts to illustrate the hydrolysis process of sensors, we prepared the hydrolysis product in ethanol and Tris buffer at pH 8.5 which is the suitable pH to generate hydrolysis product in water. According to the ¹H-NMR spectra in Figure 4.11, the hydrolysis product of **F-oBOH** shows the proton signals at 10.15, 8.25, 7.50 ppm in consistent with ¹H-NMR spectra of 2-formylphenyl boronic acid. However, the **F-oBOH** is still remaining in the reaction. These results strongly support the evidence of the hydrolysis product of **F-oBOH**. Furthermore, the hydrolysis product of **F-mBOH** and **F-pBOH** were evaluated along with the similar method preparation. The results showed that the hydrolysis products of **F-mBOH** and **F-pBOH** are similar to those of **F-oBOH**.

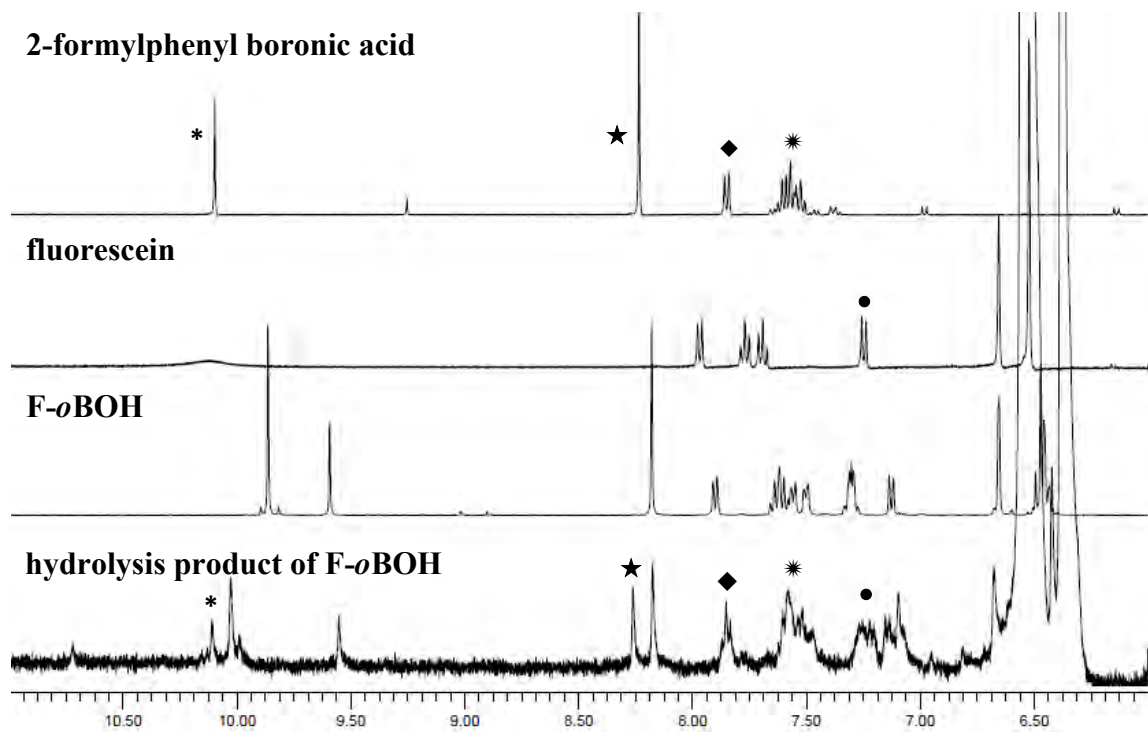
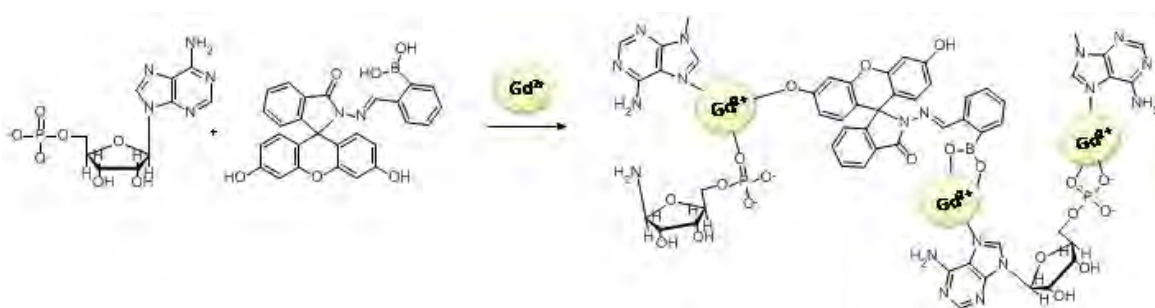


Figure 4.10 Comparing experiment of hydrolysis product of **F-*o*BOH** with **F-*o*BOH**, fluorescein, and 2-formylphenyl boronic acid

4.8 Preparation of F-*o*BOH doped nucleotide/lanthanide CNPs (F-*o*BOH-AMP/Gd³⁺ CNPs)

Due to the hydrolysis phenomenon of receptors composing of hydrazone unit, it represents a promising problem and inspires researchers to create other receptors which highly stable in an appropriate aqueous media. In addition, their applications in many disciplines such as cell culture and antitubercular are very attractive. [53-54] To overcome this limitation, we especially took forward efforts to search for the new strategy of a fluorescence turn-on sensor system without hydrolysis process. We manipulated adaptive self-assembly of subunits which could spontaneously form with a following of the shape of guest molecule in water. Nishiyabu [40-41] reported that the coordination nanoparticles (CNPs) were naturally formed in water by incorporation of nucleotides, lanthanide ions, and dye molecules. In this research, the coordination nanoparticles were prepared according to the Nishiyabu procedure by adding gadolinium(III) nitrate (Gd(NO₃)₃) into an aqueous mixture of adenosine monophosphate (AMP) and F-*o*BOH under stirring. The schematic 4.5 describes the formation possibility of coordination nanoparticles of F-*o*BOH-AMP/Gd³⁺ CNPs. Nanoparticles of F-*o*BOH-AMP/Gd³⁺ CNPs with average diameter of 60 nm were spontaneously formed and characterized by scanning and transmission electron microscopy (SEM and TEM, Figure 4.12 a, b).



Scheme 4.5 A schematic illustration of nanoparticles formation through the self-assembly of F-*o*BOH, AMP, and Gd³⁺ ion (F-*o*BOH-AMP/Gd³⁺ CNPs).

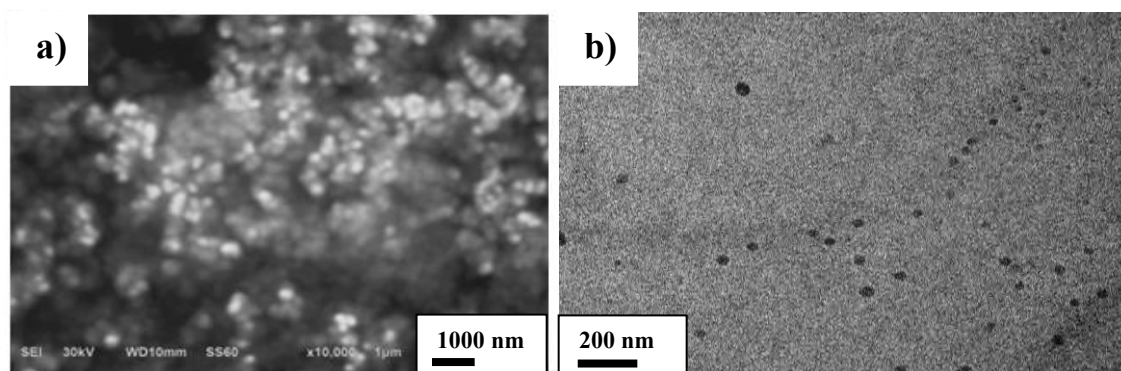


Figure 4.11 a) SEM image of **F-oBOH-AMP/Gd³⁺** CNPs b) TEM image of **F-oBOH-AMP/Gd³⁺** CNPs

4.9 The stability study of **F-oBOH-AMP/Gd³⁺** CNPs

In our hypothesis, the coordination nanoparticles were expected to protect the hydrazone unit from hydrolysis due to the interior hydrophobic shell of coordination nanoparticles. Then, the stability of **F-oBOH-AMP/Gd³⁺** CNPs was examined by monitoring the fluorescence spectra of **F-oBOH-AMP/Gd³⁺** CNPs \subset copper(II) under various time from 0-120 minutes. The fluorescence intensity at 515 nm of **F-oBOH-AMP/Gd³⁺** CNPs \subset copper(II) is constant during the measurement (shown in Figure 4.12). This implied that **F-oBOH** is stable in aqueous solution with an assistance of AMP/Gd³⁺ nanoparticles.

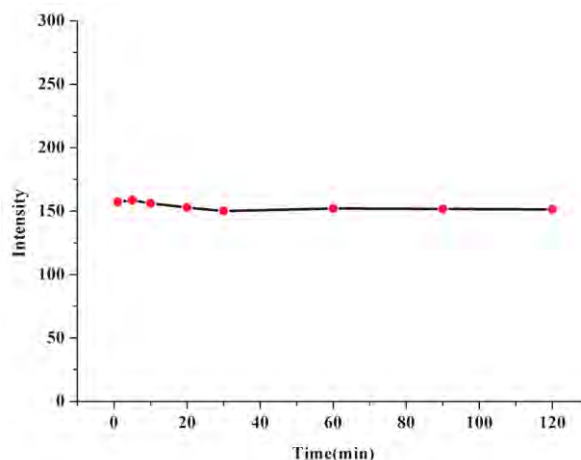


Figure 4.12 Fluorescence intensity at 515 nm for **F-oBOH-AMP/Gd³⁺** CNPs \subset copper(II) under various time from 0-120 minutes. ($\lambda_{ex} = 492$ nm)

4.10 Complexation studies of **F-oBOH-AMP/Gd³⁺ CNPs** \subset **copper(II)** with various anions: fluoride, chloride, bromide, iodide, hydroxide, nitrate, perchlorate, benzoate, dihydrogenphosphate, thiocyanate, and cyanide

According to the previous study of **F-oBOH** in acetonitrile, the results explained that **F-oBOH** shows a selectivity toward copper(II) ion. Therefore, the copper(II) ion is selected to be used for opening the spirolactam ring of **F-oBOH** in **F-oBOH-AMP/Gd³⁺ CNPs**. As described in scheme 4.5, the boronic acid of **F-oBOH** has a vacancy site, thus, anion is expected to react at the boronic site of **F-oBOH-AMP/Gd³⁺ CNPs**. Therefore, in this section, the selectivity of **F-oBOH-AMP/Gd³⁺ CNPs** \subset **copper(II)** toward various anions was evaluated by fluorescence spectrophotometry. As depicted in Figure 4.13, a large change of fluorescence response of **F-oBOH-AMP/Gd³⁺ CNPs** \subset **copper(II)** was observed in the presence of cyanide anion. These results revealed that **F-oBOH-AMP/Gd³⁺ CNPs** \subset **copper(II)** had an excellent selectivity for cyanide anion.

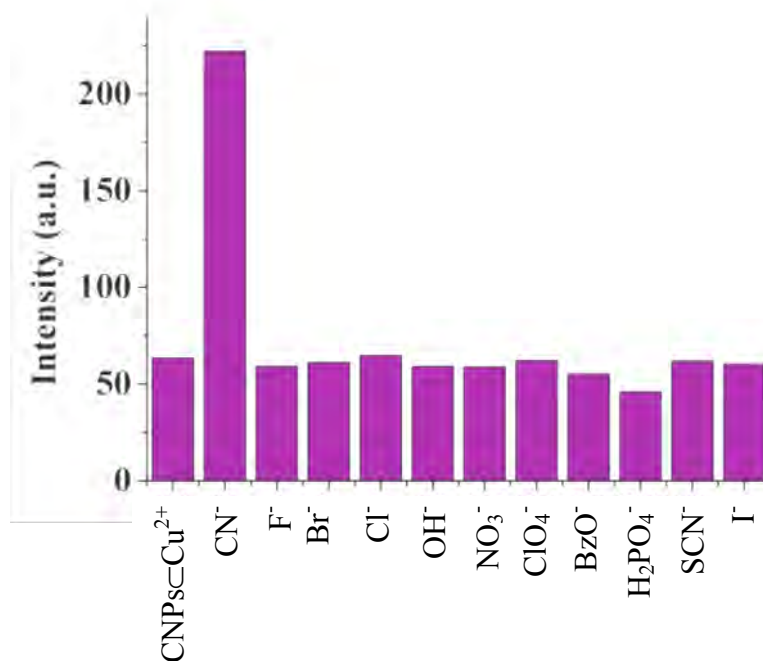


Figure 4.13 Fluorescence intensity of **F-oBOH-AMP/Gd³⁺ CNPs** \subset **copper(II)** at 515 nm in the presence of different anions (500 μ M) in HEPES (0.1M) pH 7.4 ($\lambda_{\text{ex}} = 492$ nm)

Furthermore, the fluorescence spectra of **F-*o*BOH-AMP/Gd³⁺** CNPs exhibited very low intensity at 515 nm after adding copper(II) ion (shown in Figure 4.14a). Similarly, a very low fluorescence intensity of **F-*o*BOH-AMP/Gd³⁺** CNPs was observed upon addition of cyanide anion (shown in Figure 4.14b). Interestingly, the fluorescence spectra of **F-*o*BOH-AMP/Gd³⁺** CNPs in the presence of copper(II) was significantly increased after adding of cyanide anion (shown in Figure 4.15).

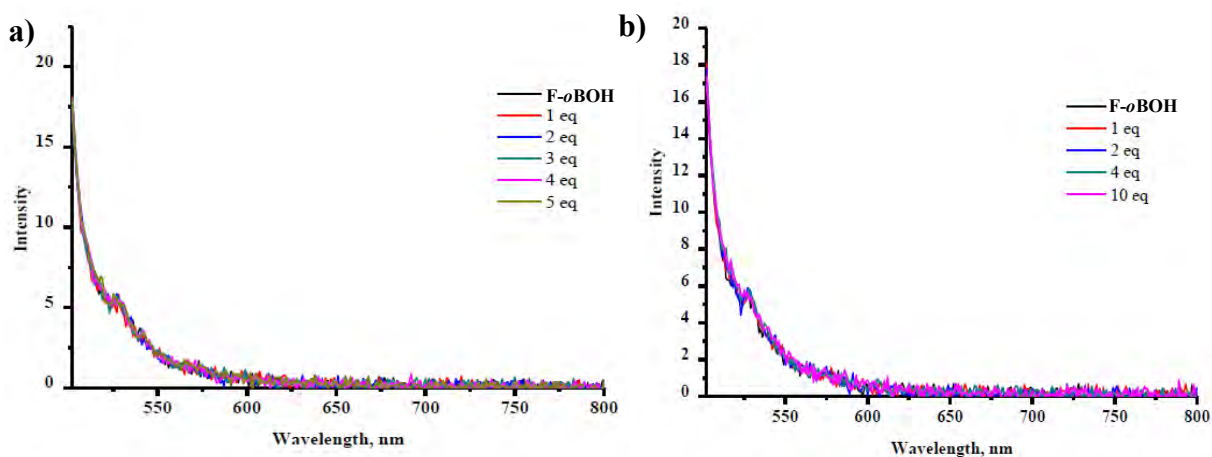


Figure 4.14 Fluorescence spectra of **F-*o*BOH-AMP/Gd³⁺** CNPs in the presence of different amount of (a) copper(II) ion and (b) cyanide anion in HEPES buffer pH 7.4.

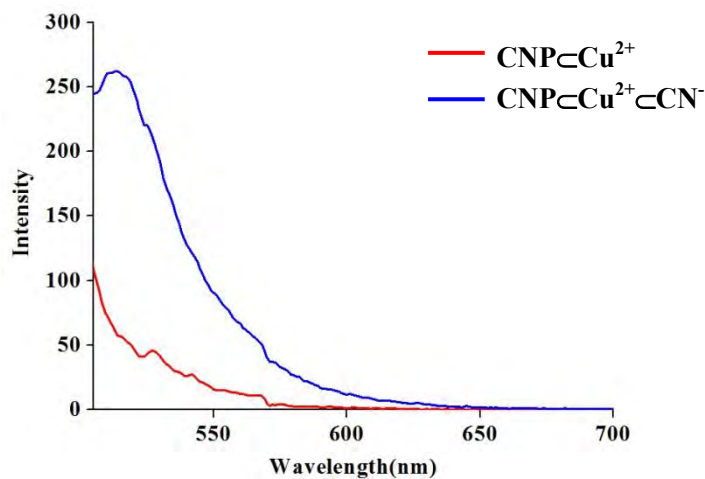


Figure 4.15 Fluorescence spectra of **F-*o*BOH-AMP/Gd³⁺** CNPs in the presence of copper(II) upon addition of cyanide anion in HEPES buffer pH 7.4.

Moreover, the naked-eyes investigation was performed as illustrated in Figure 4.16. The obvious color changes from colorless to sky blue of **F-oBOH-AMP/Gd³⁺** CNPs=Copper(II) upon addition of cyanide anion are shown in Figure 4.16a. In addition, the samples were illuminated by the 356 nm UV light and showed a strong luminescence of **F-oBOH-AMP/Gd³⁺** CNPs=Cu²⁺ after adding cyanide anion. Furthermore, the coordination nanoparticles of AMP/Gd³⁺ CNPs=Cu²⁺ without **F-oBOH** did not exhibit a change after adding cyanide anion. This suggested that the large color and luminescence changes were caused by **F-oBOH** incorporated in AMP/Gd³⁺ CNPs.

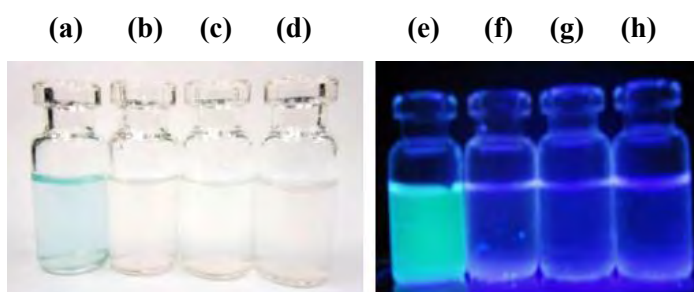


Figure 4.16 Photograph of Naked-eyes of (a) **F-oBOH-AMP/Gd³⁺** CNPs in the presence of Cu²⁺ 45 equiv and CN⁻ 90 equiv (b) **F-oBOH-AMP/Gd³⁺** CNPs in the presence of Cu²⁺ 45 equiv (c) AMP/Gd³⁺ CNPs in the presence of Cu²⁺ 45 equiv and CN⁻ 90 equiv (d) AMP/Gd³⁺ CNPs in the presence of Cu²⁺ 45 equiv and Luminescent of (e) **F-oBOH-AMP/Gd³⁺** CNPs in the presence of Cu²⁺ 45 equiv and CN⁻ 90 equiv (f) **F-oBOH-AMP/Gd³⁺** CNPs in the presence of Cu²⁺ 45 equiv (g) AMP/Gd³⁺ CNPs in the presence of Cu²⁺ 45 equiv and CN⁻ 90 equiv (h) AMP/Gd³⁺ CNPs in the presence of Cu²⁺ 45 equiv. Samples were illuminated by the 356 nm UV light.

4.11 Job's plot analyses for F-*o*BOH-AMP/Gd³⁺ CNPs⊂copper(II) with cyanide anion and F-*o*BOH-AMP/Gd³⁺ CNPs⊂cyanide with copper(II) by fluorescence spectrophotometry

In the section 4.10, the result showed the selectivity of F-*o*BOH-AMP/Gd³⁺ CNPs⊂copper(II) toward cyanide anion. Herein, the stoichiometry between F-*o*BOH-AMP/Gd³⁺ CNPs⊂copper(II) and cyanide anion was determined by Job's continuous variation method. The maximum of the corresponding Job's plot shown in Figure 4.17 indicated the stoichiometry in 1:1 complexation of F-*o*BOH-AMP/Gd³⁺ CNPs⊂copper(II) and cyanide anion observing from a maximal value at 0.5.

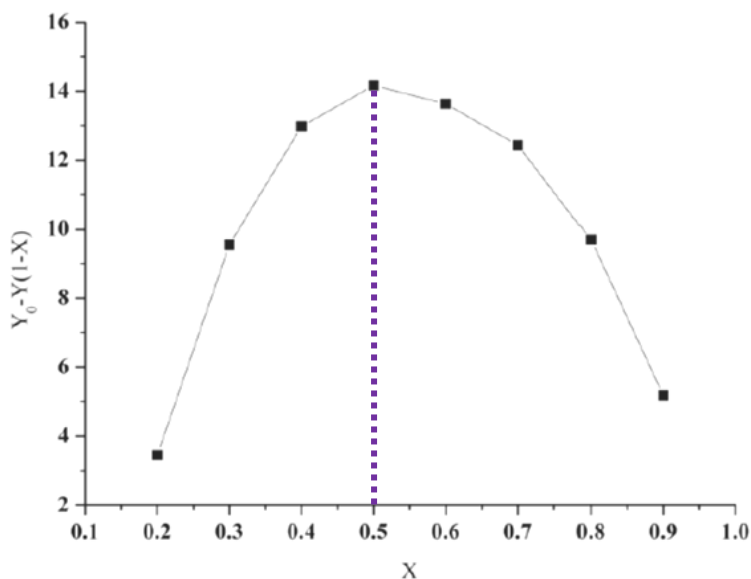


Figure 4.17 Job's plot analysis of fluorescence intensity for the complexation of the F-*o*BOH-AMP/Gd³⁺ CNPs⊂copper(II) and cyanide anion. The molar ratio of F-*o*BOH-AMP/Gd³⁺ CNPs⊂copper(II) CNPs to cyanide anion was varied: 2:8, 3:7, 4:6, 5:5, 6:4, 7:3, 8:2, 9:1.

Due to the previous studies of **F-oBOH** in acetonitrile demonstrated that **F-oBOH** can bind with copper(II) ion in a ratio of 1:2 referring to the binding of copper(II) cation at a spirolactam and hydroxy groups of boronic acid. In scheme 4.5, the proposed structure of **F-oBOH-AMP/Gd³⁺** CNPs illustrated the coordination of boronic acid with gadolinium(III), therefore, copper(II) ion can coordinate with **F-oBOH-AMP/Gd³⁺** CNPs at spirolactam ring only. In order to prove the stoichiometry of **F-oBOH-AMP/Gd³⁺** CNPs and copper(II) ion, Job's plot method was used to determine the stoichiometry. Firstly, **F-oBOH-AMP/Gd³⁺** CNPs was doped with cyanide anion and provided the complex of **F-oBOH-AMP/Gd³⁺** CNPs \subset cyanide. After substitution of the cyanide anion on the boron center, the electron poor property was converted to be an electron rich center which can assist the binding of copper(II) ion at a spirolactam ring of **F-oBOH**. The Job's plot shown in Figure 4.18, is indicative of the 1:1 stoichiometry of **F-oBOH-AMP/Gd³⁺** CNPs \subset cyanide and copper(II) ion. This result tremendously confirms that the boronic acid moiety cannot coordinate with copper(II) ion but possibly coordinate with gadolinium(III) cation.

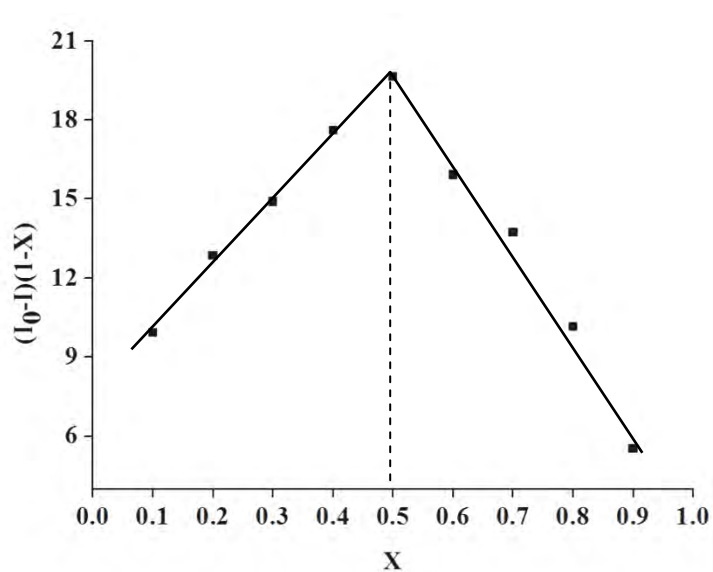
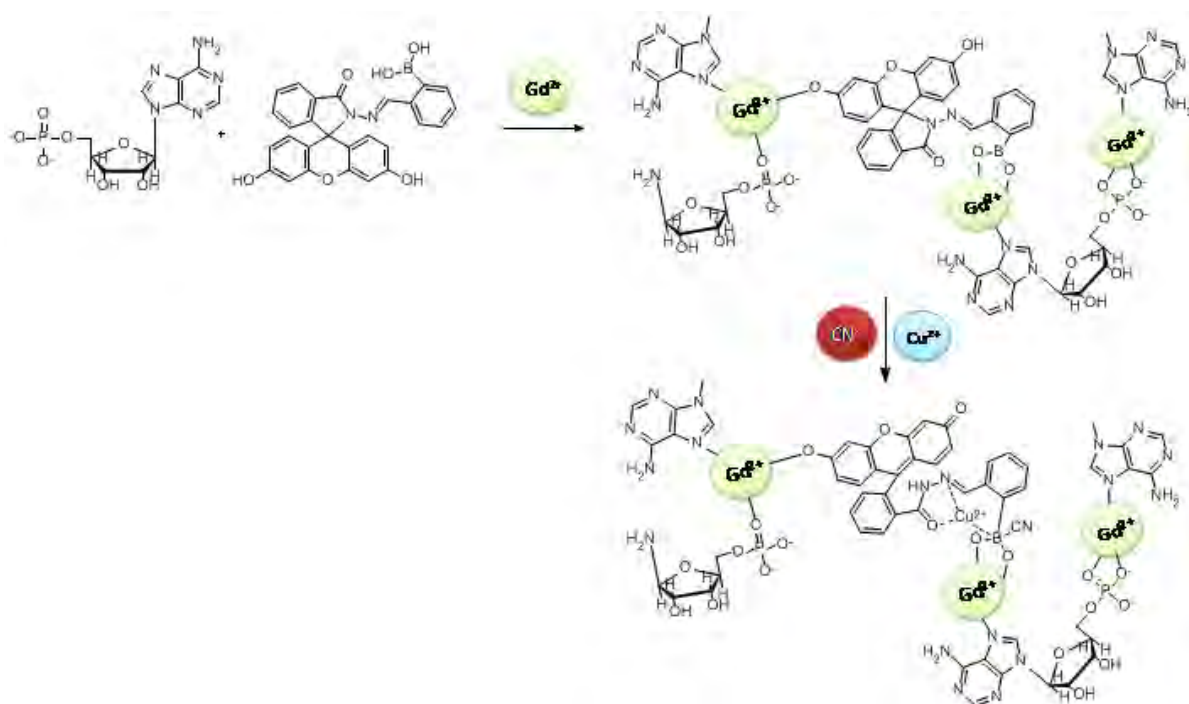


Figure 4.18 Job's plot analysis of fluorescence intensity for the complexation of the **F-oBOH-AMP/Gd³⁺** CNPs \subset cyanide and copper(II). The molar ratio of **F-oBOH-AMP/Gd³⁺** CNPs \subset cyanide and copper(II) was varied: 1:9, 3:7, 4:6, 5:5, 6:4, 7:3, 8:2, 9:1.

The possible mechanism of **F-*o*BOH-AMP/Gd³⁺** CNPs≃copper(II) with cyanide anions is shown in Scheme 4.6. It suggests that cyanide anions react with a vacancy site at boron center of **F-*o*BOH-AMP/Gd³⁺** CNPs≃copper(II). Therefore, both cyanide anion and copper(II) cation can support the ring opening of **F-*o*BOH** resulting in the enhancement of fluorescence response.



Scheme 4.6 The description of nanoparticles formation through the self-assembly of **F-*o*BOH**, AMP, and Gd^{3+} and the proposed mechanism of **F-*o*BOH-AMP/Gd³⁺** CNPs after adding copper(II) and cyanide anions.

To verify the incorporation of copper(II) ion into **F-oBOH-AMP/Gd³⁺** CNPs, the energy dispersive X-ray (EDX) analysis was investigated. The **F-oBOH-AMP/Gd³⁺** CNPs-copper(II)-cyanide anion was prepared and washed with water several times to remove the remaining copper(II) ion and cyanide anion in solution. The **F-oBOH-AMP/Gd³⁺** CNPs-copper(II)-cyanide anion was collected by ultracentrifugation and redispersion in water using sonication technique. Then, the sample was brought to analyze the incorporated copper(II) ion and other composition of coordination nanoparticles by EDX analysis shown in Figure 4.19. The EDX spectrum shows the characteristic peak of copper element at 8.04 eV, attributing to the incorporated copper(II) ion in **F-oBOH-AMP/Gd³⁺** CNPs. Besides, the EDX spectrum shows the characteristic peak of gadolinium element at 6.05 eV and the characteristic peak of phosphorus at 2.01 eV assigned to the phosphorous element of adenosine monophosphate (AMP). Thus, the EDX analysis give a strong evidence of the formation of copper(II) ion incorporated into the **F-oBOH-AMP/Gd³⁺** CNPs.

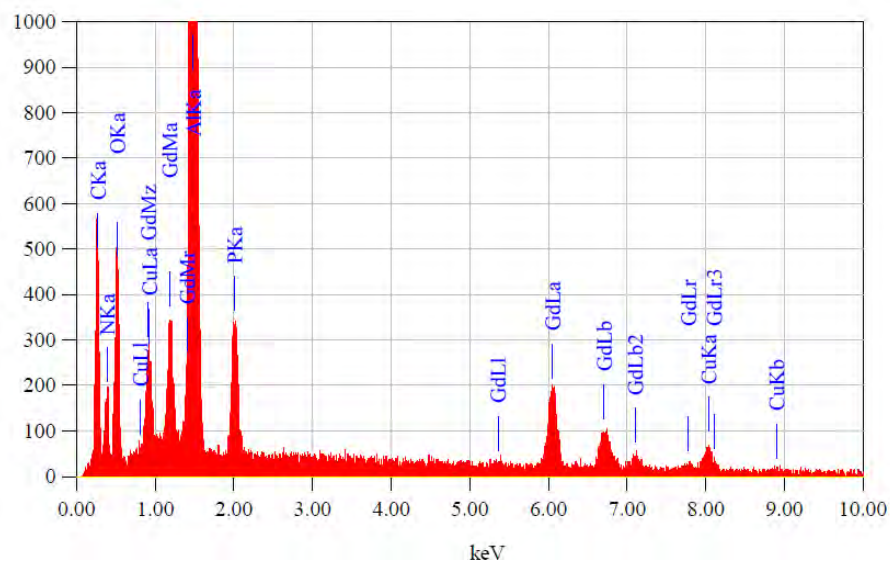


Figure 4.19 Energy dispersive X-ray (EDX) spectrum of **F-oBOH-AMP/Gd³⁺** CNPs-copper(II)-cyanide anion. (Aluminium peak is from the supporting aluminium stub)

4.12 Complexation studies of **F-oBOH-AMP/Gd³⁺ CNPs**–copper(II) with cyanide anion by fluorescence spectrophotometry

To determine the binding ability of **F-oBOH-AMP/Gd³⁺ CNPs**–copper(II) with cyanide anion, fluorescence titration was carried out in HEPES pH 7.4. Prior to fluorescence measurement, the solution mixture of **F-oBOH-AMP/Gd³⁺ CNPs**–copper(II) and cyanide anion was stirred for 2 minutes. The emission intensity at 515 nm of the complexation of **F-oBOH-AMP/Gd³⁺ CNPs**–copper(II) with cyanide anion increased as a function of cyanide concentration as shown in Figure 4.20. The fluorescence titration was measured at least twice. The stability constant of **F-oBOH-AMP/Gd³⁺ CNPs**–copper(II) with cyanide anion calculated by fitting data of titration curves at a 1:1 binding model using the Specfit 32 program gives the logK values of 3.97 (shown in Figure 4.21).

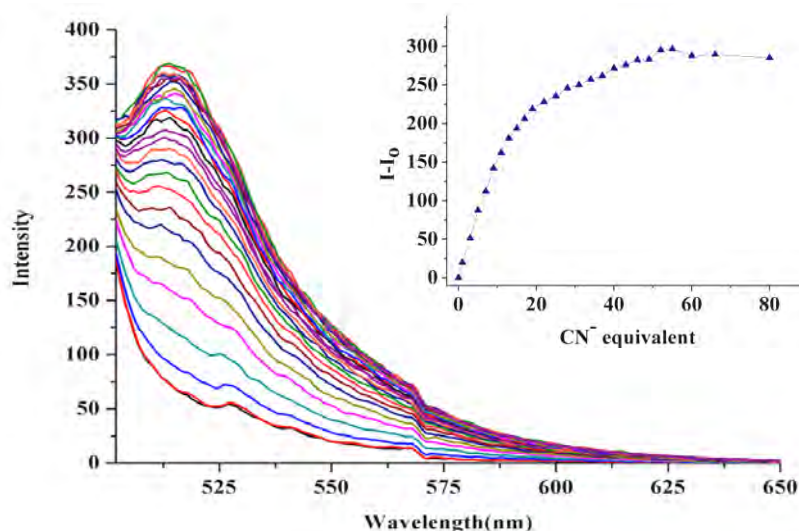


Figure 4.20 Fluorescence titration spectra of **F-oBOH-AMP/Gd³⁺ CNPs**–copper(II) in HEPES (0.1M) pH 7.4 upon addition of CN^- (0-80 equiv) at emission band at 515 nm. Inset: Titration curve of **F-oBOH-AMP/Gd³⁺ CNPs**–copper(II) and cyanide anion. ($\lambda_{\text{ex}}/\lambda_{\text{emis}} = 492/515 \text{ nm}$).

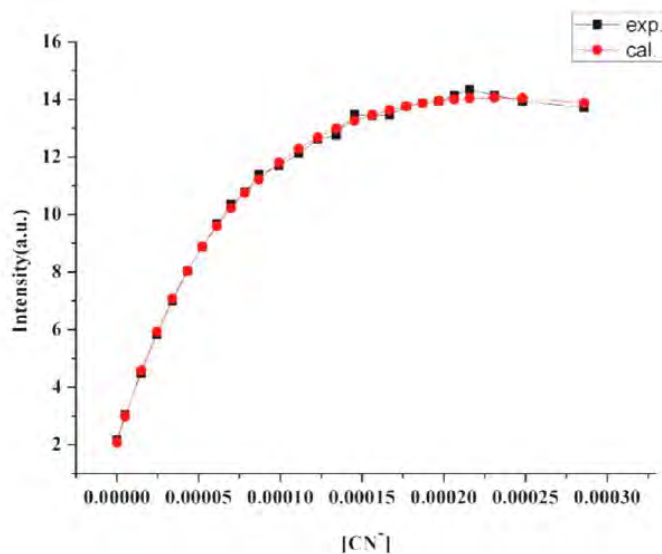


Figure 4.21 Comparing experiment and calculated data from Fluorescence titration curves of **F-*o*BOH-AMP/Gd³⁺ CNPs \subset copper(II)** and cyanide anion for calculation of stability constant ($\lambda_{\text{ex}}/\lambda_{\text{emis}} = 492/515 \text{ nm}$).

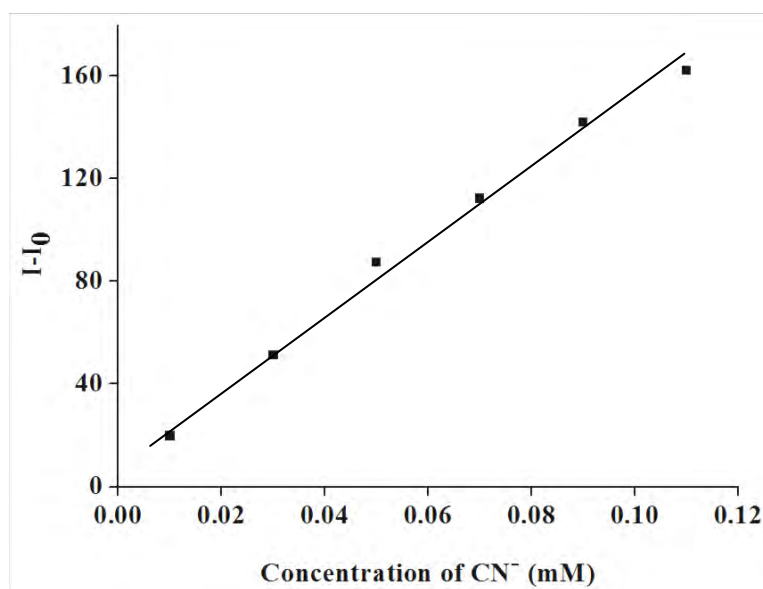
4.13 Determination of detection limit of F-*o*BOH-AMP/Gd³⁺ CNPs \subset copper(II) toward cyanide anion

4.13.1 Fluorescence spectrophotometry: Calculation method

The detection limit of **F-*o*BOH-AMP/Gd³⁺ CNPs \subset copper(II)** was observed by fluorescence spectroscopy. The 10 samples of **F-*o*BOH-AMP/Gd³⁺ CNPs \subset copper(II)** was prepared and measured the intensity (shown in Table 4.3). The standard deviation (SD) of intensity was 1.938. The linear plot was carried out between the concentration of cyanide anion and emission intensity at 515 nm displaying the best linear correlation, R^2 of 0.993 as shown in Figure 4.22. The standard deviation (SD) of the background noise was repeated three times and the detection limit of cyanide for **F-*o*BOH-AMP/Gd³⁺ CNPs \subset copper(II)** is 4.03 μM (0.198 ppm) which is nearly equal to the minimum level defined by the World Health Organization [55].

Table 4.3 The intensity of F-*o*BOH-AMP/Gd³⁺ CNPs-copper(II) (1×10^{-5} M)

Point	Intensity
1	69.53281
2	68.02630
3	68.59849
4	64.97699
5	66.84428
6	68.86111
7	63.84298
8	65.72705
9	65.43518
10	65.26340
Standard Deviation	1.938492

**Figure 4.22** Linear plot between intensity and concentration of cyanide anion

4.13.2 Naked-eyes detection limit

In addition, the naked-eyes detection limit of **F-*o*BOH-AMP/Gd³⁺** CNPs \subset copper(II) was evaluated. Accordingly, the photos of **F-*o*BOH-AMP/Gd³⁺** CNPs \subset copper(II) were shown at different concentration of the cyanide anion. Figure 4.23 demonstrates the process of color changes of **F-*o*BOH-AMP/Gd³⁺** CNPs \subset copper(II) from colorless to sky blue by adding various concentration of cyanide anion from 20 – 400 μ M. The visual detection limit of **F-*o*BOH-AMP/Gd³⁺** CNPs \subset copper(II) toward cyanide anion is 20 μ M.



Figure 4.23 Naked-eyes of **F-*o*BOH-AMP/Gd³⁺** CNPs \subset copper(II) in HEPES (0.1M) pH 7.4 in the presence of different concentrations of cyanide anion. From left to right ($\times 10 \mu$ M): **F-*o*BOH-AMP/Gd³⁺**, 0, 2.0, 4.0, 7.0, 10.0, 20.0 30.0, and 40.0.

4.14 Interference studies of F-*o*BOH-AMP/Gd³⁺ CNPs⊂copper(II) by fluorescence spectrophotometry

The effect of foreign substances was investigated by considering a standard solution of cyanide anion to the added interference species. The tolerance amount and the value (%) of relative error of F-*o*BOH-AMP/Gd³⁺ CNPs⊂copper(II) are displayed in Table 4.4. The evaluated principle for interferences is fixed at a $\pm 10\%$ relative error. From Table 4.4, it was found that the coexisting substances showing slightly effects on the determination of cyanide anion for F-*o*BOH-AMP/Gd³⁺ CNPs⊂copper(II). In the case of H₂PO₄, it cannot be determined the tolerance limit value because H₂PO₄ can interrupt the coordination nanoparticles system due to the competition binding of phosphate group with gadolinium and F-*o*BOH. Furthermore, H₂PO₄ has a pH effect on the solution of F-*o*BOH-AMP/Gd³⁺ CNPs⊂copper(II).

Table 4.4 Effect of interference anions on the determination of cyanide anion ($C_{CN} = 24.5$ ($\mu\text{g/mL}$))

Foreign Anion	equivalent	%relative error	[Interfere] M	Tolerance limit ($\mu\text{g/mL}$)
Cl ⁻	1000	0.620	0.5000	29220
Br ⁻	1000	1.248	0.5000	51450
NO ₃	1000	1.300	0.5000	42505
ClO ₄	1000	3.610	0.5000	70230
I ⁻	100	7.160	0.0500	7495
SCN ⁻	100	8.740	0.0500	4859
BzO ⁻	100	4.125	0.0500	7206
OH ⁻	10	6.743	0.0050	200
F ⁻	5	9.514	0.0025	145
H ₂ PO ₄	n.d. ^a	n.d. ^a	n.d. ^a	n.d. ^a

^anot determine

CHAPTER V

CONCLUSION

5.1 Conclusion

With the recognition of copper and cyanide ions as an objective, we have investigated the synthesis and ion binding properties of boronic sensors and spirolactam ring. In particular, the sensors **F-oBOH**, **F-mBOH**, and **F-pBOH** bearing a boronic acid and a spirolactam ring have been synthesized by the reaction of fluorescein hydrazide and formylphenyl boronic acid using sulfuric acid as a catalyst. The target sensors were obtained after recrystallization in hexane and ethyl acetate (**F-oBOH** as a white solid 85%, **F-mBOH** as pale yellow solid 92%, and **F-pBOH** as pale yellow solid 90%). Then, all sensors were characterized by using $^1\text{H-NMR}$, $^{13}\text{C-NMR}$ and ESI-HRMS spectroscopy. According to the $^1\text{H-NMR}$ spectra of **F-oBOH**, **F-mBOH**, and **F-pBOH** showed a singlet signal of imine proton ($\text{N}=\text{CH}$) at 9.584, 8.784, and 8.952, respectively. The $^{13}\text{C-NMR}$ spectra of **F-oBOH**, **F-mBOH**, and **F-pBOH** illustrated a characteristic peak of spirolactam carbon at 65.447, 64.623, and 65.413, respectively. In addition, the ESI-HRMS spectra confirmed the structure of **F-oBOH**, **F-mBOH**, and **F-pBOH** containing methanol and hydronium ion and showed the main intense peak at m/z 529.1542, 529.1552, and 529.1481, respectively. According to all characterization results, the obtained sensors have a structure corresponding to the structure of **F-oBOH**, **F-mBOH**, and **F-pBOH**.

Initially, the **F-oBOH**, **F-mBOH**, and **F-pBOH** were studied on the complexation abilities with several cation including Cu^{2+} , Cd^{2+} , Ni^{2+} , Ag^+ , Zn^+ , Co^{2+} , Mg^{2+} in acetonitrile performed on UV-Vis spectrophotometry. The UV-Vis spectra of **F-oBOH**, **F-mBOH**, and **F-pBOH** displayed the absorption band at 437 nm after adding Cu^{2+} ion, indicating the opened form of spirolactam ring of sensors. This suggested that our sensors have a selectivity toward copper(II) ion. Then, the binding competency of each sensors with copper(II) ion were measured by using UV-vis and fluorescence titration techniques. The $\log\beta$ values evaluated by UV-vis titration of **F-oBOH**, **F-mBOH**, and **F-pBOH** in acetonitrile were 6.67, 8.87, and 9.88, respectively. In comparison, the $\log\beta$ values

evaluated by fluorescence titration of **F-*o*BOH**, **F-*m*BOH**, and **F-*p*BOH** in acetonitrile were 8.02, 8.48, and 11.53, respectively. Furthermore, we studied the binding properties of sensors with cyanide anion in acetonitrile by UV-vis spectrophotometry. The results showed that cyanide anion can remove the copper(II) ion from the spirolactam ring of sensor. In contrast, it could not remove copper(II) ion from the hydroxy group of boronic acid but it can substituted on boron center.

Then, the stability of **F-*o*BOH**, **F-*m*BOH**, and **F-*p*BOH** studied by $^1\text{H-NMR}$ spectroscopy and fluorescence spectrophotometry was found that **F-*o*BOH** could be hydrolyzed by water and **F-*m*BOH**, and **F-*p*BOH** might be changed to be other forms. Thereafter, we designed the new strategy to turn-on fluorescence sensor of **F-*o*BOH** to avoid the hydrolysis phenomenon by applying the coordination nanoparticles (CNPs) network of **F-*o*BOH-AMP/Gd $^{3+}$** CNPs. The **F-*o*BOH-AMP/Gd $^{3+}$** CNPs has the average size approximately 60 nm characterized by scanning and transmission electron microscopy. Since, **F-*o*BOH** bound selectively to copper(II) ion, it was selected to be the generator of the opening spirolactam ring in **F-*o*BOH-AMP/Gd $^{3+}$** CNPs. The stability of **F-*o*BOH-AMP/Gd $^{3+}$** CNPs \subset copper(II) was tested by fluorescence spectrophotometry. The stability of **F-*o*BOH-AMP/Gd $^{3+}$** CNPs \subset copper(II) in aqueous solution was observed possibly caused by the interior hydrophobic shell of CNPs that can prevent **F-*o*BOH** to be hydrolyzed by water.

Moreover, the **F-*o*BOH-AMP/Gd $^{3+}$** CNPs \subset copper(II) toward various anions was investigated by fluorescence spectrophotometry and found that **F-*o*BOH-AMP/Gd $^{3+}$** CNPs \subset copper(II) gave a selective response toward cyanide anion. The stoichiometry between **F-*o*BOH-AMP/Gd $^{3+}$** CNPs \subset copper(II) and cyanide anion was 1:1 while the ratio of **F-*o*BOH-AMP/Gd $^{3+}$** CNPs \subset cyanide and copper(II) ion was 1:1 determined by Job's plot method. This results revealed that the hydroxy group on the boron center of **F-*o*BOH** incorporated in AMP/Gd $^{3+}$ CNPs bound with gadolinium(III) cation.

In addition, the stability constant of **F-*o*BOH-AMP/Gd³⁺** CNPs-copper(II) and cyanide anion showed the logK values of 3.97 evaluated by Specfit 32 program. The detection limit of **F-*o*BOH-AMP/Gd³⁺** CNPs-copper(II) toward cyanide anion evaluated by fluorescence technique and the visual change was 4.03 μM and 20 μM , respectively. Furthermore, no interference anions interfered to the detection of cyanide anion for **F-*o*BOH-AMP/Gd³⁺** CNPs-copper(II). Finally, the synthesized sensors can be served as a potential tool for detect cyanide anion in water. Interestingly, the use of self-assembly coordination in terms of lanthanide cation and AMP can eliminate the problem of hydrolysis toward **F-*o*BOH** and has a promising selectivity and sensitivity for detection of cyanide anion in water.

5.2 Future work

Future work in the areas of self-assembly coordination nanoparticles sensors should include further investigation on the effect of other lanthanide ions and nucleotide species. It would be great importance to look for some applications in real sample of **F-*o*BOH-AMP/Gd³⁺** CNPs because it composed of gadolinium(III) ion which could be used as MRI contrasting agent and also investigated in other applications. In addition to studying the ability of sensors **F-*o*BOH**, **F-*m*BOH**, and **F-*p*BOH** with cyanide anion should also be evaluated deeply in details.

REFERENCES

- [1] Lehn, J.M. *Supramolecular Chemistry Concepts and Perspective*, Wiley-VCH, Weinheim, 1995.
- [2] Steed, J. W., Turner, D.R., and Wallace, K.J. *Core concepts in Supramolecular Chemistry and Nanochemistry*, John Wiley & Sons, New York, 2007.
- [3] Ariga, K., and Kunitake, T. *Supramolecular Chemistry Fundamentals and Application*, Springer-Verlag Heidelberg, New York, 2006.
- [4] Jeffery, G.A. *An Introduction to Hydrogen Bonding*, Oxford University Press, Oxford, UK, 1997.
- [5] Bianchi, E., Bowman, J. K., and Garcia E. E. *Supramolecular Chemistry of Anions*, Wiley-VCH, New York, 1997.
- [6] Desvergne, J. P., and Czarnik, A. W. *Chemosensors for Ion and Molecule Recognition*, NATO Asi Series, Series C, Kluwer Academic Publishers, London, 1997.
- [7] Quang, D.T., and Kim, J.S. “*Fluoro- and Chromogenic Chemodosimeter for Heavy Metal Ion Detection in Solution and Biospecimens*” *Chem. Rev.* 2010, 110, 6280–6301.
- [8] Valeur, B. *Molecular Fluorescence: principles and Application*, Wiley-VCH Verlag GmbH, New York, 2001.
- [9] Lakowicz, J. R. *Principle of Fluorescence Spectroscopy*, 3rd ed, Springer Science, New York, 2006.
- [10] Bourson, J., and Valeur, B. “*Ion-Responsive fluorescent compounds. 2. Cation-steered Intramolecular Charge Transfer in a crowned Merocyanine*” *J. Phys. Chem.* 1989, 93, 3871-3876.

- [11] Fery-Forgues, S., Le Bris, M.T., Guette, J.P., and Valeur, B. “*First Crown Ether Derivative of Benzoxazone; a New Fluoroionophore for Alkaline Earth Metals Recognition*” *J. Chem. Soc. Chem. Commun.* 1988, 384-385.
- [12] Miller, J. N. and Miller, J. C. *Statistic and chemometric for analytical chemistry*, Prentice Hall, Harow, 2000.
- [13] <http://www.sciencedaily.com/articles/n/nanoparticle.htm> (accessed March 16, 2011)
- [14] <http://www.understandingnano.com/nanoparticles.html> (accessed March 16, 2011)
- [15] <http://en.wikipedia.org/wiki/Nanoparticle> (accessed March 16, 2011)
- [16] Heywood, J.A. *Microscopy Environmental Analysis:Elemental Analysis in the scanning electron microscope*, International Scientific Communication, Connecticut, 1981.
- [17] Chae, M. Y., Czarnik, A. W. “*Fluorometric Chemodosimetry. Mercury(II) and Silver(I) Indication in Water via Enhanced Fluorescence Signaling*” *J. Am. Chem. Soc.* 1992, *114*, 9704-9705.
- [18] Dujols, V., Ford, F., and Czarnik, A. W. “*A Long-Wavelength Fluorescent Chemodosimeter Selective for Cu(II) Ion in Water*” *J. Am. Chem. Soc.* 1997, *119*, 7386-7383.
- [19] Yang, Y. K., Yook, K. J., and Tae, J. “*A Rhodamine-Based Fluorescent and Colorimetric Chemodosimeter for the Rapid Detection of Hg²⁺ Ions in Aqueous Media*” *J. Am. Chem. Soc.* 2005, *127*, 16760-16761.
- [20] Wang, X. C., Li, Z., Wei, B. G., and Yang, J. Y. “*Synthesis of 2-(4-Methoxyphenyloxy-Acetylamido)-5-Aryloxymethyl-1,3,4-Oxadiazoles under Microwave Irradiation*” *Synth. Commun.* 2002, *32*, 1097-1103.
- [21] Zou, X. J., and Jin, G. Y. “*Synthesis of Pyridazinone-substituted 1,3,4-Thiadiazoles, -1,3,4-Thiadiazoles, -1,3,4-Oxadiazoles and -1,2,4-Triazoles*” *J. Heterocycl. Chem.* 2001, *38*, 993-996.

- [22] Wu, J. S., Hwang, I. C., Kim, K. S., and Kim, J. S. “*Rhodamine-Based Hg²⁺-Selective Chemodosimeter in Aqueous Solution: Fluorescent OFF-ON*” *Org. Lett.* 2007, 9, 907-910
- [23] Kaim, W., and Schwederski, B. *Bioinorganic Chemistry: Inorganic Elements in the Chemistry of Life*, John Wiley & Sons Ltd, England, 1991.
- [24] Khatua, S., Choi, S.H., Lee, J., Huh, J. O., Do, Y., and Churchill D.G. “*Highly Selective Fluorescence Detection of Cu²⁺ in Water by Chiral Dimeric Zn²⁺ Complexes through Direct Displacement*” *Inorg. Chem.* 2009, 48, 1799-1801.
- [25] Kim, H. J., Park, S. Y., Yoon, S., and Kim, J. S. “*FRET-Derived Ratiometric Fluorescence Sensor for Cu²⁺*” *Tetrahedron*, 2008, 64, 1294-1300.
- [26] Weng, Y. Q., Yue, F., Zhong, Y. R., and Ye, B. H. “*A Copper(II) Ion-Selective On-Off-Type Fluoroionophore Based on Zinc Porphyrin-Dipyridylamino*” *Inorg. Chem.* 2007, 46, 7749-7755.
- [27] Chen, X., and Ma, H. “*A Selective Fluorescence-On Reaction of Spiro Form Fluorescein Hydrazide with Cu(II)*” *Anal. Chim. Acta.*, 2006, 575, 217-222.
- [28] Li, T., Yang, Z., Li, Y., Liu, Z., Qi, G., and Wang, B. “*A Novel Fluorescein Derivative as A Colorimetric Chemosensor for Detecting Copper(II) Ion*” *Dyes Pigm.*, 2011, 88, 103-108.
- [29] Zhou, Y., Wang, F., Kim, Y., Kim, S.J., and Yoon, J. “*Cu²⁺-Selective Ratiometric and “Off-On” Sensor Based on the Rhodamine Derivative Bearing Pyrene Group*” *Org. Lett.*, 2009, 11, 4442-4445.
- [30] Kaim, W., and Schwederski, B. *Bioinorganic Chemistry: Inorganic Elements in the Chemistry of Life*, John Wiley & Sons Ltd, England, 1991, Chapter 10, pp208.
- [31] Lou, X., Qianh, L., Qin, J., and Li, Z. “*A New Rhodamine-Based Colorimetric Cyanide Chemosensor: Convenient Detecting Procedure and High Sensitivity and Selectivity*” *ACS Appl. Mater. Interfaces*, 2009, 1, 2529-2535.

- [32] Cho, D., Kim, J.H., and Sessler, J.L. “*The Benzil–Cyanide Reaction and Its Application to the Development of a Selective Cyanide Anion Indicator*” *J. Am. Chem. Soc.* 2008, *130*, 12163-12167.
- [33] Hudnall, T.W. and Gabbai, F.P. “*Ammonium Boranes for the Selective Complexation of Cyanide or Fluoride Ions in Water*” *J. Am. Chem. Soc.* 2007, *129*, 11978-11986.
- [34] Yang, Y.K., and Tae, J. “*Acridinium Salt Based Fluorescent and Colorimetric Chemosensor for the Detection of Cyanide in Water*” *Org. Lett.*, 2006, *8*, 5721-5723.
- [35] Happ, J. W., Janzen, E. G., and Rudy, B. C. “*Electron Spin Resonance Studies of Radical Formation in Nucleophilic Addition Reactions. III. Mechanism of Radical Formation and Chemiluminescence in the Cyanide Addition and Oxygenation of N-methylacridinium Chloride*” *J. Org. Chem.* 1970, *35*, 3382-3389.
- [36] Jamkratoke, M., Ruangpornvisuti, W., Tumcharern, G., Tuntulani, T., and Tomapatanaget, B. “*A-D-A Sensors Based on Naphthoimidazoledione and Boronic Acid as Turn-On Cyanide Probes in Water*” *J. Org. Chem.* 2009, *74*, 3919–3922.
- [37] Badugu, R., Lakowicz, J.R., and Geddes, C.D. “*Enhanced Fluorescence Cyanide Detection at Physiologically Lethal Levels: Reduced ICT-Based Signal Transduction*” *J. Am. Chem. Soc.* 2004, *127*, 3635-3641.
- [38] Li, Z., Lou, X., Yu, H., Li, Z., and Qin, J. “*An Imidazole-Functionalized Polyfluorene Derivative as Sensitive Fluorescent Probe for Metal Ions and Cyanide*” *Macromolecules.* 2008, *41*, 7433-7439.
- [39] Morikawa, M., Yoshihara, M., Endo, T., and Kimizuka, N. “*ATP as Building Blocks for the Self-Assembly of Excitonic Nanowires*” *J. Am. Chem. Soc.* 2005, *127*, 1358-1359.

- [40] Nishiyabu, R. et al. “*Nanoparticles of Adaptive Supramolecular Networks Self-Assembled from Nucleotides and Lanthanide Ions*” *J. Am. Chem. Soc.* 2005, *131*, 2151-2158.
- [41] Nishiyabu, R., Aim, C., Gondo, R., Noguchi, T., and Kimzuka, N. “*Confining Molecules within Aqueous Coordination Nanoparticles by Adaptive Molecular Self-Assembly*” *Angew. Chem. Int. Ed.* 2009, *48*, 9465–9468.
- [42] X. Chen, and H. Ma. (2006) “*A Selective Fluorescence-on reaction of spiro form fluorescein hydrazide with Cu(II)*” *Analytica Chim. Acta*, 2006, *575*, 217-222.
- [43] James, T.D., and Phillips M. D., Shinkai, S. *Boronic Acid in Saccharide Recognition*, The Royal Society of Chemistry, London, 2006.
- [44] Steed, J. W., and Atwood, J. L. *Supramolecular Chemistry*, 2nd ed, Anthony Rowe Ltd, Wilshire, UK, 2009.
- [45] Yang, H., Zhou, Z., Huang, K., Yu, M., Li, F., and Yi, T. “*Multisignaling Optical-Electrochemical Sensor for Hg²⁺ Based on a Rhodamine Derivative with a Ferrocene Unit*” *Org. Lett.* 2007, *9*, 4729-4732.
- [46] Kwon, J. Y. et al. “*A Highly Selective Fluorescent Chemosensor for Pb²⁺*” *J. Am. Chem. Soc.* 2005, *127*, 10107-10111.
- [47] Xiang, Y., and Tong, A. “*A New Rhodamine-Based Chemosensor Exhibiting Selective Fe^{III}-Amplified Fluorescence*” *Org. Lett.*, 2006, *8*, 1549–1552.
- [48] (a) Zhou, Y., Wang, F., Kim, Y., Kim S. J., and Yoon J. “*Cu²⁺-Selective Ratiometric and “Off-On” Sensor Based on the Rhodamine Derivative Bearing Pyrene Group*” *Org. Lett.* 2009, *11*, 4442-4445.
- [49] Swamy, K.M.K. et al. “*Boronic Acid-Link Fluorescent and Colorimetric Probes for Copper Ions*” *Chem. Commun.*, 2008, 5915-5917.
- [50] Adamczyk, M., and Grote, J. “*Synthesis of Novel Spirolactams by Reaction of Fluorescein Methyl Ester with Amines*” *Tetrahedron Lett.* 2000, *41*, 807-809.

- [51] Adamczyk, M., and Grote, J. “Efficient synthesis of rhodamine conjugates through the 20-position” *Bioorg. Med. Chem.* 2000, 10, 1539-1541.
- [52] Hyman, L. M., Stephenson, C. J., Dickens, M. G., Shimizu, K. D., and Franz, K.J. “Toward the Development of Prochelators as Fluorescent Probes of Copper-Mediated Oxidative stress” *Dalton Trans.*, 2010, 39, 568-576.
- [53] Ventura, C., and Martins, F. “Application of Quantitative Structure–Activity Relationships to the Modeling of Antitubercular Compounds. 1. The Hydrazide Family” *J. Med. Chem.* 2008, 51, 612-624.
- [54] Kalinowski, D.S., Sharpe, P.C., Bernhardt, P.V., and Richardson, D.R. “Structure–Activity Relationships of Novel Iron Chelators for the Treatment of Iron Overload Disease: The Methyl Pyrazinylketone Isonicotinoyl Hydrazone Series” *J. Med. Chem.* 2008, 51, 331-344.
- [55] *Guidelines for drinking-water quality*, 3rd ed.; World Health Organization, Geneva, 2004, 363.

APPENDIX

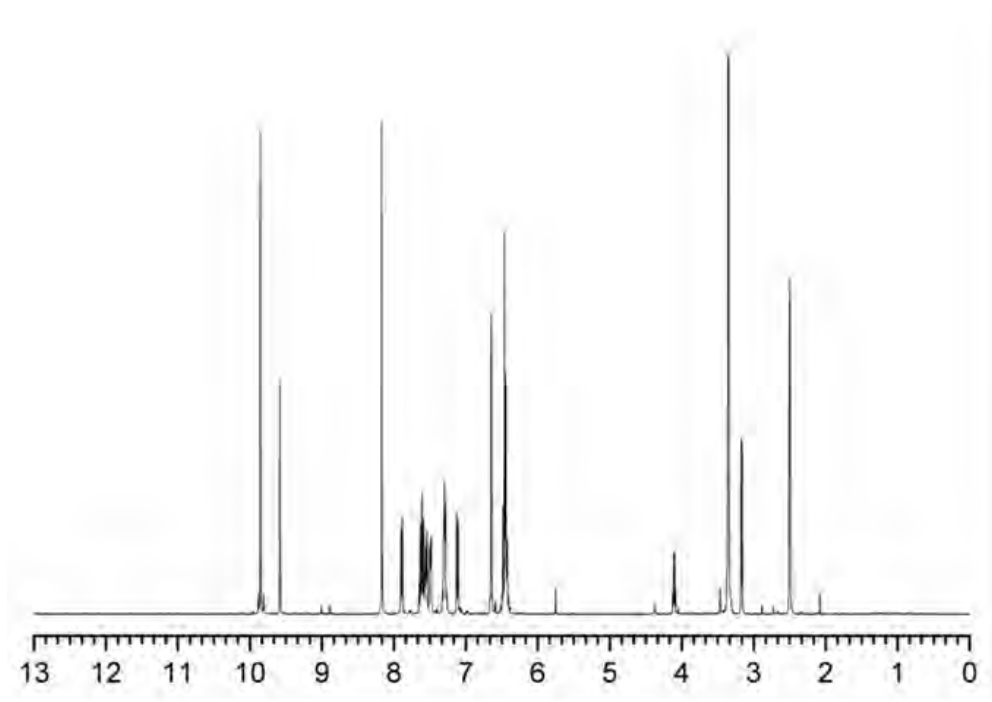


Figure S1 The $^1\text{H-NMR}$ spectrum of **F-oBOH** in $\text{DMSO-}d_6$

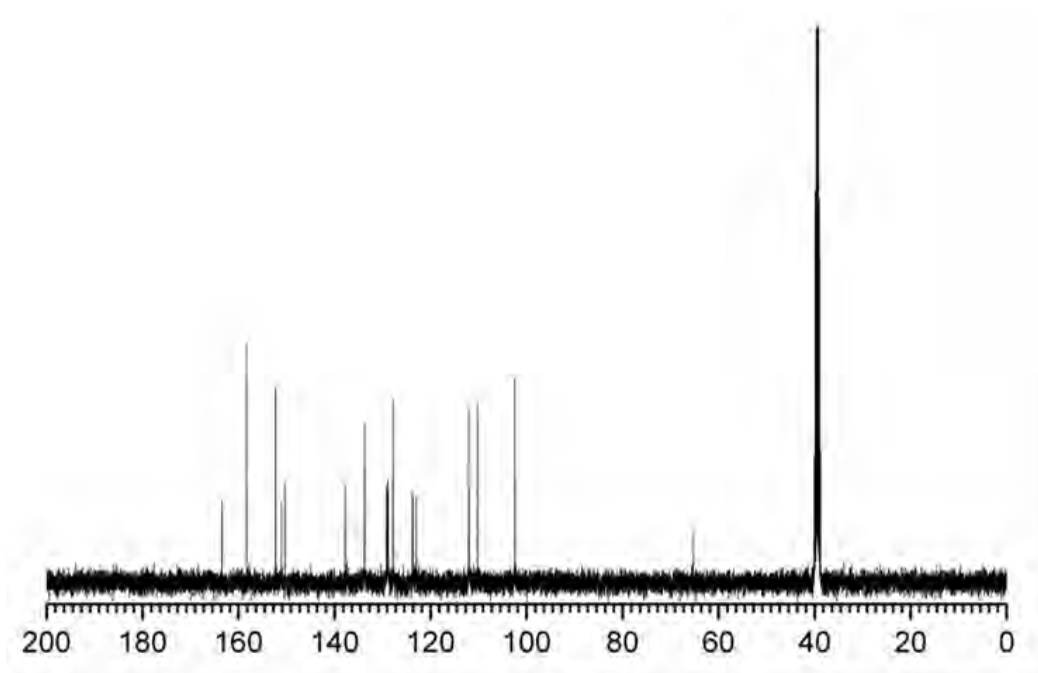


Figure S2 The $^{13}\text{C-NMR}$ spectrum of **F-oBOH** in $\text{DMSO-}d_6$

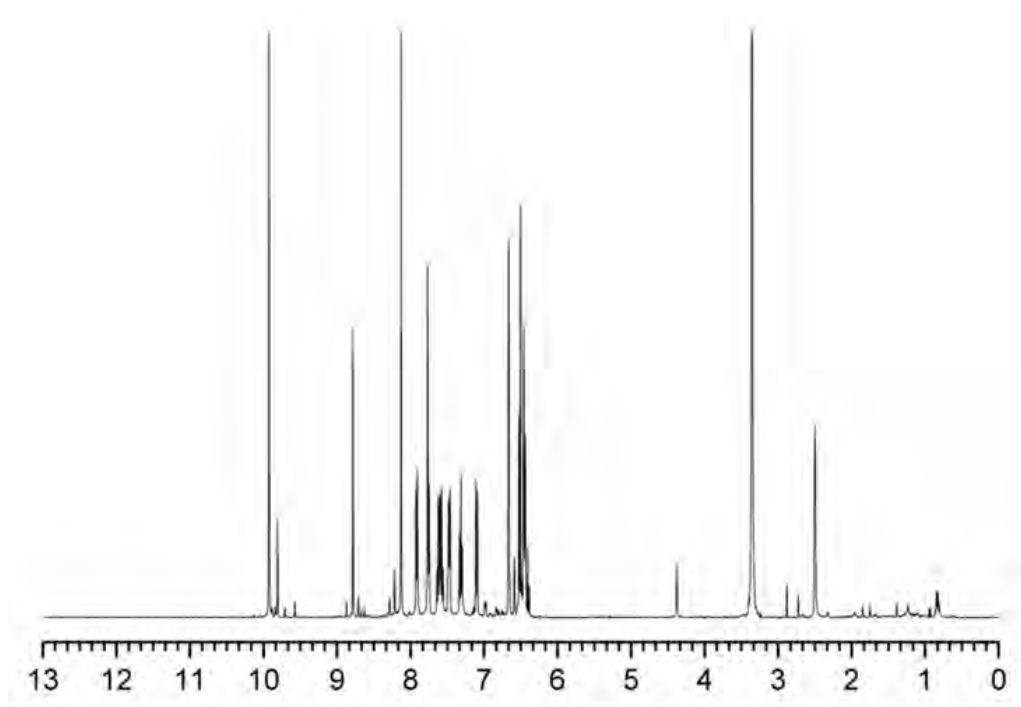


Figure S3 The $^1\text{H-NMR}$ spectrum of **F-*m*BOH** in $\text{DMSO-}d_6$

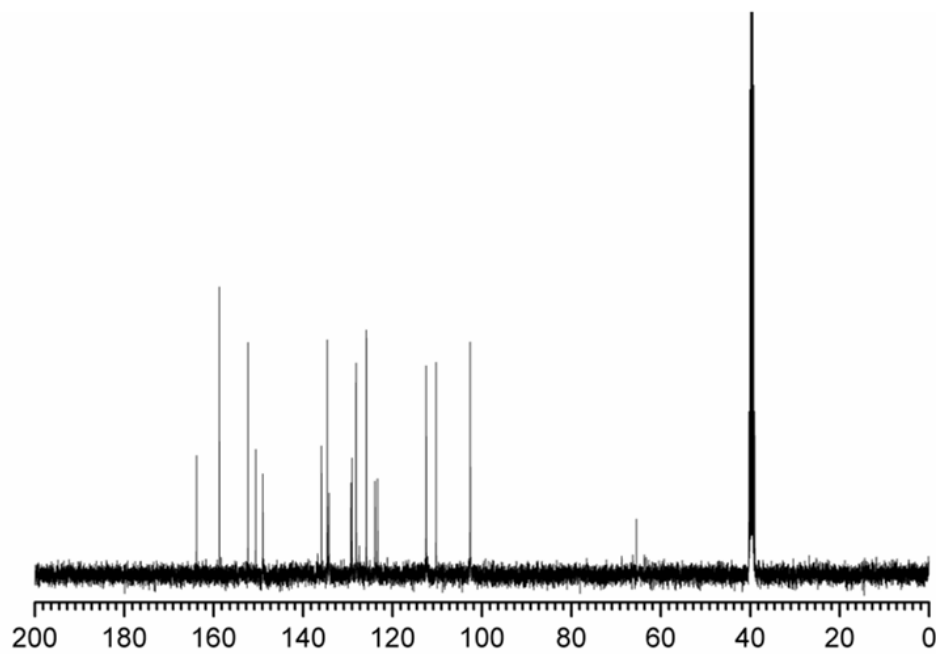


Figure S4 The $^{13}\text{C-NMR}$ spectrum of **F-*m*BOH** in $\text{DMSO-}d_6$

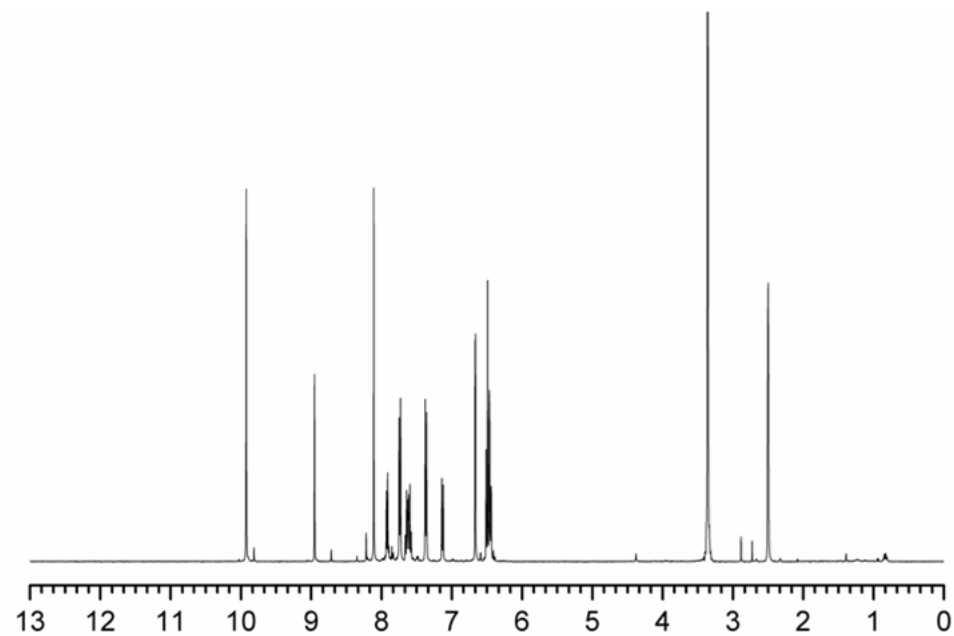


Figure S5 The $^1\text{H-NMR}$ spectrum of **F-pBOH** in $\text{DMSO-}d_6$

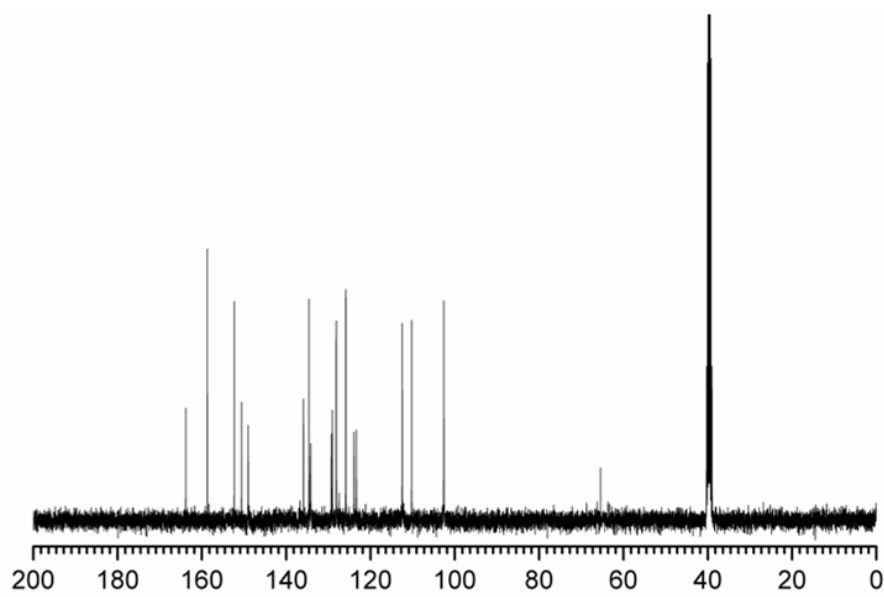


Figure S6 The $^{13}\text{C-NMR}$ spectrum of **F-pBOH** in $\text{DMSO-}d_6$

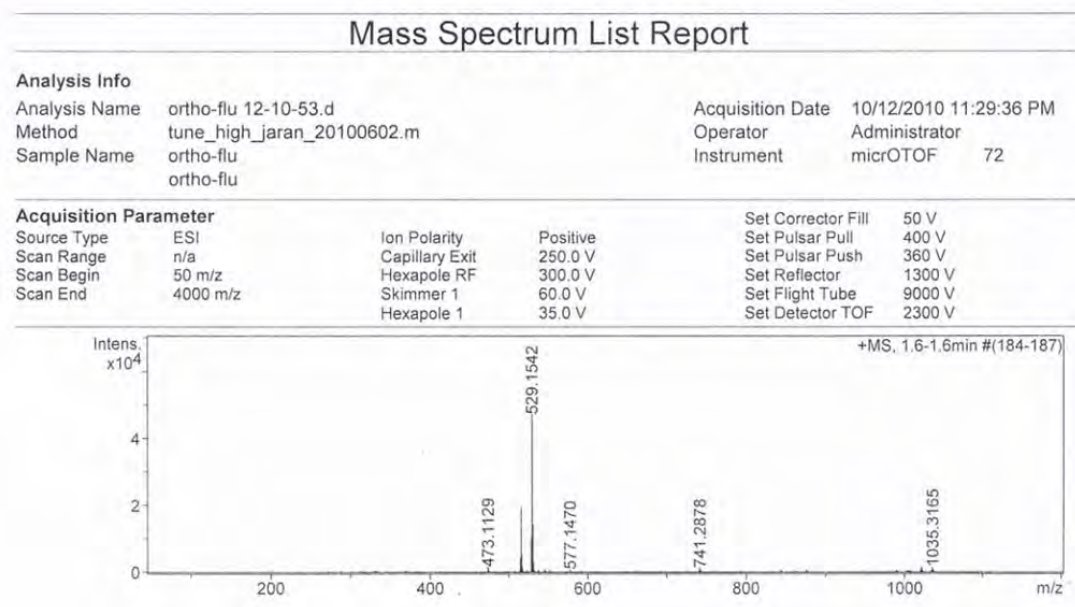


Figure S7 The ESI-High Resolution Mass spectrum of **F-*o*BOH**

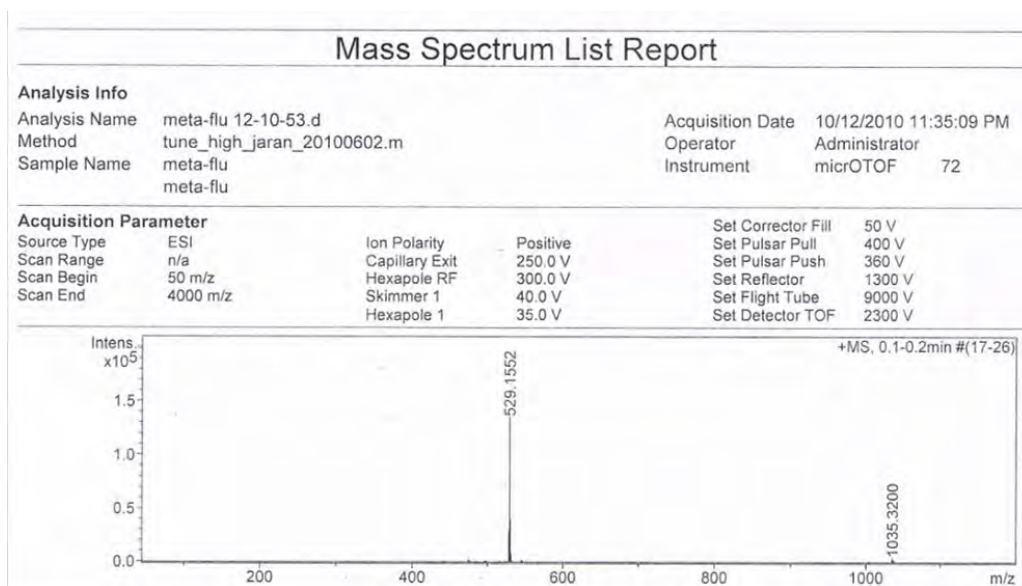


Figure S8 The ESI-High Resolution Mass spectrum of **F-*m*BOH**

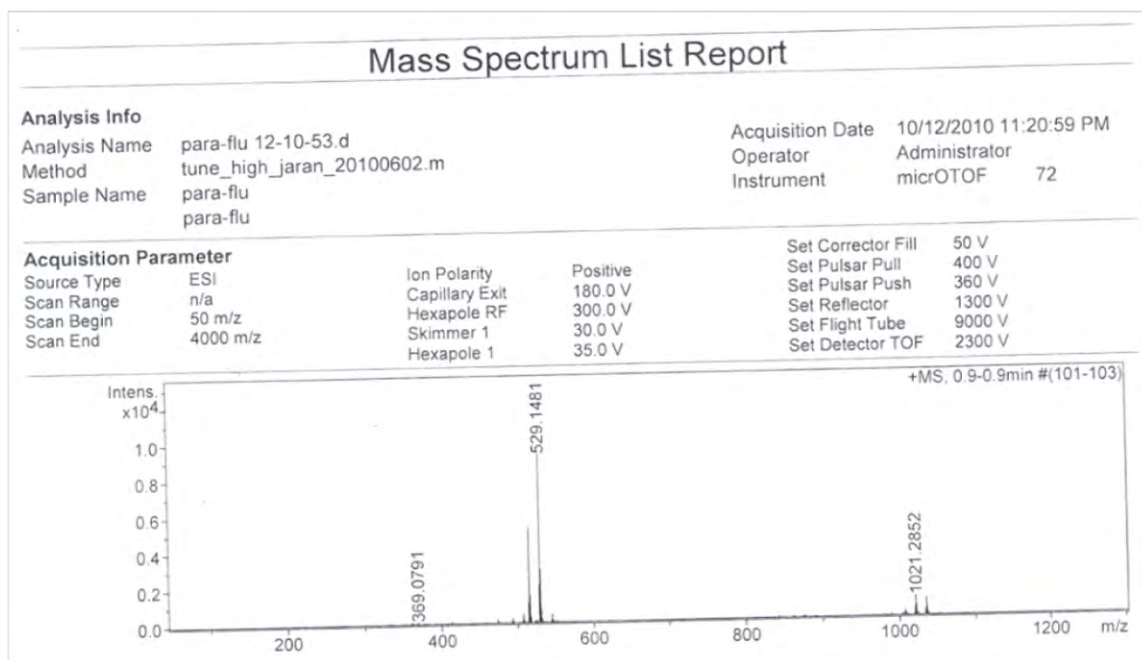


Figure S9 The ESI-High Resolution Mass spectrum of **F-pBOH**

VITA

General Biographical Information

Miss Sirinan Kulchat was born on October, 4, 1986 in Kalasin, Thailand. She graduated with a high school diploma from Buakhao School, Kuchinarai, Kalasin in 2005. Thereafter, she has become a member of supramolecular research unit since 2006 till now under supervision of Assistant Professor Dr. Boosayarat Tomapatanaget. She obtained her Bachelor's degree of Science in Chemistry with a second class honor from Chulalongkorn University in 2008. She finished her Master's degree of Science in the academic year 2010.

Awards and Experiences

- Participant in the 59th Meeting of Nobel Laureates dedicated to Chemistry 2009
in Lindau, Germany
- Research at Texas A&M University (USA) in Gabbai Research Group 2008
with Professor Francois P. Gabbai entitled "*Cationic silyl ether as chemosensor of fluoride ion in chloroform*"

Fellowships & Scholarships

- Junior Science Talent Project (JSTP) Scholarship Program, 2004-2011
Nation Science and Technology Development agency (NSTDA) to support covering full tuition and stipend in academic program at Chulalongkorn University, Thailand.

Publication

- Chaicham, A.; **Kulchat, S.**; Tumcharern, G.; Tuntulani, T.; Tomapatanaget, B.
"Synthesis, photophysical properties and cyanide detection in aqueous solution of *BF₂-curcumin dyes*" *Tetrahedron*, **2010**, 66, 6217-6223.